AD_______________

Award Number: W81XWH-10-1-0661

TITLE: SIRT3 is a Mitochondrial Tumor Suppressor and Genetic Loss Results in a Murine Model for ER/PR Positive Mammary Tumors Connecting Metabolism and Carcinogenesis

PRINCIPAL INVESTIGATOR: David Gius, M.D., Ph.D.
Sarki Abdulkadir, M.D., Ph.D.

CONTRACTING ORGANIZATION: Vanderbilt University
Nashville TN 37240

REPORT DATE: September 2011

TYPE OF REPORT: Annual

PREPARED FOR: U.S. Army Medical Research and Materiel Command
Fort Detrick, Maryland 21702-5012

# REPORT DOCUMENTATION PAGE

*Form Approved*
*OMB No. 0704-0188*



| 1. REPORT DATE | 2. REPORT TYPE | 3. DATES COVERED |
|---|---|---|
| September 2011 | Annual | 1 September 2010 – 31 August 2011 |

**4. TITLE AND SUBTITLE**

SIRT3 is a Mitochondrial Tumor Suppressor and Genetic Loss Results in a Murine Model for ER/PR Positive Mammary Tumors Connecting Metabolism and Carcinogenesis

**5a. CONTRACT NUMBER**

**5b. GRANT NUMBER**
W81XWH-10-1-0661

**5c. PROGRAM ELEMENT NUMBER**

**6. AUTHOR(S)**

David Gius, M.D., Ph.D.

**E-Mail:** david.gius@Vanderbilt.Edu

**5d. PROJECT NUMBER**

**5e. TASK NUMBER**

**5f. WORK UNIT NUMBER**

**7. PERFORMING ORGANIZATION NAME(S) AND ADDRESS(ES)**

Vanderbilt University
Nashville TN 37240

**8. PERFORMING ORGANIZATION REPORT NUMBER**

**9. SPONSORING / MONITORING AGENCY NAME(S) AND ADDRESS(ES)**
U.S. Army Medical Research and Materiel Command
Fort Detrick, Maryland 21702-5012

**10. SPONSOR/MONITOR'S ACRONYM(S)**

**11. SPONSOR/MONITOR'S REPORT NUMBER(S)**

**12. DISTRIBUTION / AVAILABILITY STATEMENT**
Approved for Public Release; Distribution Unlimited

**13. SUPPLEMENTARY NOTES**

**14. ABSTRACT**

The last year, which was funded by the DOD collaborative Breast Cancer Idea Award, has resulted in several important translational and basic science findings. Specifically, the most significant finding during the research period were: (1) the identification of MnSOD as a legitimate Sirt3 deacetylation target that for the first time shows that post-translation modifications of mitochondrial proteins plays a role in mitochondrial function (published in Molecular Cell); (2) that Sirt3 is first mitochondrial tumor suppressor protein that may play a role in the development of human luminal B breast malignancies; (3) that Sirt3 regulates the ATP synthase complex and the aberrant regulation of ATP synthase may play a role, at least in part, in breast carcinogenesis; (4) that tumors lacking Sirt3 may require the dysregulation of HIF-1 suggesting that there may be a sub-group of human tumors that may response to HIF-1 inhibitors in both chemoprevention as potentially as anti-cancer agents; and (5) that MnSOD function as both a molecular mechanism in breast cancers as well as the suggestion that agents that activate MnSOD may be agents for chemoprevention.

**15. SUBJECT TERMS**
Luminal B (ER+) breast cancer, murine models, chemoprevention, ROS, Sirtuins, Sirt3.

| 16. SECURITY CLASSIFICATION OF: | | | 17. LIMITATION OF ABSTRACT | 18. NUMBER OF PAGES | 19a. NAME OF RESPONSIBLE PERSON |
|---|---|---|---|---|---|
| | | | | | USAMRMC |
| a. REPORT | b. ABSTRACT | c. THIS PAGE | | | 19b. TELEPHONE NUMBER *(include area code)* |
| U | U | U | UU | | |

## Table of Contents

## INTRODUCTION:

The overarching goal of this proposal is to determine if the mitochondrial sirtuin *SIRT3* is a tumor suppressor gene (TSG) that may be used to: (1) establish a murine model to investigate the mechanisms of carcinogenesis in ER/PR-positive mammary tumors; and (2) determine if SIRT3 may serve as a new molecular biomarker that correlates with clinically and pathologically significant outcomes including response to therapy, local tumor control, disease free survival, and overall survival. Preliminary data from our laboratory demonstrated that: (1) *Sirt3* knockout mice exhibit decreased mitochondrial integrity and are genomically unstable when exposed to genotoxic agents; (2) Sirt3$^{-/-}$ MEFs transformed by either Myc or Ras have aberrant intracellular metabolism including increases in glycolysis, superoxide levels, and chromosomal abnormalities; (3) MnSOD prevents immortalization of *Sirt3*$^{-/-}$ MEFs by a single oncogene; (4) *Sirt3* knockout mice develop ER/PR-positive mammary tumors; and (6) SIRT3 expression is decreased in human breast tumors. Based on these results we initially proposed a hypothesis that longevity genes impact the process of carcinogenesis via the maintenance of mitochondrial integrity and oxidative metabolism. Specifically, loss of sirtuin expression could result in mitochondrial damage and a phenotype permissive for mammary tumors. In this regard, we proposed to: **(i)** Identify SIRT3 mitochondrial deacetylation targets and determine if these targets are regulated by extracellular stimuli known to activate sirtuin function (resveratrol). These targets will subsequently be knocked down (siRNA) to determine if there is a mechanistic connection between the increase in superoxide and stress-induced genomic instability observed in Sirt3$^{-/-}$ cells. **(ii)** Determine if exposure to resveratrol or overexpression of a MnSOD gene will prevent increases in ROS in MEFs and/or decrease the development of mammary tumors in SIRT3 knockout mice and transformation in Sirt3$^{-/-}$ MEFs. **(iii)** Determine if loss of SIRT3 protein in ER/PR-positive and negative breast samples correlates with clinically significant endpoints including response to therapy, tumor control, disease free survival, and overall survival.

**BODY:**

**Statement of Work - Task 1 - Identify Sirt3 mitochondrial deacetylation targets and determine if these targets are regulated by extracellular stimuli known to activate sirtuin function (e.g., resveratrol). These targets will subsequently be knocked down (with siRNA) to determine if there is a mechanistic connection between the increase in superoxide and the stress-induced genomic instability observed in SIRT3$^{-/-}$ cells (months 1-18).**

**I. Sirt3-Mediated Deacetylation of Evolutionarily Conserved Lysine 68 and 122 Regulates MnSOD Activity in Response to Stress. (Tao et al., 2010, Molecular Cell, See Appendix A).**

The work proposed in task 1 has made the most progress as one might expect since many of these experiments were proposed to provide data and reagents that are required to conduct the work in task 3. In addition, task 2 should take the longest since these experiments are in vivo chemoprevention work and will take most of, and perhaps all of the two years requested under this proposal. In regards to task 1, we have shown that genetic deletion of *Sirt3* results in increased mitochondrial superoxide, a tumor permissive environment, and mammary tumor development. As such, it was proposed in task 1 to determine if any Sirt3-dependent reversible acetyl-lysines that are regulated via Sirt3 by extracellular stimuli known to activate sirtuin function including resveratrol, fasting, and other exogenous agents that induce cellular oxidative stress. To address this we exposed mice to several such agents and determined any proteins in the mitochondria that are deacetylated by Sirt3. The first protein that we identified was MnSOD that appeared to have altered acetylation as well as the function activity in cells lacking Sirt3. Specifically, livers of Sirt3$^{-/-}$ mice contained hyperacetylated MnSOD as well as exhibited decreased MnSOD activity, but not immunoreactive protein, relative to wild-type livers. Re-introduction of wild-type, but not deacetylation null Sirt3, into Sirt3$^{-/-}$ MEFs deacetylated lysine and restored MnSOD activity. Site-directed mutagenesis of MnSOD lysine 122 to an arginine, mimicking deacetylation (lenti-MnSOD$^{K122-R}$), increased MnSOD activity when expressed in MnSOD$^{-/-}$ MEFs, suggesting acetylation directly regulates function. Furthermore, infection of Sirt3$^{-/-}$ MEFs with lenti-MnSOD$^{K122-R}$ inhibited in vitro immortalization by an oncogene (Ras), inhibited IR-induced genomic instability, and decreased mitochondrial superoxide. This work was subsequently published last December in *Molecular Cell* (Tao et al., 2010)[1]. Finally, lysine specific antibodies were made to these two lysine and these two antibodies will be used in task 3 to identify potential molecular targets for chemoprevention and molecular biomarkers that may be used to develop personalized treatment protocols. Thus, this work showed for the first time that there may be a connection between loss of *Sirt3* and the aberrant regulation of reactive oxygen species levels in the mitochondria that may play a role, at least in part, in the mechanism by which the mice lacking *Sirt3* develop ER+ tumors as well as develop spontaneous genomic instability.

**II. OSCP Contains an Evolutionarily Conserved Lysine that is Deacetylated by Sirt3 that Directs ATP Synthase Activity. (Pennington et al., 2011, Submitted, See Appendix B)**

Genetic deletion of *Sirt3* in vitro and in vivo decreases mitochondrial ATP levels suggesting a mechanistic connection to aberrant energy homeostasis and preferential use of glycolysis by the mammary tumors that develops in the *Sirt3* knockout mice. As such, we investigated if the aberrant energy production in mice lacking Sirt3 may play a role in why these mice develop mammary tumors. ATP synthase is made up of multiple proteins and it is primarily responsible for the production of ATP and since the mice lacking *Sirt3* have decreased ATP levels and increased glycolysis it seemed logical to propose that the dys-regulation of ATP synthase may play a role in the ER+ tumor permissive phenotype observed in these mice.

OSCP sits atop the ATP synthase (F1Fo ATPase) that uses chemiosmotic energy across the inner mitochondrial membrane to convert ADP and orthophosphate to ATP[2-4]. We have shown that OSCP contains at least one nutrient status-reversible acetyl-lysine that is evolutionarily conserved in multiple species. In this regard, mass spectrometry demonstrated that lysine 139 is hyperacetylated in *Sirt3* knockout livers, as compared to the control, wild-type mice. Re-introduction of wild-type, but not deacetylation null *Sirt3*, into $Sirt3^{-/-}$ MEFs deacetylated OSCP and increased mitochondrial ATP levels. IP experiments showed a physical interaction between OSCP and Sirt3. A series of in vitro and in vivo analysis demonstrated that OSCP lysine 139 is deacetylated by Sirt3. Finally, OSCP lysine 139 was mutated to arginine, mimicking deacetylation ($CMV\text{-}OSCP^{K139\text{-}R}$) and expression of $CMV\text{-}OSCP^{K139\text{-}R}$ increased mitochondrial ATP levels demonstrating that Sirt3 post-translational acetyl signaling contributes to mitochondrial energy homeostasis by deacetylating OSCP. Finally, a lysine specific antibody was made to this lysine and this antibody will be used in task 3 to identify potential molecular targets and/or biomarkers. These results not only identify an additional Sirt3 target but also for the first time showed that the production of ATP in the mitochondrial is regulated by a mechanism involving the post-translation modification of a reversible acetyl lysine. This work has recently been submitted and is in review at *PNAS* and the manuscript has been included in appendix B.

***SIRT3 deacetylates several potential reversible acetyl-lysines in ATP synthase alpha and beta.*** Since OSCP appeared to have a reversible acetyl-lysine it seems reasonable to propose that the other major proteins in the ATP synthase complex, including ATP synthase alpha and beta, might also have Sirt3-dependent reversible acetyl-lysine(s). To address this question a series of in vitro deacetylation assays were preformed.

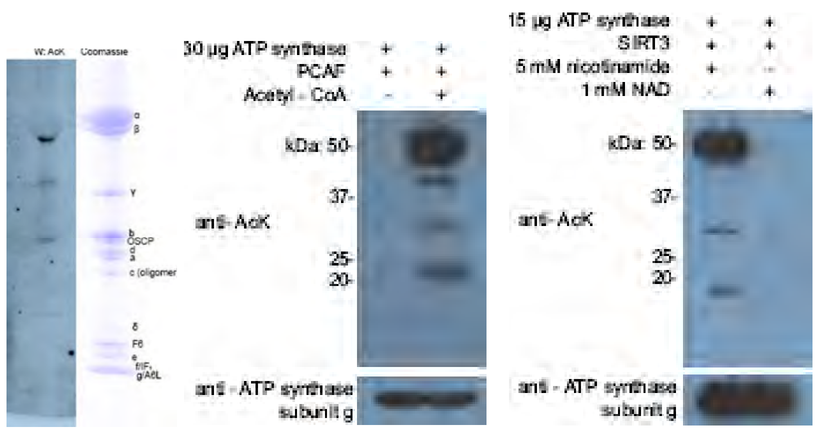


**Figure 1. The ATP Synthase complex contains multiple Sirt3-dependent reversible acetyl-lysines**. 50 mg samples of highly purified bovine F1Fo ATP synthase were separated and immunoblotted with an anti-acetyl antibody (left panels). These samples were mixed with PCAF to acetylated lysines (middle panels). Finally, an in vitro Sirt3 deacetylation assay was done as describe above and samples were separated and immunoblotted with an anti-acetyl antibody (right panel).

Affinity purified ATP synthase was obtained from bovine mitochondria with a GST-tagged inhibitor protein (I1-60) that was obtained (a kind gift from J.E. Walker, MRC, unpublished). Subunits from two 50 µg samples were resolved by SDS-PAGE and immunoblotted with an anti-acetyl-lysine antibody (Fig. 1, left panel lane 1) or stained with Coomassie (lane 2). These results suggest that in addition to OSCP, ATP synthase proteins alpha and beta may also contain specific reversible acetyl-lysines. These samples were subsequently treated with PCAF, which is an acetyl transferase previously shown to acetylate potential sirtuin targets, separated, and immunoblotted with an anti-acetyl antibody (Fig. 1, middle panel, lane 1 vs. 2). Finally, the PCAF-treated ATP synthase samples from lane 2, middle panel were mixed with recombinant SIRT3 without and with NAD for an in vitro deacetylation assay, similar to the experiments above (Fig. 1, right panel, lane 1 vs. 2). In these blots the ATP synthase alpha and beta proteins run at similar locations, and based on the differences in band intensity, it seems reasonable to assume that these two proteins contain multiple reversible acetyl-lysines (Fig. 1, right panel, lane 1 vs. 2). Finally, the samples in Fig. 1, right panel, lanes 5 and 6, were isolated and analyzed by mass spectrometry (that was done in Dr.

Liebler's Proteinomics group) and these results identified 10 alpha and 5 beta *in vitro* reversible acetyl-lysines (Supporting Data, pages 1 and 2). When these results were combined with published results that identified mitochondrial reversible acetyl-lysines after CR or fasting (12 hrs) (Supporting Data) we determined that ATP synthase alpha contains 7 reversibly acetylated lysines that appear in all three data sets and 3 that appear in two data sets. In addition, beta contains 3 reversible lysines that appear in two data sets. These combined findings strongly suggest that the ATP synthase alpha and beta, which are critical to the generation of mitochondrial ATP, may also be SIRT3 deacetylation targets that respond to stress or changes in cellular nutrient status. We are in the process of determining if these lysines are function in the regulation of ATP synthase activity and when this is done antibodies will also be made against the specific lysine as outlined above. Thus, this work has shown for the first time that ATP production via Sirt3 acetylation of proteins within the ATP synthase complex is regulated by Sirt3 and may play a role, at least in part, in the tumor permissive phenotype observed in mice lacking *Sirt3*. This work is not ready for publication yet but we anticipate that this work in will submitted sometime in the spring of 2012. In conclusion, the work outlined above has made very good progress in addressing the research proposed in task 1.

**Statement of Work - Task 2 - Determine if exposure to resveratrol or overexpression of a MnSOD gene will prevent increases in ROS in MEFs and/or decrease the development of mammary tumors in *Sirt3* knockout mice and transformation in SIRT3$^{-/-}$ MEFs (months 7-24).**

**I.** The research proposed in task 2 should take the longest since these experiments are in vivo chemoprevention work and will take most of, and perhaps all of the two years under this proposal. In addition, these experiments were not slated to start until month seven and as such, this work has only just begun. However, I have included the proposed experiments and the mice housing, breeding, and generation protocol / schema that is nearly completed. All mice for this study will be housed in barrier facilities in accordance with the standards set by the Vanderbilt Committee on Animal Care and according to our Institutional IACUC protocol number M/10/078. All mice will be examined daily and housed in a specific-pathogen-free animal facility. All the breeding is done in the barrier facility and 3 to 4 breeding pairs of all mice strains will be maintained at all times as founders to maintain the colonies as well as for breeding for the proposed experiments.

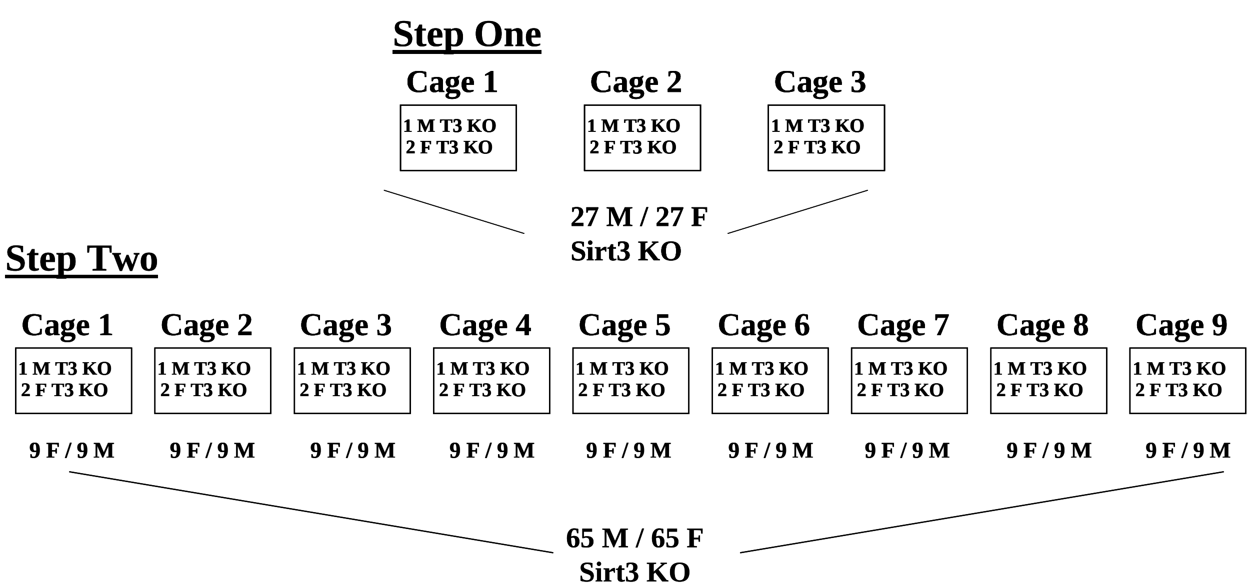


**Figure 2. Generation of SIRT3 KO (shown) and wild-type mice (not shown) for task 2.**

For the proposed experiments in Aim 1, a total of 130 female *SIRT3* knockout mice are required for each of the two groups that will contain 65 mice each (control and resveratrol). An outline is provided showing how we will generate roughly 65 female mice (Fig. 2). The number will be slight greater than 65 to adjust for decreased liter sizes and other issues so as the desired number of 65 mice will be obtained. This breeding scheme will be done in a very similar manner to generate the number of mice necessary for the control group. These mice are all genetically identical, originating from the same group of 2 to 4 females that are continuously maintained in a barrier facility in the Medical Center North (MCN) mouse facility at Vanderbilt.

For the resveratrol experiments wild-type and *Sirt3* knockout mice will be treated with resveratrol (AKSci, Cat. No. 60512A) supplemented drinking water daily (7.5 mg/mL) while the control group will be treated with carrier drinking water (DMSO 0.015%) daily. The drinking water will be kept away from light and changed every 3 days, and the mice will be maintained on resveratrol treatment until tumor formation or death. This regimen has previously been used to decrease tumors in mice.

These experiments have been somewhat delayed due to are relocation to Vanderbilt from the NCI however, they were recently started. Generation of the mice required for the work in task 2 is straightforward but somewhat more complex than the mice above. Step 1 involves the generation of the MnSOD-Sirt3$^{-/-}$ mice that this will be done by crossing the transgenic MnSOD mice with the Sirt3 knockout mice and then these mice will be back crosses to obtain the MnSOD-Sirt3$^{-/-}$ mice. To obtain roughly 9 male mice, one cage will be set up that contains 2 females and 1 male. From this round of breeding 8 MnSOD-Sirt3$^{-/-}$ males and 16 SIRT3$^{-/-}$ females will be mated as shown in Figure 3. Since both the MnSOD$^{+/+}$-Sirt3$^{-/-}$ males and Sirt3$^{-/-}$ females are homogenous for loss of *Sirt3*, all these offspring will be Sirt3$^{-/-}$. In addition, since all the male mice contain the *MnSOD* gene on both chromosomes, the offspring will only receive one copy of the exogenous *MnSOD* gene (Fig. 3). As such, after 10 weeks, 16 Sirt3$^{-/-}$ females and 8 MnSOD-Sirt3$^{-/-}$ males will be used to set up 8 cages of 2 females and 1 male. This should result in roughly 65 females and 65 males that contain one copy of the exogenous *MnSOD* gene that also lack both copies of *Sirt3* (MnSOD$^{+}$-Sirt3$^{-/-}$), of which 65 will be used for the experiments proposed in Aim 2. This should take roughly 6 months. The *Sirt3* knockout mice that will act as controls will be generated as described above (Figure 2). Finally, an additional 5 mice will be added to each group to account for mice that may become infect or sick and these mice will assure that the number of mice that can be evaluated will remain at or above 65 mice per group.

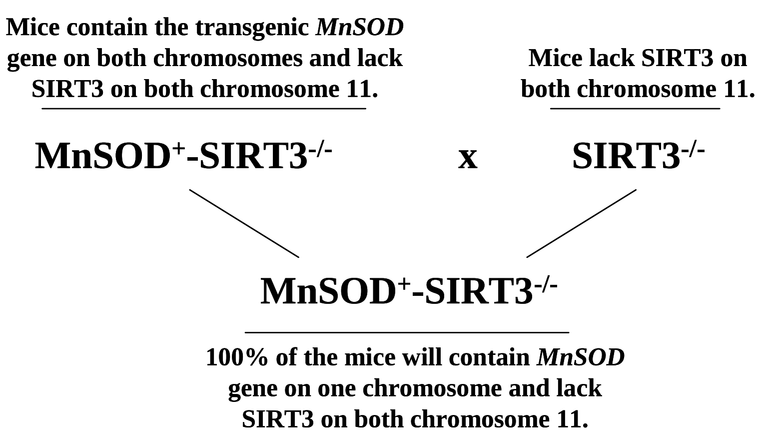


**Figure 3. Generation of the MnSOD$^{+}$-SIRT3$^{-/-}$ Mice**

**II. Procedures for reducing discomfort, and stress:** Injection procedures, if necessary, will be performed as outlined in our murine protocols as well as with the guidance and approval of the Vanderbilt veterinarians. For anesthesia, and when required, mice will be anesthetized prior to all injections using Ketamine at a dosage of 100 mg/kg body weight and Xylazine at a dosage of 15

mg/kg body weight by intraperitoneal injection. The depth of anesthesia will be monitored by respiratory rate and toe-pinch reflex. Animals will be monitored daily and euthanized when ill. The animals will be housed in groups of up to 5 animals per cage when possible; however, for CR only two mice per cage will be possible. Animals are removed from the sight of other animals for procedures requiring anesthesia, and are returned to their cages as quickly as possible, usually 5-10 minutes. Mice will be terminated if they become ill (lack normal grooming and avoidance behaviors), or are unable to eat or drink.

**III. Statistical Considerations:** The primary objective of several aspects of this grant proposal is to compare the tumor development between study groups. The Vanderbilt Power and Sample Size Estimation software and the Radiation Oncology network station was used to estimate the sample size required for our proposed experiments with resveratrol (task 2). The sample size calculations are based on a two-sample chi-square test of proportions without a continuity correction. At 30 months, the incidence of ductal mammary tumors is estimated to be 60%. This number (60%) is based on our results that are already published (Kim et al., 2010, *Cancer Cell*) as well as an additional 20 mice in each arm that was just completed at the NCI. If CR decreases the tumor incidence to 35%, the number of mice needed in each arm is roughly 65 control *SIRT3* knockout mice and 66 *SIRT3* knockout mice placed on a CR diet, which will give 80% power using a Type I error of 0.05. These proposed experiments are on going and it is still too early to make any determinations at this time..

**Statement of Work - Task 3 - Determine if loss of SIRT3 ductal protein in ER/PR-positive and -negative breast samples from the Vanderbilt Breast Spore correlates with clinically significant outcomes including response to therapy, local tumor control, disease free survival, and overall survival (months 1-24).**

In this task we proposed to conduct H & E stained of human samples or slides that will be reviewed to assess the diagnosis and grade, in a blinded manner with no prior knowledge of IHC results. In addition, we will determine clinicopathologic variables including age, tumor grade, stage, mitotic count, and ER and PR status and these will be assesses by response to therapy, local tumor control, disease free survival, and overall survival. These endpoints will be determined via Kruskal-Wallace non-parametric analysis of variance will be done to determine how marker expression varies with grade. The log-rank test will be used to evaluate the statistical significance of disease-free survival by the Kaplan–Meier method for univariate analysis. Finally, log-plots will be used to estimate survival function to test the proportional hazards assumption. The Wald test will be used for Cox proportional hazards regression analysis, and data will first be tested to ensure they meet the assumptions for using the Cox test.

This work is on going and has been slightly delayed to accommodate the new antibodies were validated and are discussed in the "statement of work – task 1 section" that may be molecular biomarkers. In addition, new preliminary data from our laboratory and others, has demonstrated that mice lacking *Sirt3* exhibit increased ROS, including superoxide levels ($O_2^{\cdot-}$), due to: (1) the aberrant acetylation of oxidative phosphorylation complex I-III proteins; and (2) the aberrant regulation of MnSOD ROS scavenging activity (Tao et al, 2010, *Molecular Cell*, Appendix A) that may be early steps in carcinogenesis. In addition, we and others have also shown that cells lacking *Sirt3* also exhibit increased HIF-1α as well as the expression of HIF-1α-dependent pro-proliferative proteins resulting in cellular metabolic reprogramming (Warburg effect).

**I. Sirt3 directs cellular metabolic reprogramming that mirrors the Warburg effect**

Tumor cells exhibit reprogramming of cellular metabolism involving an increase in glucose consumption described by Otto Warburg 60 years ago and referred to as the "Warburg effect." Interestingly, any underlying cellular processes linking aberrant mitochondrial metabolism and increased ROS to the Warburg effect have, until recently, remained unclear. In this regard, we have shown that Sirt3$^{-/-}$ cells exhibit increased glucose uptake that is preferentially used to make ATP as a result of what appears to be the aberrant acetylation and decreased activity of ETC complex III[5,6]. It has been previously suggested that mitochondrial ROS can induce HIF-1α activity[7-9], and cells lacking Sirt3 exhibit increased ROS. Thus, is there a connection between Sirt3, HIF-1α, and changes in metabolic reprogramming? To address this issue we showed that Sirt3$^{-/-}$ MEFs exhibit increased HIF-1α protein levels (Fig. 5a, lane 1 vs. 4) as well as HIF-1α dependent gene expression, as shown by co-transfection assays using an HRE luciferase reporter (Fig. 4b, bar 1 vs. 2). In addition, exposure to NAC, which scavenges ROS, prevents the increase in HIF-1α levels (Figs 4a, lane 4 vs. 5) and HIF-1α dependent gene expression (Fig. 4b, bar 2 vs. 4).

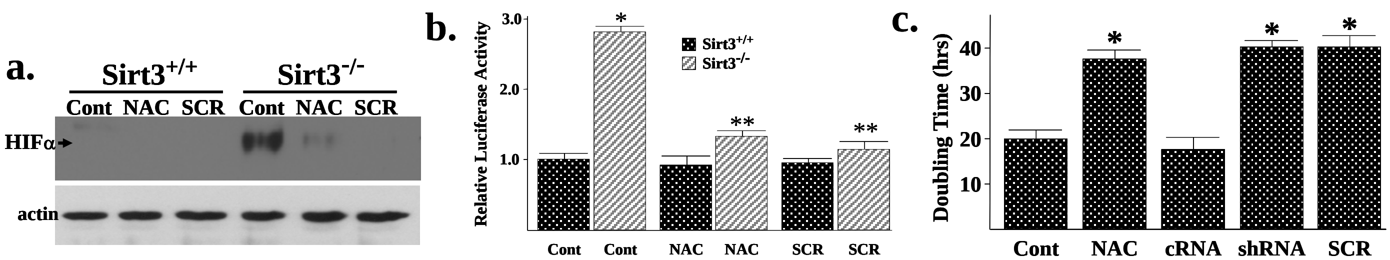


**Figure 4. Loss of Sirt3 increases HIFα protein levels and gene expression via a ROS-dependent mechanism. (a)** Cell extracts from Sirt3$^{+/+}$ and Sirt3$^{-/-}$ MEFs, with and without exposure to either NAC or stigmatellin (SCR), were blotted with an anti-HIF-1α antibody. **(b)** MEFs were co-transfected with p3x-HRE-luciferase with or without NAC or stigmatellin and 40 hours afterwards luciferase levels were determined. **(c)** MTCLT3$^{-/-}$ Cells were exposed to NAC, control shRNA, HIF-1α shRNA, or stigmatellin and cell doubling times were determined. All the experiments for this figure were done in triplicate. * indicates $P < 0.05$ by t-test.

As such, we now have scientific data demonstrating that cells lacking *Sirt3* exhibit decreased ETC complex III activity that may play a critical role, at least in part, in the elevated cellular ROS levels. Stigmatellin is a chemical agent that binds to complex III, inhibits electron transfer, and prevents generation of ROS[5]. Exposure of Sirt3$^{-/-}$ MEFs to stigmatellin decreased HIF-1α levels (Fig. 4a, lane 4 vs. 6) and HIF-1α gene expression (Fig. 4b, bar 2 vs. 6). In addition, tissue culture cells were also treated with either NAC or stigmatellin and these results clearly show that both agents decreased the growth rate of mammary tumor cells lacking *Sirt3* (Fig. 4c, lane 1 vs. 2 and 5). Finally, cells were treated with either control shRNA or HIF-1α shRNA and decreased HIF-1α protein levels were observed (data not shown) as well as an increase in the tumor cell doubling time (Fig. 4c, lane 3 vs 4). Decreases in several other *in vitro* transformation properties including growth in soft agar, foci formation, and tumor formation, were seen in nude mice (data not shown).

Thus, we propose a model where an increase in ROS and HIF-1α results in a phenotype favoring both genomic mutations (Fig. 5. blue arrow) and proliferation (purple arrow) that are established early driving events for breast tumorigenesis. Thus, it is hypothesized that ROS and/or HIF-

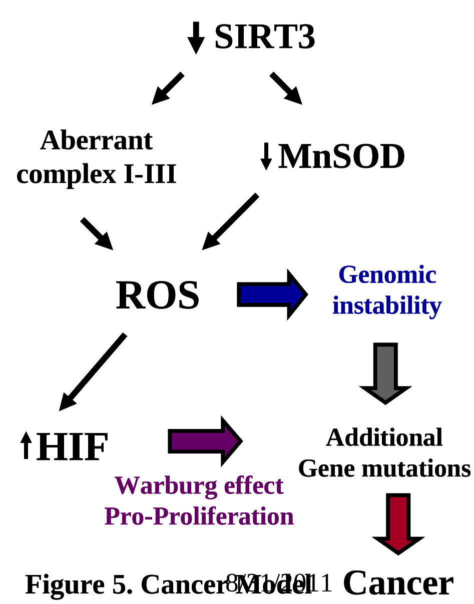


**Figure 5. Cancer Model**

1α may be molecular targets for therapeutic intervention. As such, we propose that mice lacking Sirt3 are a novel in vivo model in which to investigate the well established connection between decreased SIRT3 levels and ROS, HIF-1α, the Warburg effect, and breast malignancies. We would propose that agents thought to scavenge or decrease cellular ROS ($O_2^-$) and/or inhibit HIF-1α activity will prevent tumors in Sirt3 knockout mice. If this is true, there is a subgroup of human breast cancers with decreased SIRT3 expression or enzymatic activity for which these agents may be chemopreventive or cytotoxic on their own and/or synergize in combination with chemo- or radiation therapy. This work is being investigated in the laboratory that we feel falls under task number 3.

Over the last 10 years it has been suggested that there our four major subgroups of breast malignancies (See Prevalence Table) as determined by genetic biomarkers. Our preliminary data suggests that the tumors observed in the mice lacking *Sirt3* may be genetically similar to the luminal B cancer or more likely a subgroup of this classification that comprises roughly 15% of all breast cancers[10-12]. As such, a critical aspect of our research proposal as outlined in task 3 is the identification of a subgroup of human breast cancer tumors where loss of *SIRT3* is an early driving or initiating event in carcinogenesis. Thus, the relationship of SIRT3 expression to clinicopathologic parameters—age, tumor grade, stage, mitotic count, ER and PR status, as well as response to therapy, local tumor control, disease free survival, and overall survival is being determined with a series of biomarkers that are discussed above. These include the new antibodies that are discussed above ($OSCP^{K139}$, $MnSOD^{K68}$, and $MnSOD^{K122}$) as well as HIF-α, and the markers shown in the table above. With the recent validation of these antibodies as well as the identification of HIF-α, we have been staining both commercial human breast cancer arrays as well as the human samples in the Vanderbilt Breast Cancer SPORE sample archive. Thus, we hope to identify a subgroup of human breast cancer tumors where loss of SIRT3 is an early driving or initiating event in carcinogenesis that has a proteomic signature that also includes increased ROS and HIF-1a that is likely to be a subgroup of "Luminal B" breast malignancies. Thus, these experiments are intended to begin the scientific process of a more extensive biological characterization of the proposed *Sirt3* knockout mouse and its potential use as a model of the subtype of mammary tumors that are observed in older women. This work is on going and it is likely that a manuscript containing these results should be ready to send out some time in the summer of 2012.

| **Subtype** | **Tumor Biomarkers** | **Prevalence** |
|---|---|---|
| **Luminal A** | **ER+ and/or PR+, HER2- low Ki67** | **42 – 59%** |
| **Luminal B** | **ER+ and/or PR+, HER2+, or HER2- high Ki67** | **6 – 19%** |
| **TN/basal-like** | **ER-, PR-HER2-CK5/6+, or HER1+** | **15 – 20%** |
| **HER2+** | **ER-, PR-, HER2+** | **7 – 12%** |

## KEY RESEARCH ACCOMPLISHMENTS:

1. The identification of MnSOD as a legitimate Sirt3 deacetylation target that for the first time shows that post-translation modifications of mitochondrial proteins plays a role in mitochondrial detoxification. This work was published in *Molecular Cell*.

2. Sirt3 is activated in vivo by 36 hours of fasting showing for the first time that Sirt3 is a nutrient distress protein.

3. Sirt3 is the first mitochondrial tumor suppressor protein that may play a role in the development of luminal B breast malignancies.

4. Sirt3 regulates the ATP synthase complex and the aberrant regulation of ATP synthase may play a role, at least in part, in breast cancers that are similar to luminal B human breast malignancies.

5. Tumors lacking Sirt3 may require the dysregulation of HIF-1$\alpha$ suggesting that there may be a sub-group of human tumors that may response to HIF-1$\alpha$ inhibitors in both chemoprevention as potentially as anti-cancer agents.

6. The identification of MnSOD function as both a molecular mechanism in breast cancers as well as the suggestion that agents that activate MnSOD or scavenge superoxide may be agents in chemo-prevention. In addition, these agents may also be anticancer in luminal B breast tumors.

## REPORTABLE OUTCOMES:

### Manuscripts supported by this award:

1. Tao, R., Coleman, M.C., Pennington, J.D., Ozkan, O., Park, S-H., Jiang, H., Kim, H-S., Flynn, C.R., Hill, S., McDonald, W.H., Olivier, A.K., Spitz, D.R., and D. Gius. Sirt3-Mediated Deacetylation of Evolutionarily Conserved Lysine 122 Regulates MnSOD Activity in Response to Stress. *Molecular Cell* 40:893-904, 2010.
2. Kim, H-S., Vassilopoulos, A., Wang, R-H., Lahusen, T., Xu, Z., Wang, X.W., Gius, D., and Deng, C-X. Mitotic dysfunction leads to genetic instability and tumorigenesis in mice lacking Sirt3. *Cancer Cell*, (In Press), 2011.

### Animal models supported by this award:

1. The Sirt3 knockout mouse supported by this award is now available to other researchers who wish to work on ER+ murine breast cancer models.

### Training supported by this award

1. Ozkan Ozden, Ph.D. (2010 - present). Post Doctoral Fellow.
2. Seong Park, Ph.D. (2010 – present). Post Doctoral Fellow.

## CONCLUSION:

The incidence of human malignancies increases significantly with age, suggesting a mechanistic connection between aging (longevity) and carcinogenesis. Breast cancer has a very specific age-related incidence that increases until menopause and then increases more slowly until the mid 60's, when a second significant increase in incidence is observed. Breast malignancies that develop over time very likely represent a spectrum of cancers arising from different types of hereditary and spontaneous tumors. Murine models for hereditary breast cancer in younger women have been established by altering the expression of BRCA genes, and these mice develop triple negative (ER/PR negative, her2neu) tumors. In contrast, there are no murine models for the spontaneous breast cancers that are more common in older women. The work supported by this DOD idea award has allows us to not only validate the first ER+ in vivo murine model for breast cancers but is has also allowed the discovery of several potential molecular targets that may potential be used for either chemoprevention or as anticancer agents. We have also developed three antibodies that along with the human SIRT3 antibody that will allow us to determine potential sub-groups of women with breast cancer that may benefit from specific anticancer therapies. In addition, these antibodies will allow the further sub-classification of women with breast malignancies that other researcher may find helpful in their own research into the mechanisms of both breast carcinogenesis as well as the potential development of anticancer agents.

## REFERENCES:


1. Tao, R., *et al.* Sirt3-mediated deacetylation of evolutionarily conserved lysine 122 regulates MnSOD activity in response to stress. *Molecular cell* **40**, 893-904.
2. Walker, J.E., Gay, N.J., Powell, S.J., Kostina, M. & Dyer, M.R. ATP synthase from bovine mitochondria: sequences of imported precursors of oligomycin sensitivity conferral protein, factor 6, and adenosinetriphosphatase inhibitor protein. *Biochemistry* **26**, 8613-8619 (1987).
3. Walker, J.E., Lutter, R., Dupuis, A. & Runswick, M.J. Identification of the subunits of F1F0-ATPase from bovine heart mitochondria. *Biochemistry* **30**, 5369-5378 (1991).
4. Rees, D.M., Leslie, A.G. & Walker, J.E. The structure of the membrane extrinsic region of bovine ATP synthase. *Proc Natl Acad Sci U S A* **106**, 21597-21601 (2009).
5. Bell, E.L., Emerling, B.M., Ricoult, S.J. & Guarente, L. SirT3 suppresses hypoxia inducible factor 1alpha and tumor growth by inhibiting mitochondrial ROS production. *Oncogene*.
6. Kim, H.S., *et al.* SIRT3 Is a Mitochondria-Localized Tumor Suppressor Required for Maintenance of Mitochondrial Integrity and Metabolism during Stress. *Cancer cell* **17**, 41-52 (2010).
7. Archer, S.L., *et al.* Mitochondrial metabolism, redox signaling, and fusion: a mitochondria-ROS-HIF-1alpha-Kv1.5 O2-sensing pathway at the intersection of pulmonary hypertension and cancer. *Am J Physiol Heart Circ Physiol* **294**, H570-578 (2008).
8. Comito, G., *et al.* HIF-1alpha stabilization by mitochondrial ROS promotes Met-dependent invasive growth and vasculogenic mimicry in melanoma cells. *Free Radic Biol Med*.
9. Hwang, A.B. & Lee, S.J. Regulation of life span by mitochondrial respiration: the HIF-1 and ROS connection. *Aging (Albany NY)* **3**, 304-310.
10. Sorlie, T., *et al.* Repeated observation of breast tumor subtypes in independent gene expression data sets. *Proc Natl Acad Sci U S A* **100**, 8418-8423 (2003).
11. Sorlie, T., *et al.* Gene expression patterns of breast carcinomas distinguish tumor subclasses with clinical implications. *Proc Natl Acad Sci U S A* **98**, 10869-10874 (2001).
12. Herschkowitz, J.I., *et al.* Identification of conserved gene expression features between murine mammary carcinoma models and human breast tumors. *Genome Biol* **8**, R76 (2007).

# Supporting Data

**Previously identified and published reversible acetyl-lysines present in ATP synthase proteins alpha, beta, and gamma.**

**Lombard et al., 2010. Aging Cell [1] in black letters**
**Kim et al., 2006. Molecular Cell [2] in blue letters**
**Gius lab (unpublished data) [3] in purple**
**in more than data set.**

| Gene Name | Amino Acid | Sequence |
|---|---|---|
| ATP synthase subunit alpha | 132 | LIKEGDVVK*R [3] |
| | 161 | VVDALGNAIDGK*GPIGSK [1,3] |
| | 167 | VVDALGNAIDGKGPIGSK*T [1,3] |
| | 230 | TSIAIDTIINQK*R [1,2,3] |
| | 239 | FNDGTDEK*K [1,2] |
| | 240 | FNDGTDEKK*K [1] |
| | 261 | RSTVAQLVK*R [1,2,3] |
| | 427 | AMK*QVAGTMK [1,2,3] |
| | 531 | SDGK*ISEQSDAKLK [1,2] |
| | 539 | ISEQSDAK*LK [3] |
| *In vitro* SIRT3 deacetylation assay | 261 | STVAQLVK*R [1,3] |
| | 161 | VVDALGNAIDGKGPIGSKAR [1,3] |
| | 167 | VVDALGNAIDGKGPIGSK*AR [1,3] |
| | 175 | VGLK*APGIIPR [3] |
| | 230 | TSIAIDTIINQK*R [1,2,3] |
| | 427 | AMK*QVAGTMK [1,2,3] |
| | 434 | QVAGTMK*LELAQYR [3] |
| ATP synthase subunit beta | 133 | VLDSGAPIK*IPVG [2] |
| | 259 | GVINLK*DATSK [2] |
| | 522 | KADK*LAEEHGS [2] |
| *In vitro* SIRT3 deacetylation assay | 55 | AAQASPSPK*AGATTGR |
| | 124 | GQK*VLDSGAPIRIPVGPET [3] |
| | 259 | EGNDLYHEMIESGVINLKDATSK [3] |
| | 426 | GVQKILQDYK [3] |
| | 522 | KADK*LAEEHS [2,3] |

| | | |
|---|---|---|
| <u>ATP synthase gamma-subunit</u> | 89 | ADIKAPEDKK*K |
| | 90 | ADIKAPEDKKK* |
| | 138 | IK*GILYR |
| | 154 | THSDQFLVSFK*DVGR |
| *In vitro* SIRT3 deacetylation assay | 49 | SMK*MVAAAK |
| | 115 | QMK*SEAANLAAAGK |
| | 259 | TAMDNASK*NASEMI SEAANLAAAGKEVK |

# APPENDIX A

Molecular Cell
Article

# Sirt3-Mediated Deacetylation of Evolutionarily Conserved Lysine 122 Regulates MnSOD Activity in Response to Stress

Randa Tao,[1,8] Mitchell C. Coleman,[2,8] J. Daniel Pennington,[1] Ozkan Ozden,[4,5] Seong-Hoon Park,[4,5] Haiyan Jiang,[4,5] Hyun-Seok Kim,[4,5] Charles Robb Flynn,[6] Salisha Hill,[7] W. Hayes McDonald,[7] Alicia K. Olivier,[3] Douglas R. Spitz,[2] and David Gius[4,5,*]

[1]Howard Hughes Medical Institute and Molecular Radiation Oncology, Radiation Oncology Branch, Center for Cancer Research, NCI, NIH, Bethesda, MD 20892, USA
[2]Free Radical and Radiation Biology Program, Department of Radiation Oncology, Holden Comprehensive Cancer Center
[3]Department of Pathology, Carver College of Medicine
University of Iowa, Iowa City, IA 52242, USA
[4]Department of Radiation Oncology
[5]Department of Pediatrics
Vanderbilt University Medical Center, Nashville, TN 37232, USA
[6]Department of Surgery
[7]Mass Spectrometry Research Center
VanderbiltUniversity School of Medicine, Nashville, TN 37232, USA
[8]These authors contributed equally to this work
*Correspondence: david.gius@vanderbilt.edu
DOI 10.1016/j.molcel.2010.12.013

## SUMMARY

**Genetic deletion of the mitochondrial deacetylase sirtuin-3 (*Sirt3)* results in increased mitochondrial superoxide, a tumor-permissive environment, and mammary tumor development. MnSOD contains a nutrient- and ionizing radiation (IR)-dependent reversible acetyl-lysine that is hyperacetylated in Sirt3$^{-/-}$ livers at 3 months of age. Livers of Sirt3$^{-/-}$ mice exhibit decreased MnSOD activity, but not immunoreactive protein, relative to wild-type livers. Reintroduction of wild-type but not deacetylation null *Sirt3* into Sirt3$^{-/-}$ MEFs deacetylated lysine and restored MnSOD activity. Site-directed mutagenesis of MnSOD lysine 122 to an arginine, mimicking deacetylation (lenti-MnSOD$^{K122-R}$), increased MnSOD activity when expressed in MnSOD$^{-/-}$ MEFs, suggesting acetylation directly regulates function. Furthermore, infection of Sirt3$^{-/-}$ MEFs with lenti-MnSOD$^{K122-R}$ inhibited in vitro immortalization by an oncogene (*Ras*), inhibited IR-induced genomic instability, and decreased mitochondrial superoxide. Finally, IR was unable to induce MnSOD deacetylation or activity in Sirt3$^{-/-}$ livers, and these irradiated livers displayed significant IR-induced cell damage and microvacuolization in their hepatocytes.**

## INTRODUCTION

The incidence of human malignancies increases exponentially as a function of age, suggesting a mechanistic connection between aging and carcinogenesis (Finkel et al., 2009). Mammalian cells contain tumor suppressor (TS) genes, such as p53, and loss of TS function results in a damage-permissive phenotype (Sherr and McCormick, 2002) that is an early event in carcinogenesis. *Sirt3* is one of three sirtuins localized to mitochondria (Onyango et al., 2002; Schwer et al., 2002) and is the primary mitochondrial protein deacetylase (Lombard et al., 2007). Since cancer is a disease of aging and sirtuin genes appear to defend against cellular damage during aging, it has been proposed that *Sirt3* plays an anticarcinogenic role and functions as a TS protein (Kim et al., 2010).

Mitochondria are thought to be central to aging, and the correct function of mitochondria impedes the processes of aging and carcinogenesis by tightly regulating the reactive oxygen species generated as a byproduct of normal respiration activities (Singh, 2006). Mitochondrial abnormalities associated with altered oxidative metabolism are observed in tumor cells in vitro and in vivo and appear to contribute to a chronic condition of oxidative stress (Aykin-Burns et al., 2009). One intriguing finding from our previous work demonstrated that cells lacking *Sirt3* exhibited altered metabolism, including a significant increase in mitochondrial superoxide levels when exposed to IR. In this regard, manganese superoxide dismutase (MnSOD) is the primary mitochondrial scavenging enzyme that converts superoxide to hydrogen peroxide, which is subsequently converted to water by catalase (Spitz and Oberley, 1989). Since MnSOD enzymatically scavenges superoxide, which is increased in irradiated cells lacking *Sirt3* (Kim et al., 2010), it seemed logical to suggest that cells lacking *Sirt3* might have altered regulation of MnSOD.

*Sirt3* knockout mice develop invasive ductal mammary tumors, and Sirt3$^{-/-}$ mouse embryonic fibroblasts (MEFs) are easily immortalized and transformed by infection of a single oncogene (Kim et al., 2010). SIRT3 levels are also decreased in human breast malignancies as compared to normal breast

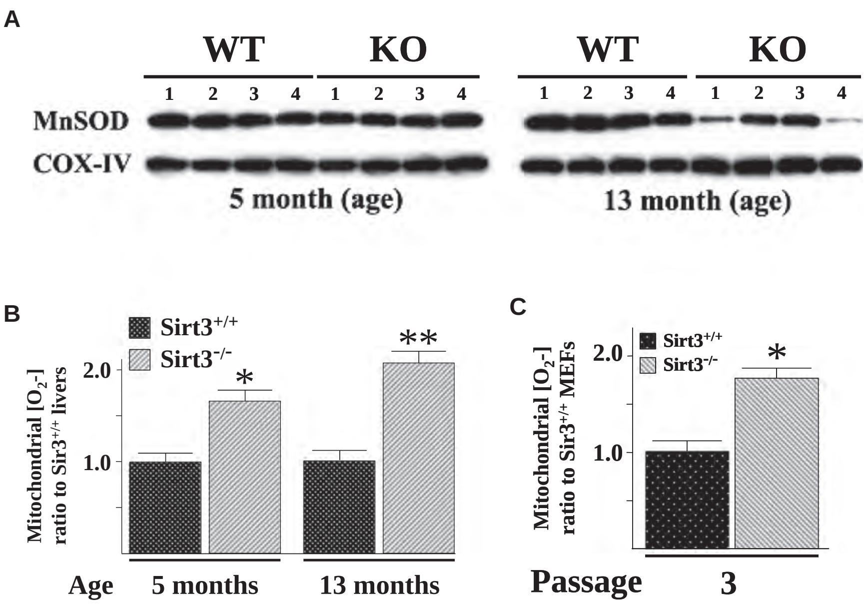


**Figure 1. MnSOD Protein and Superoxide Levels in *Sirt3* Wild-Type and Knockout Mouse Livers and MEFs**

(A) Livers from four Sirt3$^{+/+}$ and Sirt3$^{-/-}$ mice at 5 and 13 months of age were harvested, and mitochondrial extracts were made. Lysates were separated by SDS-PAGE, transferred onto nitrocellulose, and processed for immunoblotting with an anti-MnSOD antibody (Santa Cruz Biotechnology, Inc.; Santa Cruz, CA).

(B) Mitochondrial superoxide levels, assessed using MitoSOX oxidation, were determined in the *Sirt3* wild-type and knockout mouse livers at 5 and 13 months of age. Superoxide levels were measured as previously described.

(C) Mitochondrial superoxide levels were determined in wild-type and Sirt3$^{-/-}$ MEFs using MitoSOX oxidation at culture passage number three, as previously described (Kim et al., 2010). Results in this figure are the mean of at least three separate experiments. Error bars represent one standard deviation. * indicates $p < 0.05$ and ** indicates $p < 0.01$ by t test.

tissues, as well as in several other human malignancies (Kim et al., 2010), suggesting that *Sirt3* is a nuclear-encoded, mitochondria-localized TS. A biochemical examination of the in vitro transformed Sirt3$^{-/-}$ MEFs, as well as murine tumors, strongly suggested a potential connection between aberrant mitochondrial superoxide levels and a transformation/tumor-permissive cell phenotype. Specifically, a statistically significant decrease in mitochondrial MnSOD protein levels was observed at roughly 1 year that corresponded with the first incidence of murine mammary tumors (Kim et al., 2010). In addition, MnSOD transcription, via a mechanism involving decreased FOXO3a acetylation, was shown to decrease at roughly the same time that the first tumors were observed in the *Sirt3* knockout mice. Finally, viral overexpression of *MnSOD* prevented in vitro immortalization and transformation of the Sirt3$^{-/-}$ MEFs by an oncogene as well as preventing IR-induced increases in mitochondrial superoxide levels, further suggesting a role of MnSOD in the carcinogen-permissive phenotype observed in cells lacking *Sirt3*.

However, if increased mitochondrial superoxide levels play a role in carcinogenesis, it would seem logical that the decrease in MnSOD protein/activity would occur at a time point earlier than 1 year when it was observed that mammary tumors begin to appear in the Sirt3$^{-/-}$ animals. Thus, while the mechanistic connection between the Sirt3$^{-/-}$ mouse in vivo tumor-permissive phenotype and increased mitochondrial superoxide seemed strong, the definition of its role as an early event in carcinogenesis seemed incomplete. Thus, we proposed that Sirt3 might regulate mitochondrial superoxide levels via a second mechanism that occurs much earlier than 1 year and is independent of total mitochondrial MnSOD protein levels. If this is the case, then loss of *Sirt3* might also result in decreased MnSOD enzymatic activity by a posttranslational mechanism, presumably via protein/lysine acetylation, which might account for the aberrant increase in mitochondrial superoxide levels, while mitochondrial MnSOD protein levels remain unchanged.

## RESULTS

### The Kinetics of MnSOD Protein Levels Do Not Correlate with Mitochondrial Superoxide Levels

The *Sirt3* knockout mice develop tumors beginning at roughly 13 months, and these tumors, as well as the in vitro transformed MEFs, exhibit significant aberrant mitochondrial metabolism, including elevated superoxide levels (Kim et al., 2010). In this regard, a decrease in MnSOD transcription and mitochondrial MnSOD protein is also observed between 9 and 13 months in the *Sirt3* knockout mice, as compared to the wild-type mice (Figures 1A and S1A). Interestingly, mitochondrial superoxide levels are significantly increased in the livers of Sirt3$^{-/-}$ mice at 5 months of age (Figure 1B), when the levels of mitochondrial MnSOD protein in the *Sirt3* wild-type and knockout mice are identical (Figure 1A).

Mitochondrial superoxide levels were also increased in Sirt3$^{-/-}$ MEFs at passage three, as compared to the Sirt3$^{+/+}$ MEFs (Figure 1C), while MnSOD levels are identical (Figure S1B). No changes in catalase activity (Figure S1C) or catalase protein levels were observed between these mice (Figure S1D). Thus, these results suggested that Sirt3 may be involved in the regulation, at least in part, of mitochondrial superoxide levels via a mechanism involving a posttranslational modification of MnSOD. Since Sirt3 is the primary mitochondrial lysine deacetylase (Lombard et al., 2007), it seemed reasonable to propose that Sirt3 may regulate MnSOD enzymatic dismutase activity via changes in MnSOD lysine acetylation.

### MnSOD Contains a Reversible Acetyl-Lysine, and MnSOD Activity Is Decreased in Sirt3$^{-/-}$ Cells

Evidence that MnSOD contains reversibly acetylated lysine residues was obtained when wild-type mice at 3 months of age were fasted for 36 hr and liver extracts were harvested, immunoprecipitated (IPed) with an anti-MnSOD antibody, separated into

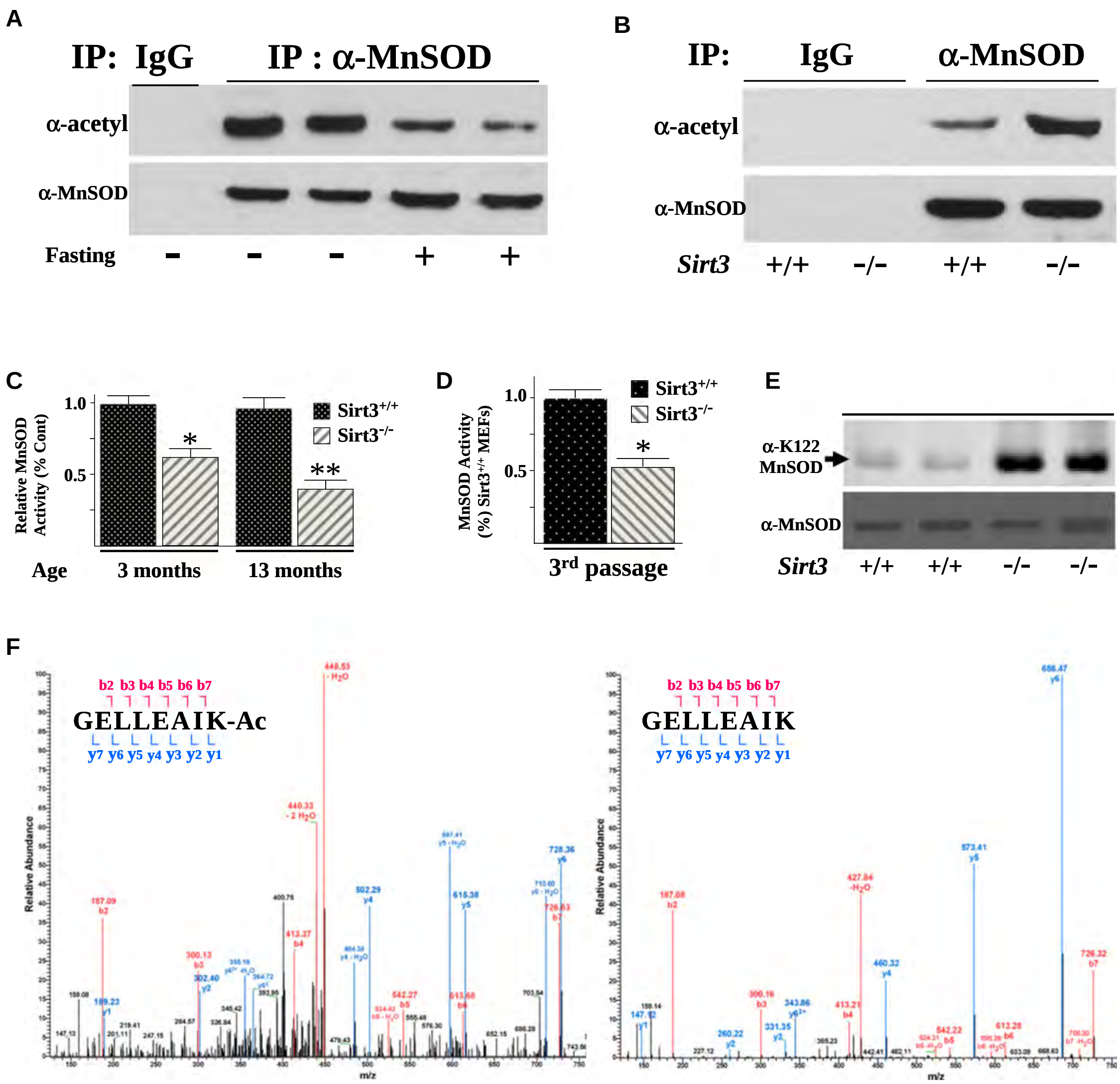


**Figure 2. MnSOD Contains a Reversibly Acetylated Lysine Residue, and Protein Deacetylation and SOD Activity Are Decreased in *Sirt3*$^{-/-}$ Cells**

(A) Isogenic, 3-month-old, age-matched Sirt3$^{+/+}$ mice were fasted for 36 hr, and livers were harvested, IPed with an anti-MnSOD antibody (Santa Cruz Biotechnology, Inc.), separated into two equal fractions, and subsequently immunoblotted with an anti-acetyl (Abcam; Cambridge, MA) or anti-MnSOD antibody.

(B) Livers from isogenic, 3-month-old, age-matched Sirt3$^{+/+}$ and Sirt3$^{-/-}$ mice were harvested, IPed with an anti-MnSOD antibody, separated into two equal fractions, and immunoblotted with either an anti-acetyl or anti-MnSOD antibody. Representative gels are shown for (A) and (B).

(C and D) MnSOD activity in *Sirt3* wild-type and knockout mouse livers at 3 and 13 months of age (C) and MEFs at passage number three (D). MnSOD activity was measured via a competitive inhibition assay as described (Spitz and Oberley, 1989). Activity data for MnSOD are presented as units of SOD activity per milligram of protein. Results in this figure are the mean of at least three separate experiments. Error bars represent one standard deviation. * indicates $p < 0.05$ and ** indicates $p < 0.01$ by t test.

(E) Livers from isogenic, 3-month-old, age-matched Sirt3$^{+/+}$ and Sirt3$^{-/-}$ mice were harvested and immunoblotted with an anti-K122-MnSOD antibody (Epitomics, Inc.; The Rabbit Monoclonal Antibody Company) recently produced for the laboratory.

(F) Tandem mass spectrometry from MnSOD demonstrates acetylated lysine 122 in vivo. Liver mitochondria from wild-type and Sirt3$^{-/-}$ mice were resolved by SDS-PAGE, followed by in-gel trypsin digestion, separation by nanoscale reverse-phase chromatography on reverse-phase columns, and analysis by OrbiTrap analyzer via an electrospray interface. See Supplemental Experimental Procedures for complete description. The spectrum represents the fragmentation of the m/z ratios of the MnSOD peptide sequences GELLEAIK (+2 charge = 436.7580 monoisotopic mass) and GELLEAIK-ac (+2 charge = 457.7633 monoisotopic mass).

equal fractions, resolved, and then immunoblotted with either an anti-acetyl (Figure 2A, upper panel) or anti-MnSOD antibody (lower panel). These experiments showed a decrease in acetylated MnSOD (Figure 2A, upper panel), while IPed MnSOD (lower panel) and total mitochondrial MnSOD protein levels were similar (Figure S2A). In addition, no difference in MnSOD protein acetylation (Figure S2B, upper panel), IPed MnSOD (lower panel), or total mitochondrial MnSOD protein (Figure S2C, lane 1 versus 3)

was observed in the livers of the Sirt3$^{-/-}$ mice at 3 months of age or when these mice were fasted, as compared to the fed mice.

Livers from isogenic, 3-month-old, age-matched wild-type and Sirt3$^{-/-}$ mice were also harvested, IPed with an anti-MnSOD antibody, separated into two equal fractions, resolved, and immunoblotted with either an anti-acetyl (Figure 2B, upper panel) or anti-MnSOD antibody (lower panel). These results showed that MnSOD acetylation was increased in the Sirt3$^{-/-}$ livers (Figure 2B), while no difference in total MnSOD (lower panel) or mitochondrial MnSOD (Figure S2C, lane 1 versus 2) was observed. Nicotinamide phosphoribosyl transferase (NAMPT) enhances cellular NAD levels and increases Sirt1 transcriptional activity in a dose-dependent manner (Revollo et al., 2004), so it seemed reasonable to determine if NAMPT levels are increased in our fasting mice and whether this induces Sirt3. Liver samples from the Sirt3$^{+/+}$ or Sirt3$^{-/-}$ mice, with and without fasting, were immunoblotted with an anti-NAMPT antibody, and no change in NAMPT levels was observed (Figure S2D).

These results support the hypothesis that MnSOD is a target for reversible lysine acetylation mediated by Sirt3. Thus, MnSOD enzymatic activity was determined in the *Sirt3* knockout livers as well as MEFs, and these results showed that MnSOD activity was significantly decreased in liver tissues from Sirt3$^{-/-}$ mice at age 3 months and Sirt3$^{-/-}$ MEFs at passage number three (Figures 2C and 2D). Total MnSOD levels were similar in the Sirt3$^{-/-}$ livers (Figure S2C), as compared to the Sirt3$^{+/+}$ liver controls. In addition, immunoblotting with an anti-acetyl-lysine 122 MnSOD (Epitomics, Inc.; Burlingame, CA) antibody (Figure 2E) as well as mass spectrometry (Figures 2F and S2E) demonstrated an increase in the acetylation of MnSOD lysine 122 in the liver samples from Sirt3$^{-/-}$ mice at 3 months of age, as compared to age-matched wild-type mice.

### Re-Expression of Sirt3 Deacetylates MnSOD and Restores Superoxide Dismutase Activity

To determine if Sirt3 directly deacetylates MnSOD and alters enzymatic activity, two lentiviruses were constructed that expressed either the wild-type (lenti-Sirt3-WT) or a deacetylation null mutant (lenti-Sirt3-DN) *Sirt3* gene (a gift from Toren Finkel, NHLBI) in which amino acid 248 was changed from histidine to tyrosine (Ahn et al., 2008). These viruses were used to infect Sirt3$^{-/-}$ MEFs. Infection with lenti-Sirt3-WT, but not lenti-Sirt3-DN, decreased MnSOD acetylation (Figure 3A, lane 3 versus 4, upper panel), while infection of these lentiviruses expressed similar levels of exogenous Sirt3 wild-type and mutant protein (Figure 3B). Lenti-Sirt3-WT, but not lenti-Sirt3-DN, also increased MnSOD activity (Figure 3C) and decreased mitochondrial superoxide levels (Figure 3D), while the levels of IPed MnSOD were similar in the control and infected Sirt3$^{-/-}$ MEFs (Figure 3A, lower panel). These results support the hypothesis that Sirt3 directly deacetylates MnSOD, leading to increased dismutase activity.

To more rigorously determine if MnSOD is a legitimate Sirt3 deacetylation target, an in vitro SIRT3 deacetylation assay was performed. IPed, purified MnSOD was mixed without or with purified SIRT3 with 1 mM NAD+, separated, and immunoblotted with an anti-acetyl, anti-SIRT3, or anti-MnSOD antibody. These experiments showed that Sirt3 decreased MnSOD acetylation (Figure 3E, lane 1 versus 2), and removal of NAD+ (lane 3) or the addition of nicotinamide (lane 4) prevented the deacetylation of MnSOD, suggesting that SIRT3 directly deacetylates MnSOD in vitro. Finally, these experiments were repeated using a specific anti-MnSOD lysine 122 antibody, showing that lysine 122 is deacetylated in vitro by SIRT3 (Figure 3F).

### SIRT3 Interacts with MnSOD

Since Sirt3 deacetylates MnSOD, it seemed reasonable to propose that these two proteins might physically interact. As such, HCT116 cells were used that have been genetically altered to overexpress a myc-tagged wild-type *Sirt3* gene (HCT116$^{myc\text{-}SIRT3WT}$ cells). These cells were lysed and IPed with either an anti-MnSOD or anti-myc antibody. The samples were divided into three equal fractions, separated, and subsequently immunoblotted with an anti-myc (Figure 4A, upper panel), anti-SIRT3 (middle panel), or anti-MnSOD (lower panel) antibody. Reverse IPs were also done with anti-SIRT3 (upper panel) or anti-MnSOD (lower panel) antibodies, demonstrating that endogenous SIRT3 and MnSOD appear to form a protein interaction (Figure 4B). These results suggest a potential physical interaction between Sirt3 and MnSOD. In addition, the HCT116 cells were grown on slides that were subsequently stained with anti-MnSOD, anti-SIRT3, DAPI, and MitoTracker (Figure 4C). The immunohistochemical experiments using the anti-MnSOD and anti-SIRT3 staining were also subsequently merged (Figure 4D) and suggest that the SIRT3 and MnSOD proteins colocalized to each other and to the mitochondria. However, these results also show areas where these proteins do not colocalize, as might be expected, since most enzyme/substrate interactions are highly dynamic and may be very transient.

### MnSOD Contains an Evolutionarily Conserved Lysine that Directly Regulates Activity

MnSOD is an old, evolutionarily conserved protein present in almost all species, and as such, if a specific MnSOD lysine is an acetylation target in the regulation of enzymatic activity, then it seems reasonable that this lysine would be conserved in multiple mammalian and nonmammalian species. A BLAST search demonstrated a conserved 13 amino acid motif (GELLEAIK*RDFGS) at amino acid 122 that is conserved in human, murine, bovine, etc. (Figure 5A) as well as at position 121 in *C. elegans*. Interestingly, the MnSOD protein in four primates (Rhesus macaque, *Callithrix jacchus*, common gibbon, and chimpanzee) contains an identical 13 amino acid consensus motif; however, it is located 24 amino acids upstream of the human sequence, and the conserved lysine is present at position 98. The consensus motif is also shifted in multiple nonmammalian species, including *Xenopus tropicalis* and zebrafish, to a slightly different protein location (lysine 124 versus 122) (Figure 5A). Thus, it seems reasonable to propose that this conserved 13 amino acid motif, which has remained roughly intact in multiple species, while in some cases being moved to slightly different locations within the MnSOD protein, suggests that this lysine may be of potentially significant

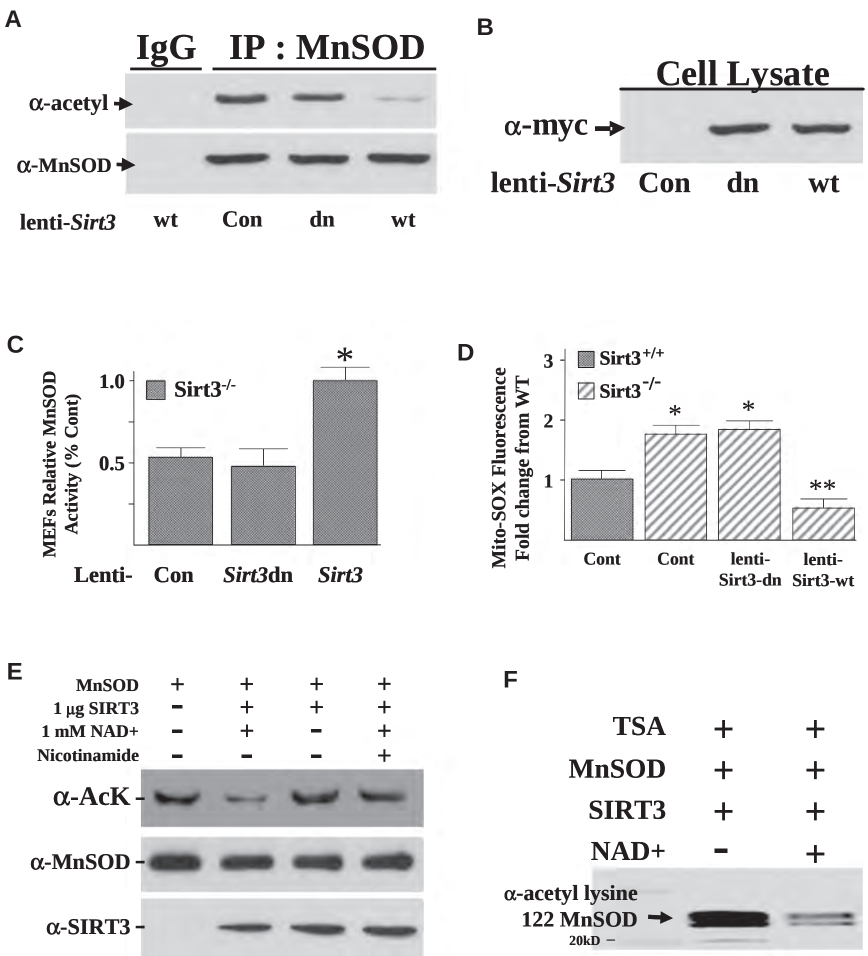


**Figure 3. Re-expression of *Sirt3* in Sirt3$^{-/-}$ MEFs Deacetylates MnSOD and Restores SOD Activity**

(A) Expression of wild-type but not a deacetylation null mutant of *Sirt3* deacetylates MnSOD. Third-passage Sirt3$^{-/-}$ MEFs were transfected with a control lentivirus, virus expressing a wild-type *Sirt3* (lenti-Sirt3-WT), or deacetylation null gene (lenti-Sirt3-DN). Forty hours after infection, Sirt3$^{-/-}$ MEFs were harvested and mitochondrial extracts were IPed with an anti-MnSOD antibody, separated into two equal fractions, and immunoblotted with either an anti-acetyl or an anti-MnSOD antibody.

(B) The mitochondrial samples above were also separated and immunoblotted with an anti-myc antibody (Santa Cruz Biotechnology, Inc.).

(C) Expression of wild-type but not a deacetylation null mutant *Sirt3* gene increases mitochondrial MnSOD activity. Sirt3$^{-/-}$MEFs were infected with lenti-Sirt3-WT or lenti-Sirt3-DN and assayed for MnSOD activity in 50 mM potassium phosphate buffer. MnSOD activity was determined using an indirect competitive inhibition assay as described in the Experimental Procedures (Spitz and Oberley, 1989). Results in this figure are the mean of at least three separate experiments, and error bars represent one standard deviation. * indicates $p < 0.05$ by t test.

(D) Expression of wild-type but not a deacetylation null mutant *Sirt3* gene decreases mitochondrial superoxide levels. Mitochondrial superoxide levels were determined after infection as described above by the addition of MitoSOX (1 μM) to the cells, followed by incubation for an additional 10 min before being trypsinized and resuspended. Fluorescence was measured via flow cytometry.

(E) SIRT3 directly deacetylates MnSOD in vitro. IPed purified MnSOD was mixed without (lane 1) or with (lanes 2–4) recombinant human SIRT3 with NAD+ (lanes 2 and 4) or nicotinamide (lane 4) and incubated. Samples were separated, followed by immunoblotting with an anti-acetyl antibody. Immunoblotting for SIRT3 and MnSOD were done as internal controls.

(F) IPed, purified MnSOD was mixed in vitro with recombinant human SIRT3 without and with NAD+, separated, and immunoblotted with an anti-K122-MnSOD antibody (Epitomics, Inc.; The Rabbit Monoclonal Antibody Company).

biological and physiological importance. Finally, an examination of the published three-dimensional structure of the MnSOD protein (PDB accession number 1PL4), which is a functional tetramer in vivo, shows that lysine 122 is on the outside of the protein complex in an ideal position to interact with other proteins, such as Sirt3 (Figure S3A).

It has previously been shown that substitution of a lysine with a glutamine mimics an acetylated amino acid state, while substitution with an arginine mimics deacetylation (Li et al., 2007; Schwer et al., 2006). Thus, mutating lysine 122 to arginine would be predicted to mimic a deacetylated lysine, while substitution with a glutamine would be expected to mimic an acetylated lysine (Figure 5B). As such, lenti-MnSOD$^{K122}$ (wild-type), lenti-MnSOD$^{K122\text{-}R}$, lenti-MnSOD$^{K122\text{-}Q}$, and a control virus were used to infect MEFs that have *MnSOD* genetically deleted (MnSOD$^{-/-}$ MEFs) (a kind gift from Prahbat Goswami, University of Iowa). The MnSOD$^{-/-}$ MEFs have previously been shown to have significantly increased mitochondrial superoxide levels as compared to wild-type MEFs (Du et al., 2009).

Infection of the MnSOD$^{-/-}$ MEFs at passage 20 with the various MnSOD lentiviruses resulted in similar levels of cellular exogenous protein (Figure S3B). In addition, infection with the K122-R mutant (lenti-MnSOD$^{K122\text{-}R}$) resulted in increased MnSOD activity (Figure 5C) and decreased mitochondrial superoxide levels (Figure 5D), while the K122-Q mutant displayed the opposite results, when compared to cells infected with the wild-type *MnSOD* lentivirus (Figures 5C and 5D). To make a stronger mechanistic connection between Sirt3 and MnSOD lysine 122, MnSOD$^{-/-}$ MEFs were infected with the wild-type or mutant *MnSOD* viruses and lenti-Sirt3-WT or lenti-Sirt3-DN. These experiments showed that infection of wild-type *Sirt3*, but not the deacetylation null gene, increased MnSOD activity in the MnSOD$^{-/-}$ MEFs expressing wild-type *MnSOD* (Figure 5E, bar 1 versus 2). In contrast, infection with lenti-Sirt3-WT or lenti-Sirt3-DN did not alter the activity of MnSOD in MnSOD$^{-/-}$ MEFs coinfected with either lenti-MnSOD$^{K122\text{-}R}$ or lenti-MnSOD$^{K122\text{-}Q}$. Finally, infection of the MnSOD$^{-/-}$ MEFs with the wild-type- and mutant-MnSOD-expressing lentiviruses did

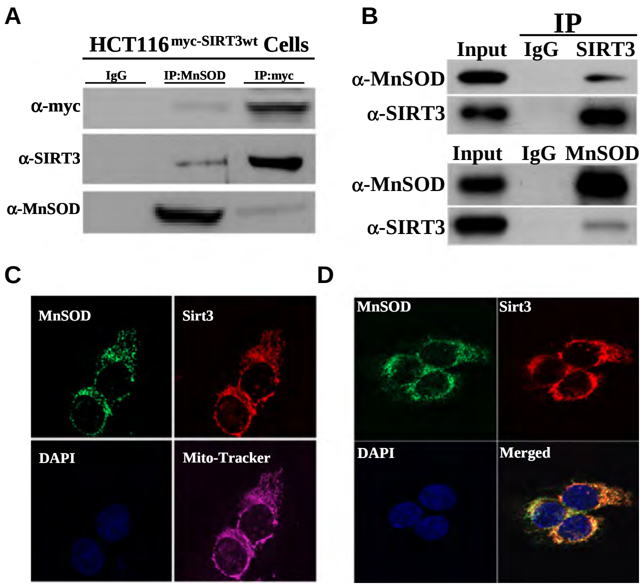


**Figure 4. Sirt3 Appears to Interact with MnSOD in the Mitochondria**

(A–D) HCT116$^{myc\text{-}Sirt3}$ cells that are genetically altered to overexpress a myc-tagged wild-type *Sirt3* gene (A) and HCT116 cells (B) were harvested and IPed with an anti-SIRT3 or an anti-MnSOD antibody and separated into equal fractions. The samples were resolved and immunoblotted with either an anti-SIRT3 or anti-MnSOD antibody. HCT116 cells were stained with an anti-SIRT3 and anti-MnSOD antibody as well as with DAPI and MitoTracker (C) or with an anti-SIRT3 and anti-MnSOD antibody and DAPI (D), and the images were merged. Representative gels or micrographs for this figure are shown. Results for the panels in this figure are the mean of at least three separate experiments.

not alter cellular $H_2O_2$ levels (Figure S3C). These results suggest that acetylation of MnSOD lysine 122 directly regulates MnSOD enzymatic dismutase activity.

It has previously been shown that exposure to ionizing radiation (IR) decreases contact inhibition, as measured by increased foci formation, in *MnSOD* knockout MEFs (Du et al., 2009). Infection of the MnSOD$^{K122\text{-}R}$ mutant lentivirus into the MnSOD$^{-/-}$ MEFs (Figure S3B) demonstrated a significant decrease in IR-induced foci formation, while the foci number in the MEFs infected with the MnSOD$^{K122\text{-}Q}$ mutant was identical to the control virus (Figure 5F). Consistent with the idea that MnSOD activity is regulated, at least in part, by acetylation of lysine 122, infection of the MnSOD$^{-/-}$ MEFs with lenti-MnSOD$^{K122\text{-}R}$ also decreased IR-induced mitochondrial superoxide levels (as determined by MitoSOX oxidation) (Figure S3D, lane 5 versus lane 2). In contrast, infection with lenti-MnSOD$^{K122\text{-}Q}$ resulted in MitoSOX oxidation similar to the control cells (lane 4 versus lane 2). These experiments were repeated after coinfection of the MnSOD$^{-/-}$ MEFs with either lenti-Sirt3-WT or lenti-Sirt3-DN. Overexpression of *Sirt3* decreased the number of foci in MnSOD$^{-/-}$ MEFs coinfected with lenti-MnSOD$^{K122}$ (Figure 5G, bar 2 versus 3) to the about same number of foci observed in MEFs infected with lenti-Sirt3-WT or lenti-Sirt3-DN and lenti-MnSOD$^{K122\text{-}R}$ (bar 3 versus 4 and 5). In contrast, infection of lenti-Sirt3-WT or lenti-Sirt3-DN did not change the number of foci in MEFs infected with lenti-MnSOD$^{K122\text{-}R}$ or lenti-MnSOD$^{K122\text{-}Q}$.

Antimycin A, a mitochondrial electron transport chain (Complex III) inhibitor, represents a metabolic stress that is shown to increase superoxide levels (Aykin-Burns et al., 2009). Exposure of MnSOD$^{-/-}$ MEFs to Antimycin A significantly increased superoxide levels (Figure 5H, lane 1), as has been previously shown (Kim et al., 2010). Infection of the MnSOD$^{-/-}$ MEFs with lenti-MnSOD$^{K122\text{-}R}$ (lane 4) and, to a lesser extent, lenti-MnSOD$^{K122}$ (lane 2) prior to exposure to Antimycin A prevented the increase in mitochondrial superoxide levels. In contrast, infection with lenti-MnSOD$^{K122\text{-}Q}$ had no effect on Antimycin A-induced mitochondrial superoxide levels (lane 3) as compared to the control virus-infected cells (lane 1). These results suggest that acetylation of MnSOD regulates MnSOD activity following stress, and this in turn could significantly impact oxidative stress-induced superoxide levels and foci formation, a surrogate marker of in vitro transformation frequency.

## MnSOD$^{K122\text{-}R}$ Reverses IR-Induced Increases in Superoxide and Genomic Instability in Sirt3$^{-/-}$ MEFs

The tumor-permissive environment seen in Sirt3$^{-/-}$ animals correlates with the observation that Sirt3$^{-/-}$ MEFs can be immortalized by overexpression of a single oncogene (*Ras* or *Myc*). In addition, exposure of Sirt3$^{-/-}$ MEFs to IR increases mitochondrial superoxide levels and genomic instability (Kim et al., 2010). When Sirt3$^{-/-}$ MEFs were infected with lenti-MnSOD$^{K122\text{-}R}$, but not with lenti-Sirt3$^{K122\text{-}Q}$, immortalization induced by lentivirus-mediated overexpression of *Ras* or *Myc* was inhibited (Table S1). Consistent with this effect being mediated by the activity of MnSOD, infection with lenti-MnSOD$^{K122\text{-}R}$, but not lenti-MnSOD$^{K122\text{-}Q}$, prevented IR-induced increases in steady-state levels of mitochondrial superoxide, as determined by MitoSOX oxidation (Figure 6A), as well as genomic instability, as indicated by IR-induced changes in ploidy (Figure 6B). Western immunoblotting confirmed similar levels of expressed exogenous wild-type and mutant MnSOD protein in the infected Sirt3$^{-/-}$ MEFs (Figure S4A). No change in cellular $H_2O_2$ levels was observed in the Sirt3$^{-/-}$ MEFs infected with these MnSOD-expressing lentiviruses (Figure S4B).

We have previously shown that Sirt3$^{-/-}$ MEFs immortalized and transformed by infection with *Ras* (referred to as Sirt3$^{-/-}$ Ras cells) exhibit increased growth in soft agar, foci formation, and mitochondrial superoxide levels (Kim et al., 2010). Consistent with the results above, infection with lenti-MnSOD$^{K122\text{-}R}$ and, to a lesser extent, lenti-MnSOD$^{K122}$, but not lentiMnSOD$^{K122\text{-}Q}$, resulted in decreased growth in soft agar (Figure 6C), decreased foci formation (Figure 6D), and decreased mitochondrial superoxide levels (Figure S4C) in the transformed Sirt3$^{-/-}$ Ras cells. Western immunoblotting confirmed similar levels of expressed exogenous wild-type and mutant MnSOD protein in the infected Sirt3$^{-/-}$ Ras cells (Figure S4D).

## In Vivo Liver MnSOD Activity, MnSOD Acetylation, and Radiosensitivity in the Sirt3$^{-/-}$ Mice

The results above suggest that acetylation of MnSOD may alter in vivo responses to radiation exposure. In order to test this hypothesis, Sirt3$^{+/+}$ and Sirt3$^{-/-}$ mice were exposed to 2 Gy of whole-body IR on 2 consecutive days, and liver mitochondria

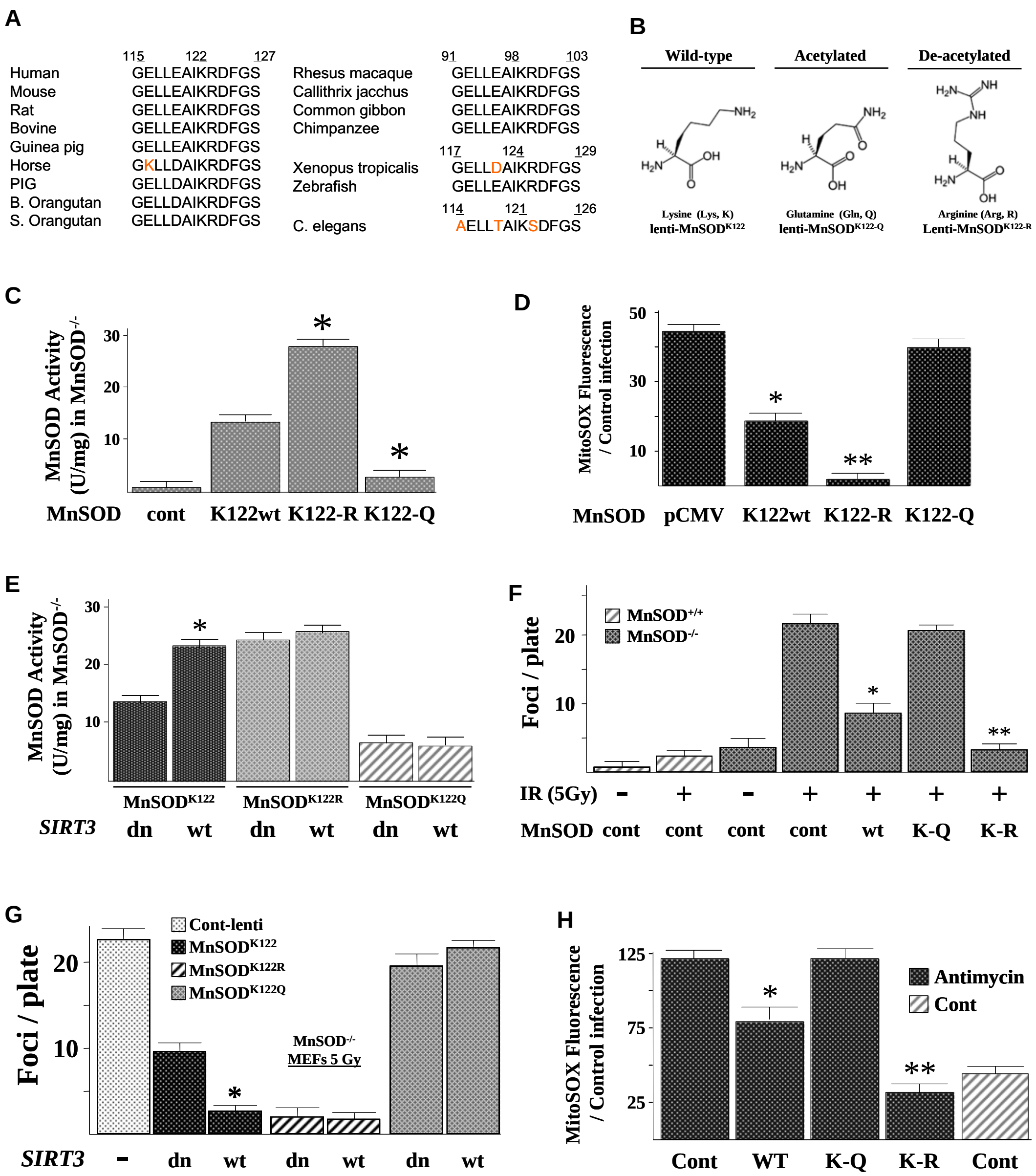


**Figure 5. MnSOD Contains an Evolutionarily Conserved Lysine Residue that Regulates SOD Activity**

(A) Multiple species contain a potentially reversibly acetylated lysine residue. The MnSOD protein sequence from multiple species was BLASTed based on the reversibly acetylated lysine located at amino acid 122 in mice. A 13 amino acid motif (GELLEAIK*RDFGS) was identified that is present in multiple species.

(B) Substitution of a lysine with a glutamine (Q) mimics an acetylated amino acid state, while substitution with an arginine (R) mimics a deacetylated amino acid state (Li et al., 2007; Schwer et al., 2006).

(C) MnSOD lysine acetylation status directs dismutase activity. MnSOD$^{-/-}$ MEFs were infected with a control lentivirus or lenti-MnSOD$^{WT}$, lenti-MnSOD$^{K122-Q}$, or lenti-MnSOD$^{K122-R}$. Twenty-four hours after infection, MnSOD activity was determined as outlined above (Figure 3 legend).

(D) Mitochondrial superoxide levels are decreased in cells overexpressing a *MnSOD*$^{K122-R}$ mutant gene. MnSOD$^{-/-}$ MEFs were infected with the various MnSOD lentiviruses, and superoxide levels were determined as described above.

(E) MnSOD$^{-/-}$ MEFs were infected with the wild-type and mutant MnSOD lentiviruses with either lenti-Sirt3-WT or lenti-Sirt3-DN and assayed for MnSOD activity.

(F) The MnSOD$^{K122-R}$ mutant decreases IR-induced contact inhibition in the *MnSOD* knockout MEFs. MnSOD$^{-/-}$ MEFs were infected with the MnSOD lentiviruses, plated at $1 \times 10^6$/100 mm dish, and exposed to 5 Gy IR, followed by long-term culture (28 days), staining with crystal violet, and measurement of foci formation.

(G) MnSOD$^{-/-}$ MEFs were infected with the wild-type and mutant MnSOD lentiviruses with either lenti-Sirt3-WT or lenti-Sirt3-DN and measured for foci formation as above.

(H) Mitochondrial superoxide levels in MnSOD$^{-/-}$ MEFs exposed to Antimcyin A are decreased by infection with lenti-MnSOD$^{K122-R}$; Sirt3$^{-/-}$ MEFs were treated with 5 μM of Antimycin A for 3 hr, and mitochondrial superoxide levels were determined as described above. Results for all the panels in this figure are the mean of at least three separate experiments, and error bars represent one standard deviation. * indicates $p < 0.05$ and ** indicates $p < 0.01$ by t test.

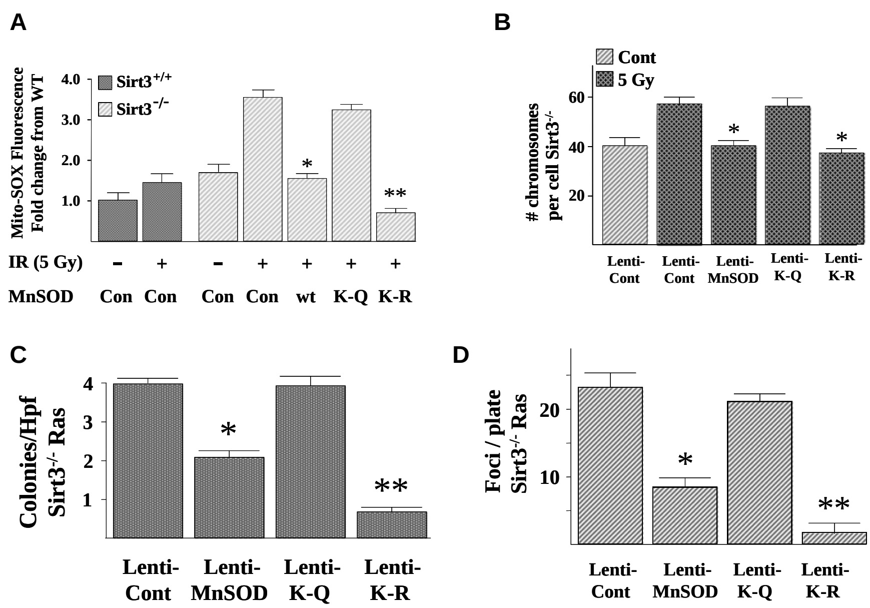


**Figure 6. The MnSOD$^{K122-R}$ Mutant Reverses the Increase in IR-Induced Superoxide Levels and Genomic Instability in the Primary or *Ras*-Transformed Sirt3$^{-/-}$ MEFs**

(A) Wild-type and Sirt3$^{-/-}$ MEFs were exposed to 5 Gy IR, and mitochondrial superoxide levels were determined by the addition of MitoSOX (1 μM) to the cells.

(B) The MnSOD$^{K122-R}$ mutant prevents aneuploidy in *Sirt3* knockout MEFs exposed to IR. Sirt3$^{-/-}$ MEFs were infected with a control lentivirus or lenti-MnSOD$^{WT}$, lenti-MnSOD$^{K122-Q}$, or lenti-MnSOD$^{K122-R}$ and exposed to 5 Gy IR. Whole-mount chromosomes were counted in a blinded fashion. Bars show the mean chromosome number per cell from 100 separate counts.

(C and D) The MnSOD$^{K122-R}$ mutant reverses the transformed phenotype in Sirt3$^{-/-}$ MEFs infected with *Ras*. The transformed Sirt3$^{-/-}$ Ras cells were infected with the *MnSOD* lentiviruses outlined above, and growth in soft agar (C) and spontaneous foci formation (D) were determined as described above. For growth in soft agar, Sirt3$^{-/-}$ Myc/Ras cells were seeded, and colonies were stained with methylene blue after 12 days and counted. Results for all panels in this figure are the mean of at least three separate experiments, and error bars represent one standard deviation. * indicates $p < 0.05$ and ** indicates $p < 0.01$ by t test.

were harvested 24 hr following the second exposure to radiation. These experiments showed a significant IR-induced increase in liver MnSOD activity (Figure 7A) as well as a decrease in lysine 122 MnSOD acetylation (Figures 7B and S5A) in liver mitochondria of Sirt3$^{+/+}$ animals. In contrast, no change in MnSOD activity or lysine acetylation was observed in the liver mitochondria isolated from IR-exposed Sirt3$^{-/-}$ mice (Figures 7A and 7B). Total mitochondrial MnSOD immunoreactive protein levels in the irradiated and control groups were identical (Figure S5B). These results support the hypothesis that Sirt3$^{-/-}$ liver mitochondria lack the capacity to induce MnSOD activity in response to IR because of an inability to deacetylate MnSOD.

If *Sirt3* knockout mice are unable to induce MnSOD activity in response to IR, then it seems reasonable to hypothesize that this loss of the ability to induce a potentially protective response could result in enhanced IR-induced liver damage. As such, livers from Sirt3$^{+/+}$ and Sirt3$^{-/-}$ mice exposed to 2 Gy of radiation on 2 consecutive days were harvested at 24 hr. Histological examination of the irradiated *Sirt3* knockout mice exposed to IR demonstrated marked periportal to midzonal hepatocellular swelling, with dilation of the cytoplasm by clear space, as well as poorly defined vacuoles (Figure 7C). Hepatocellular swelling in the irradiated Sirt3$^{-/-}$ mice livers was significantly more severe as compared to the irradiated Sirt3$^{+/+}$ or the control Sirt3$^{+/+}$ and Sirt3$^{-/-}$ mice (Figure 7D). Liver sections processed with osmium tetroxide (stains lipid in fixed tissue) demonstrated minimal to no lipid vacuoles in the swollen hepatocytes of Sirt3$^{-/-}$ mice (Figure S5C, top panels). In addition, liver sections from irradiated Sirt3$^{-/-}$ mice stained with periodic acid-Schiff (PAS) (stains glycogen) demonstrated mild to moderate cytoplasmic glycogen with poorly defined clear spaces (Figure S5C, bottom panels). This histology displays some characteristics similar, at least in part, to those observed in microvesicular steatosis that is associated with mitochondrial dysfunction (Araya et al., 2006). Interestingly, the risk factors for steatosis include diabetes mellitus, protein malnutrition, and obesity (Araya et al., 2006), all of which have been associated with abnormalities of sirtuin function (Finkel et al., 2009).

When the livers from these mice were stained with markers for apoptosis, the *Sirt3* knockout mice exposed to irradiation demonstrated significantly more apoptosis then the irradiated wild-type mice, as well as the control Sirt3$^{+/+}$ and Sirt3$^{-/-}$ mice, as measured by TUNEL assay (Figure 7E) or staining with antibodies to cleaved caspase-3 (Figure S5D). This result is consistent with the increased cellular damage and the membrane-bound vacuoles observed in the H&E staining (Tolman and Dalpiaz, 2007).

Control and irradiated Sirt3$^{+/+}$ and Sirt3$^{-/-}$ livers were also stained with an anti-nitrotyrosine antibody as a marker for increased protein damage caused by intracellular reactive oxygen/nitrogen species, specifically $ONOO^-$, a reaction product of nitric oxide and superoxide (Kim et al., 2010). *Sirt3* knockout mouse liver cells exhibited increased anti-nitrotyrosine staining (Figure 7F), as compared the Sirt3$^{+/+}$ samples (quantified in Figure S5E, $p < 0.05$), and there was a very significant difference between the Sirt3$^{+/+}$ and Sirt3$^{-/-}$ irradiated liver samples (bar 2 versus 4, $p < 0.01$). These results suggest an oxidative stress-permissive phenotype in liver cells lacking *Sirt3* that becomes more evident upon IR-induced oxidative stress.

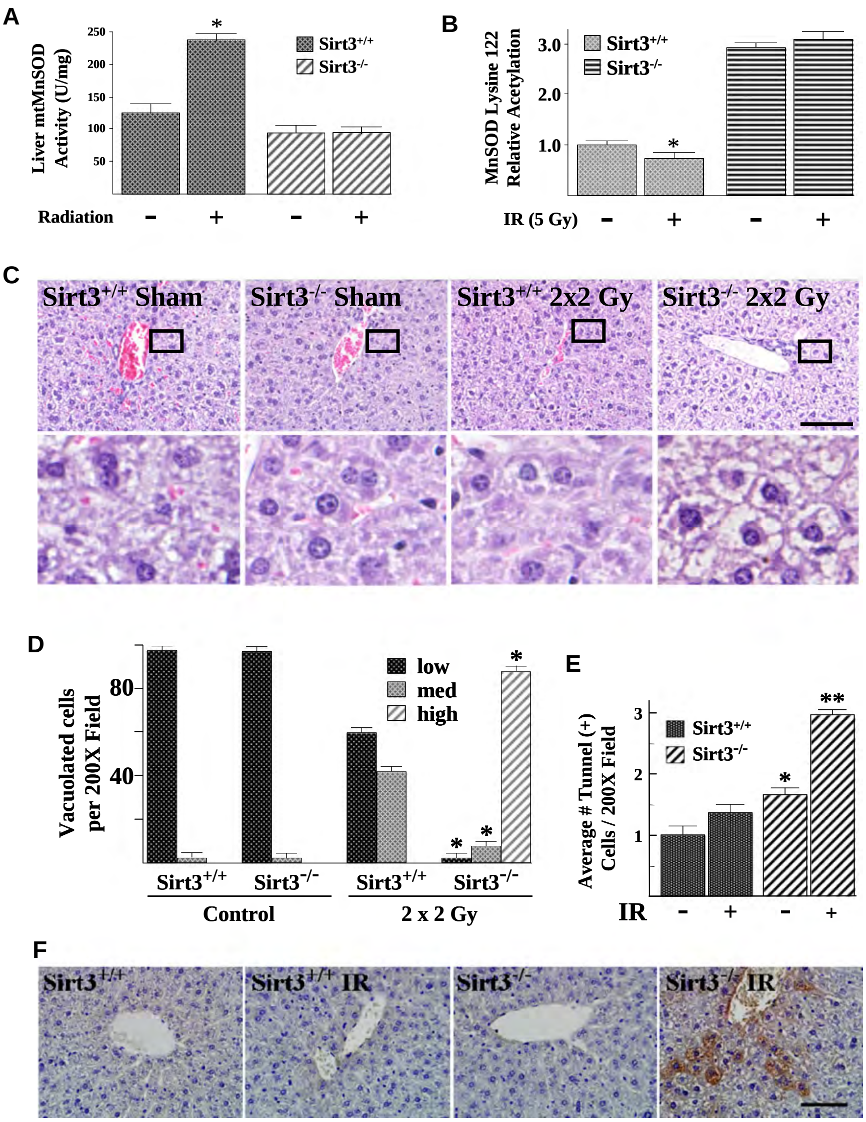


**Figure 7. MnSOD Dismutase Activity, Lysine 122 Acetylation, and the Cellular Metabolic and Damage/Cytotoxic Response Are Altered by IR**

(A) $Sirt3^{+/+}$ and $Sirt3^{-/-}$ mice at 12 weeks were exposed to ionizing radiation (2 Gy on 2 consecutive days) or sham treated every 24 hr. Livers were harvested 24 hr postexposure and mitochondria were isolated. MnSOD activity in MEFs was measured via a competitive inhibition assay as described (Spitz and Oberley, 1989). Activity data for MnSOD are presented as units of SOD activity per milligram of protein.

(B) Mitochondrial extracts from above were analyzed for acetylation of MnSOD lysine 122 via mass spectrometry. Results are presented as fold change from the untreated, wild-type mouse livers.

(C) $Sirt3^{-/-}$ mouse livers exposed to IR exhibit marked cytoplasmic vacuolation of periportal to midzonal hepatocytes. The wild-type and $Sirt3^{-/-}$ livers without and with exposure to IR were H&E stained and scored for degree of hepatocellular cytoplasmic vacuolation—low, medium, and high—by a pathologist. Representative micrographs are shown. Scale bar = 80 $\mu$m.

(D) Quantification of the H&E for liver cells. Liver cells were scored as follows: low, no detectable cytoplasmic vacuolation; med, moderate dilation of the cytoplasm by clear space primarily affecting periportal hepatocytes; high, severe dilation of the cytoplasm by clear space and poorly defined clear vacuoles primarily affecting periportal to midzonal hepatocytes.

(E) Apoptosis was determined in the $Sirt3^{+/+}$ and $Sirt3^{-/-}$ livers exposed to IR. Apoptotic cells were identified in liver sections by TUNEL assay. Sections were scored by a pathologist blinded to the groupings. TUNEL-positive cells were counted in ten randomly selected 200× fields per liver section. Results in this figure are reported as the average number of positive cells per field. Data are presented as the average ± SD. * indicates $p < 0.05$ and ** indicates $p < 0.01$.

(F) Irradiated $Sirt3^{-/-}$ mouse liver cells exhibit increased anti-nitrotyrosine IHC staining. Liver tissues from wild-type and $Sirt3^{-/-}$ mice were stained with an anti-nitrotyrosine antibody (StressMarq Biosciences Inc.; Victoria, British Columbia, Canada). A representative micrograph is shown. Scale bar = 80 $\mu$m. See Figure S5E for quantification.

## DISCUSSION

We have previously demonstrated that Sirt3 is an in vitro and in vivo TS protein and that the knockout mice spontaneously develop well-differentiated, ER/PR-positive mammary tumors (Kim et al., 2010). In addition, SIRT3 protein levels are decreased in human breast cancers as well as in several other human malignancies. These results identified Sirt3 as a genomically expressed, mitochondrially localized TS, and cells lacking *Sirt3* may be a useful in vivo model to investigate the subtype of breast cancer observed in postmenopausal or older women.

One intriguing finding from our previous work was that cells lacking *Sirt3* exhibited altered mitochondrial metabolism, as exhibited by increased mitochondrial superoxide levels during stress. These results suggested a connection between the increase in superoxide and the *Sirt3* knockout mouse tumor-permissive phenotype. However, one outstanding question from this previous work involved the observation that MnSOD transcription, via FOXO3a acetylation, was not decreased until 1 year—roughly the same time that the mammary tumors were first observed in the *Sirt3* knockout mice. Thus, while the connection between the MnSOD and increased mitochondrial superoxide seemed strong, the mechanism appeared to be more complex than a decrease in FOXO3a-driven MnSOD transcription (Kim et al., 2010). Thus, additional wild-type and *Sirt3* knockout mouse colonies were established and followed to more rigorously investigate the connection between superoxide levels and MnSOD as an early carcinogenic event in the *Sirt3*

knockout mouse tumor-permissive phenotype. These results suggested a second potential mechanism for Sirt3 regulation of MnSOD activity that is independent of *MnSOD* expression and potentially related to posttranslational modification involving acetylation.

The connection between mitochondrial damage and carcinogenesis is well established; however, the mechanism appears to be complex (Singh, 2006; Wallace, 2005). In addition, it has been suggested that the mitochondria play a role in radiation-induced malignancies, but the specific molecular steps are not completely understood (Du et al., 2009). One proposed mechanism involves the accumulation of mitochondrial ROS; these reactive molecules can damage numerous cellular processes, creating an environment permissive for genomic instability as well as carcinogenesis (Oberley, 2005). Since Sirt3 is the primary mitochondrial deacetylase, we hypothesized that the increase in mitochondrial superoxide levels in *Sirt3* knockout mice and MEFs exposed to stress may be due to aberrant acetylation and regulation of MnSOD enzymatic activity.

Our results identify MnSOD amino acid 122 as a reversibly acetylated lysine residue that is deacetylated by 36 hr of fasting, and MnSOD acetylation is significantly increased and enzymatic activity decreased in Sirt3$^{-/-}$ cells. In addition, MnSOD is deacetylated by Sirt3, suggesting that mitochondrial acetylation plays a role, at least in part, in regulation of MnSOD function. This idea was validated by a pair of MnSOD mutants that demonstrated increased activity when lysine 122 was changed to arginine (to mimic the deacetylated state). MnSOD$^{K122\text{-}R}$ also prevented IR-induced foci formation in MnSOD$^{-/-}$ cells and immortalization of Sirt3$^{-/-}$ MEFs by a single oncogene, as well as IR-induced genomic instability and loss of contact inhibition.

Finally, we show in vivo that IR induces deacetylation of MnSOD and increased enzymatic activity in irradiated wild-type mouse liver mitochondria, but not in liver mitochondria of the *Sirt3* knockout mice. While it is tempting to suggest this IR-induced damage-permissive phenotype is primarily due to changes in MnSOD activity, it seems likely that other Sirt3 deacetylation targets may also play a role in this histological and biochemical phenotype. This idea would fit the well-established data that IR-induced damage and cytotoxicity is a multifactorial process involving several cellular proreparative pathways, including redox scavenging, DNA repair, and stress-responding proteins. Taken together, the in vivo and in vitro results suggest MnSOD enzymatic activity is regulated by acetylation during stress and that Sirt3 regulates acetylation under specific conditions associated with neoplastic transformation, including IR-induced cellular damage.

A fundamental paradigm in biology is the presence of intracellular redox-sensing proteins that recognize specific cellular conditions and initiate posttranslational signaling cascades (Slane et al., 2006), and these pathways activate the cellular machinery that maintains cellular homeostasis. The most common example of this is the cytoplasmic activation of kinases that phosphorylate a series of downstream targets in response to different environmental conditions, thereby minimizing any potentially permanent cellular detrimental effects (Slane et al., 2006). In this regard, lysine acetylation has recently emerged as an important and perhaps primary posttranslational modification employed to regulate mitochondrial proteins (Lombard et al., 2007).

The results presented above support this hypothesis and, together with recent findings (Kim et al., 2010), suggest that mitochondrial sirtuins, including Sirt3, may function as fidelity proteins whose loss of function may result in a damage-permissive phenotype that leads to neoplastic transformation. The results presented above also suggest that the superoxide scavenging enzymatic function of MnSOD is regulated by changes in specific lysine acetylation. The connection between MnSOD and carcinogenesis, as well as tumor cell resistance to anticancer agents, is significant; however, the mechanism of action appears to be complex (Oberley, 2005; Aykin-Burns et al., 2009). The current work represents a paradigm shift in our understanding of the posttranslational regulation of MnSOD enzymatic function and the mechanism of its role in responses to stress. Finally, since Sirt3 is proposed to sense nutrient deprivation and oxidative stress, it also seems logical that exposure to IR, which has previously been shown to induce both oxidative stress and mitochondrial damage (Slane et al., 2006), would activate Sirt3 as a signaling pathway to protect against persistent IR-induced metabolic stress and normal tissue damage.

## EXPERIMENTAL PROCEDURES

### Cell Lines

MEFs were isolated from E14.5 isogenic *Sirt3*$^{+/+}$ and *Sirt3*$^{+/+}$ mice and maintained in a 37°C incubator with 5% $CO_2$ and 6% oxygen. MEFs and HCT-116 were cultured in McCoy's 5A media, containing 10% heat-inactivated (56°C, 30 min) FBS. Sirt3$^{+/+}$ or Sirt3$^{-/-}$ MEFs (Kim et al., 2010) were infected at P3 with lentivirus expressing either *Myc*, *Ras*, or *MnSOD* made by Applied Biological Materials, Inc. (Richmond, British Columbia, Canada), and pooled, selected cells were used for all experiments. For lentiviral infections, MEFs were infected with 5 moi of virus.

### IP and Immunoblot Analysis

IP with anti-MnSOD and anti-Sirt3 antibodies and the subsequent western analyses were done as previously described (Kim et al., 2010). The control for these IP experiments is normalized to rabbit IgG. In addition, the IPed MnSOD samples were divided into equal fractions, separated, and blotted with anti-acetyl or anti-MnSOD antibodies. Blots were incubated with horseradish peroxidase secondary antibody, using ECL (Amersham Biosciences; Piscataway, NJ), and visualized in a Fuji Las-3000 darkbox (FujiFilm Systems; Stamford, CT).

### Statistical Analysis

Data were analyzed by Student's t test, and results were considered significant at $p < 0.05$. Results are presented as mean ± SD.

### MnSOD Activity

MnSOD activity was analyzed in cell homogenates prepared on ice in 50 mM potassium phosphate buffer (Spitz and Oberley, 1989). This assay is based on the competition between MnSOD and an indicator molecule for superoxide production from xanthine and xanthine oxidase, in the presence of 5 mM NaCN to inhibit CuZnSOD activity (Spitz and Oberley, 1989). See Supplemental Experimental Procedures.

### Measurement of Mitochondrial Superoxide Levels

Superoxide production was determined as described (Kim et al., 2010) by measuring MitoSOX (1 μM) oxidation in cells that were cultured as described above and incubated for an additional 10 min before being trypsinized, resuspended, and measured by flow cytometry (see Supplemental Information).

Liver samples were used to determine in vivo superoxide levels as previously described (Kim et al., 2010).

### Cell Foci, Colony Formation, and Soft Agar Assays

For foci formation assays, cells were plated onto a 10 cm plate and grown to confluence, with medium replaced every 3 days for 28 days. All results for these experiments are the mean of at least three separate experiments. For the soft agar colony formation assay, 4000 cells were plated in 2 ml of 0.4% agar in growth medium over a 3 ml base layer of agar, also in growth medium. Each culture was topped with 1–2 ml of medium every 3–5 days. After 12 days, colonies were stained with methylene blue. The colonies (>0.5 mm size) were counted after 2 weeks under a light microscope.

### Chromosome Analysis

MEFs were exposed at passage four to irradiation and harvested after 72 hr. Whole-mount chromosomes were counted in a blinded fashion. Individual spreads were deemed countable if all chromosomes were clearly defined and clearly visible within a single cytoplasm, as previously described (Kim et al., 2010).

### Catalase Enzymatic Activity

Catalase activity was determined as described (Slane et al., 2006). Cell extracts containing 100 μg protein were combined with 30 mM $H_2O_2$ (Fisher Scientific; Suwanee, GA) in 1 ml of 50 mM potassium phosphate buffer (pH 7.0). $H_2O_2$ disappearance was measured at 240 nm for 120 s and recorded over 15 s intervals. Catalase enzymatic activity was expressed in k units per microgram protein per second (k units/μg/s): $k = 1/60 \times \ln(A0/A60)$, where A0 is the initial absorbance and A60 is the absorbance at 60 s.

### Liver Histopathology Examination, TUNEL Assay, and Cleaved Caspase-3 IHC

Liver sections were fixed in 10% neutral buffered formalin. Fixed tissues were then processed, paraffin embedded, and sectioned at 4 μm. Sections were stained with H&E or PAS reagent (for glycogen evaluation). H&E slides were scored in a blinded fashion for severity of hepatocellular vacuolation. The vacuolar change, when present, was focused in periportal to midzonal hepatocytes; therefore, scoring was based on an average of three periportal areas per liver section. For each periportal area, 100 hepatocytes were counted and given a vacuolar severity score of low, medium, or high. Low vacuolar change was characterized by mild, poorly defined cytoplasmic vacuolation consistent with glycogen accumulation. Hepatocytes with medium or high vacuolation were moderately to markedly enlarged due to dilation of the cytoplasm by clear space and few poorly defined clear vacuoles. Osmium tetroxide staining for lipid (to identify hepatocellular lipid vacuoles) was performed on formalin-fixed tissues. Formalin-fixed tissues (3 mm) were placed in potassium dichromate/osmium tetroxide (5%/2%) for 7 hr, followed by a 2 hr tap water rinse. Tissue sections were then routinely processed, paraffin embedded, and sectioned.

TUNEL assay was performed using the ApopTag Peroxidase ISOL Apoptosis Detection Kit (Millipore; Billerica, MA) according to the manufacturer's instructions. Apoptosis was detected by IHC for cleaved caspase-3 on formalin-fixed, paraffin-embedded liver tissues. Cleaved caspase-3 antibody, which is indicative of activated caspase-3 (rabbit monoclonal 1:50, Cell Signaling Technologies; Danvers, MA), was applied for 1 hr. Following several rinses, secondary antibody (Rabbit Envision HRP System, DAKO; Carpinteria, CA) and chromogen (Rabbit Envision HRP System reagents, DAB Plus, and DAB Enhancer; DAKO) kits were applied as per the manufacturer's instructions. TUNEL and caspase-3 staining were quantified by counting positive cells per 200× field. A total of 10–200× fields were counted, and means of these counts were calculated for further statistical analysis.

## SUPPLEMENTAL INFORMATION

Supplemental Information includes Supplemental Experimental Procedures, Supplemental References, six figures, and one table and can be found with this article online at doi:10.1016/j.molcel.2010.12.013.

## ACKNOWLEDGMENTS

D.G. is supported by 1R01CA152601-01 from the NCI, BC093803 from the DOD, and SPORE P50CA98131. D.R.S., A.K.O., and M.C.C. are supported by grants from the NIH and DOE (R01CA133114, T32CA078586, P30CA086862, and DE-SC0000830). J.D.P. is supported by F30AG030839. We thank Melissa Stauffer of Scientific Editing Solutions for editorial assistance.

Received: July 13, 2010
Revised: October 10, 2010
Accepted: December 6, 2010
Published: December 21, 2010

## REFERENCES

Ahn, B.H., Kim, H.S., Song, S., Lee, I.H., Liu, J., Vassilopoulos, A., Deng, C.X., and Finkel, T. (2008). A role for the mitochondrial deacetylase Sirt3 in regulating energy homeostasis. Proc. Natl. Acad. Sci. USA *105*, 14447–14452.

Araya, Q.A.V., Valera, M.J.M., Contreras, B.J., Csendes, J.A., Díaz, J.J., Burdiles, P.P., Rojas, C.J., Maluenda, G.F., Smok, S.G., and Poniachik, T.J. (2006). [Glucose tolerance alterations and frequency of metabolic syndrome among patients with non alcoholic fatty liver disease]. Rev. Med. Chil. *134*, 1092–1098.

Aykin-Burns, N., Ahmad, I.M., Zhu, Y., Oberley, L.W., and Spitz, D.R. (2009). Increased levels of superoxide and H2O2 mediate the differential susceptibility of cancer cells versus normal cells to glucose deprivation. Biochem. J. *418*, 29–37.

Du, C., Gao, Z., Venkatesha, V.A., Kalen, A.L., Chaudhuri, L., Spitz, D.R., Cullen, J.J., Oberley, L.W., and Goswami, P.C. (2009). Mitochondrial ROS and radiation induced transformation in mouse embryonic fibroblasts. Cancer Biol. Ther. *8*, 1962–1971.

Finkel, T., Deng, C.X., and Mostoslavsky, R. (2009). Recent progress in the biology and physiology of sirtuins. Nature *460*, 587–591.

Kim, H.S., Patel, K., Muldoon-Jacobs, K., Bisht, K.S., Aykin-Burns, N., Pennington, J.D., van der Meer, R., Nguyen, P., Savage, J., Owens, K.M., et al. (2010). SIRT3 is a mitochondria-localized tumor suppressor required for maintenance of mitochondrial integrity and metabolism during stress. Cancer Cell *17*, 41–52.

Li, X., Zhang, S., Blander, G., Tse, J.G., Krieger, M., and Guarente, L. (2007). SIRT1 deacetylates and positively regulates the nuclear receptor LXR. Mol. Cell *28*, 91–106.

Lombard, D.B., Alt, F.W., Cheng, H.L., Bunkenborg, J., Streeper, R.S., Mostoslavsky, R., Kim, J., Yancopoulos, G., Valenzuela, D., Murphy, A., et al. (2007). Mammalian Sir2 homolog SIRT3 regulates global mitochondrial lysine acetylation. Mol. Cell. Biol. *27*, 8807–8814.

Oberley, L.W. (2005). Mechanism of the tumor suppressive effect of MnSOD overexpression. Biomed. Pharmacother. *59*, 143–148.

Onyango, P., Celic, I., McCaffery, J.M., Boeke, J.D., and Feinberg, A.P. (2002). SIRT3, a human SIR2 homologue, is an NAD-dependent deacetylase localized to mitochondria. Proc. Natl. Acad. Sci. USA *99*, 13653–13658.

Revollo, J.R., Grimm, A.A., and Imai, S. (2004). The NAD biosynthesis pathway mediated by nicotinamide phosphoribosyltransferase regulates Sir2 activity in mammalian cells. J. Biol. Chem. *279*, 50754–50763.

Schwer, B., North, B.J., Frye, R.A., Ott, M., and Verdin, E. (2002). The human silent information regulator (Sir)2 homologue hSIRT3 is a mitochondrial nicotinamide adenine dinucleotide-dependent deacetylase. J. Cell Biol. *158*, 647–657.

Schwer, B., Bunkenborg, J., Verdin, R.O., Andersen, J.S., and Verdin, E. (2006). Reversible lysine acetylation controls the activity of the mitochondrial enzyme acetyl-CoA synthetase 2. Proc. Natl. Acad. Sci. USA *103*, 10224–10229.

Sherr, C.J., and McCormick, F. (2002). The RB and p53 pathways in cancer. Cancer Cell *2*, 103–112.

Singh, K.K. (2006). Mitochondria damage checkpoint, aging, and cancer. Ann. N Y Acad. Sci. *1067*, 182–190.

Slane, B.G., Aykin-Burns, N., Smith, B.J., Kalen, A.L., Goswami, P.C., Domann, F.E., and Spitz, D.R. (2006). Mutation of succinate dehydrogenase subunit C results in increased O2.-, oxidative stress, and genomic instability. Cancer Res. *66*, 7615–7620.

Spitz, D.R., and Oberley, L.W. (1989). An assay for superoxide dismutase activity in mammalian tissue homogenates. Anal. Biochem. *179*, 8–18.

Tolman, K.G., and Dalpiaz, A.S. (2007). Treatment of non-alcoholic fatty liver disease. Ther Clin Risk Manag *3*, 1153–1163.

Wallace, D.C. (2005). Mitochondria and cancer: Warburg addressed. Cold Spring Harb. Symp. Quant. Biol. *70*, 363–374.

**Supplemental Information**
Molecular Cell, *Volume 40*

# Sirt3-Mediated Deacetylation of Evolutionarily Conserved Lysine 122 Regulates MnSOD Activity in Response to Stress

Randa Tao, Mitchell C. Coleman, Daniel Pennington, Ozkan Ozden, Seong-Hoon Park, Haiyan Jiang, Hyun-Seok Kim, Charles Robb Flynn, Salisha Hill, W. Hayes McDonald, Alicia K. Olivier, Douglas R. Spitz, and David Gius

## Supplemental Experimental Procedures

### *Mass Spectrometry Based Proteomics and analysis*

**Mass Spectrometry Sample Preparation** - Anti-MnSOD immune complexes from $Sirt3^{+/+}$ and $Sirt3^{-/-}$ mouse liver were separated by SDS-PAGE (4-20% acrylamide) and stained with colloidal Coomassie Blue G-250 (Invitrogen). Samples were de-stained with 100 µl of 50% acetonitrile and 50 mM ammonium bicarbonate. A prominent 22 kD band present in each gel lanes was excised, finely diced, reduced with 45mM DTT for 20 minutes at 55 degrees, alkylated with 100 mM iodoacetamide for 30 minutes at room temperature, and digested overnight at 37°C with trypsin. Peptides were extracted with two rounds of 60% acetonitrile and 0.1% trifluoroacetic acid and were then lyophilized to dryness. Digests were resolubilized in 15 µl of 0.1% formic acid and analyzed by LC-MS/MS.

**Mass Spectrometry Based Proteomics** - LC-MS-MS analysis of the peptides was performed using a LTQ-Orbitrap mass spectrometer equipped with an Eksigent NanoLC-AS1 Autosampler 2.08 and the Eksigent NanoLC-1D plus HPLC pump, and Nanospray source. The peptides were resolved on a packed fused silica capillary column, 100 µm × 20 cm, packed with C18 resin (Jupiter $C_{18}$, 3 µm, 300 Å, Phenomonex, Torrance, CA), and coupled with an in-line trapping column that was 100 µm × 4 cm packed with the same C18 resin (using a frit generated with the liquid silicate Kasil 1 [1]). Liquid chromatography was carried out at ambient temperature with a flow rate of 0.5 $\mu$L /min using a gradient mixture of 0.1% (v/v) formic acid in water

(solvent A) and 0.1% (v/v) formic acid in acetonitrile (solvent B). The flow rate during the loading and desalting phase of the gradient was 1.5μL/min and during separation phase was 500 nL/min. A 95 min gradient was performed with a 10 min washing period diverted to waste after the precolumn (98% A for the first 10 min followed by a gradient to 98% A at 15 min) to allow for removal of any residual salts. After the initial washing period, a 60 min gradient was performed where the first 35 min was a slow, linear gradient from 98% A to 75% A, followed by a faster gradient to 10% A at 65 min and an isocratic phase at 10% A to 75 min.

Centroided MS/MS scans were acquired on the LTQ-Orbitrap using an isolation width of 2 *m/z*, an activation time of 30 ms, an activation *q* of 0.250 and 35% normalized collision energy using 1 microscan with a maximum injection time of 0.1 sec for each MS/MS scan and 1 microscan with a maximum injection time of 1 sec for each full orbitrap MS scan. The tune parameters were as follows: spray voltage of 2.43 kV, a capillary temperature of 200 °C, a capillary voltage of 48 V and tube lens of 85 V. The AGC target values were set at 1,000,000 for the full MS and 10000 for the MS/MS spectra. A full scan obtained for eluting peptides in the range of 400-2000 amu was collected on the Orbitrap at a resolution of 60 000, followed by five data-dependent MS/MS scans on the LTQ portion of the instrument with a minimum threshold of 1000 set to trigger MS/MS spectra. A dynamic exclusion list of the 150 previously analyzed precursors was maintained for 60 sec in which time MS/MS was not performed on those masses.

Spectra were extracted from the instrument data files using ScanSifter and then searched using SEQUEST against the mouse protein database (UniProtKB Mouse; ver 201006 ) also containing reversed protein sequences with carbamidomethyl Cys (+57), oxidized Met (+16) and acetylated lysine (42) as variable modifications. Resulting peptide matches were collated using the IDPicker algorithm (version 3.0.0; Ma *et. al.*, 2009) with a target false discovery rate of 5% with the additional requirement of a minimum of 2 distinct peptides per protein group.

Figure 2f. Tandem mass spectra for the MnSOD peptide $^{115}$GELLEAIK$^{122}$ in an A) unmodified (436.257 Da, +2 charge) and B) acetylated (457.257 Da, +2 charge) form were identified in full scan MS spectra in each of two replicate *Sirt3*$^{+/+}$ and *Sirt3*$^{-/-}$ LC-MS analyses. C-F) Selected ion chromatograms (SIC) of $^{115}$GELLEAIK$^{122}$, and $^{115}$GELLEAIK$^{122}$ -acetyl for each *Sirt3*$^{+/+}$ (C and D) and *Sirt3*$^{-/-}$ IP replicate (E and F) are shown. The area under the curve for each SIC was used to derive an average peptide ratio (unmodified/acetylated). Average *sirt3*$^{+/+}$ ratio (1.114%); Average *sirt3*$^{-/-}$ ratio (2.341%).

**MnSOD activity assay**

MnSOD activity was determined from whole cell homogenates prepared on ice following 2 freeze-thaw cycles in 50 mM potassium phosphate buffer (pH=7.8, with 1.34 mM diethylenetriaminepentaacetic acid) using an indirect competitive inhibition assay (Zhu et al., 2009). This assay is based on the competition between MnSOD and an indicator molecule (nitroblue tetrazolium) for superoxide production from xanthine and xanthine oxidase, according to the method of Spitz and Oberley (Spitz and Oberley, 1989). Incubation for at least 45 min with 5 mM sodium cyanide was used to inhibit CuZnSOD activity in order to selectively measure MnSOD activity. Activity data for MnSOD is presented as units of SOD activity per milligram of protein. Mitochondrial superoxide levels were determined in the *Sirt3* wild-type and knockout mouse livers at 5 and 13 months of age. Superoxide levels were measured as previously described (Li et al., 2001).

***In vitro* immortalization and transformation assays**

For *in vitro* immortalization, Sirt3$^{-/-}$ MEFs at passage three were infected with a lentivirus containing *Ras*, *Myc*, and/or *MnSOD* or one of the *MnSOD* mutant genes. MEFs were infected with 5 MOI of virus per 10 cm plate. Levels of Ras or exogenous MnSOD were confirmed by

western blot analysis and PCR analysis (data not shown). Cells were cultured and split every two days to prevent confluency and plated into a new 100 mm dish at 3.0 x $10^5$ cells. After 17 additional passages (20 total), cells were considered immortalized if they continued to divide.

### *The anti-MnSOD$^{Ac\text{-}K122}$ antibody preferentially binds to acetylated MnSOD lysine 122*

To begin to characterize that the monoclonal anti-MnSOD$^{Ac\text{-}K122}$ specific antibody, which was made in collaboration with Epitomics, Inc, Burlingame, CA, we obtained a series of samples from 33 monoclonal cell lines. Based on the ELISA results sample 33 was used for further experiments. To begin to more rigorously characterize a monoclonal antibody that is specific for acetylated MnSOD at amino acid lysine 122 HEK 293T cells were transfected with a CMV based plasmid expressing a Flag-tagged wild-type MnSOD protein. These cells were maintained in 1 μM TSA and after 48 hr the exogenous MnSOD was IPed with an anti-Flag antibody. Equal amounts of IPed MnSOD were incubated with purified SIRT3 protein (BioMol, Inc.) without or with NAD+ that is required to induce SIRT3 deacetylation activity. These samples were subsequently separated and incubated with the antibody obtained from Epitomics, Inc, Burlingame, CA). These results demonstrate that SIRT3 immunoreactive protein is decreased in the sample containing SIRT3 and NAD+ but not SIRT3 lacking NAD+ (Fig. S6A, lanes 1 versus 2). These *in vitro* were repeated with 2 hr of incubation with the 13 amino acid lysine 122 acetylated peptide (Ac-peptide) used to make the antibody or an identical control 13 amino acid peptide that lacks an acetyl molecular at position 122. These experiments demonstrate that incubation with the acetylated peptide prevents immunostaining with the anti-MnSOD$^{Ac\text{-}K122}$ specific antibody (Fig. S6A, lanes 3 and 4) but not with the control, non-acetylated antibody (lanes 5 and 6). These results strongly suggest that the antibody make for us by Epitomics is specific for acetylated lysine 122.

To further validate the results with anti-MnSOD$^{Ac\text{-}K122}$ specific antibody the samples used for figure S6A, lanes 1 and 2 were sent for mass spectrometry as was previously done using the Vanderbilt Proteinomics Core (see main manuscript, Fig. 2f and Fig. S2E). The left panel of appendix figure A2B has also been added to the manuscript as Fig. 3f to show that MnSOD lysine 122 is specifically deacetylated *in vitro* by recombinant SIRT3. These results showed a roughly 80% decrease in MnSOD lysine 122 acetylation (Fig. S6C) that is similar to and very consistent with the anti-MnSOD$^{Ac\text{-}K122}$ antibody Western (Fig. S6B) results. These results also show that incubation of IPed MnSOD from cells containing TSA with the purified SIRT3 results in a significant (80%), but not complete, deacetylation of MnSOD lysine 122 (Fig. S6A, lane 1 versus lane 2).

## SUPPLEMENTAL REFERENCES


Ahn, B.H., Kim, H.S., Song, S., Lee, I.H., Liu, J., Vassilopoulos, A., Deng, C.X., and Finkel, T. (2008). A role for the mitochondrial deacetylase Sirt3 in regulating energy homeostasis. Proc Natl Acad Sci U S A *105*, 14447-14452.

Gius, D., Cao, X.M., Rauscher, F.J., 3rd, Cohen, D.R., Curran, T., and Sukhatme, V.P. (1990). Transcriptional activation and repression by Fos are independent functions: the C terminus represses immediate-early gene expression via CArG elements. Mol Cell Biol *10*, 4243-4255.

Grdina, D.J., Murley, J.S., Kataoka, Y., Baker, K.L., Kunnavakkam, R., Coleman, M.C., and Spitz, D.R. (2009). Amifostine induces antioxidant enzymatic activities in normal tissues and a transplantable tumor that can affect radiation response. Int J Radiat Oncol Biol Phys *73*, 886-896.

Hadzic, T., Aykin-Burns, N., Zhu, Y., Coleman, M.C., Leick, K., Jacobson, G.M., and Spitz, D.R. Paclitaxel combined with inhibitors of glucose and hydroperoxide metabolism enhances breast cancer cell killing via H2O2-mediated oxidative stress. Free Radic Biol Med *48*, 1024-1033.

Kim, H.S., Patel, K., Muldoon-Jacobs, K., Bisht, K.S., Aykin-Burns, N., Pennington, J.D., van der Meer, R., Nguyen, P., Savage, J., Owens, K.M., *et al.* (2010). SIRT3 Is a Mitochondria-Localized Tumor Suppressor Required for Maintenance of Mitochondrial Integrity and Metabolism during Stress. Cancer cell *17*, 41-52.

Schwer, B., Eckersdorff, M., Li, Y., Silva, J.C., Fermin, D., Kurtev, M.V., Giallourakis, C., Comb, M.J., Alt, F.W., and Lombard, D.B. (2009). Calorie restriction alters mitochondrial protein acetylation. Aging Cell.

Spitz, D.R., and Oberley, L.W. (1989). An assay for superoxide dismutase activity in mammalian tissue homogenates. Analytical biochemistry *179*, 8-18.

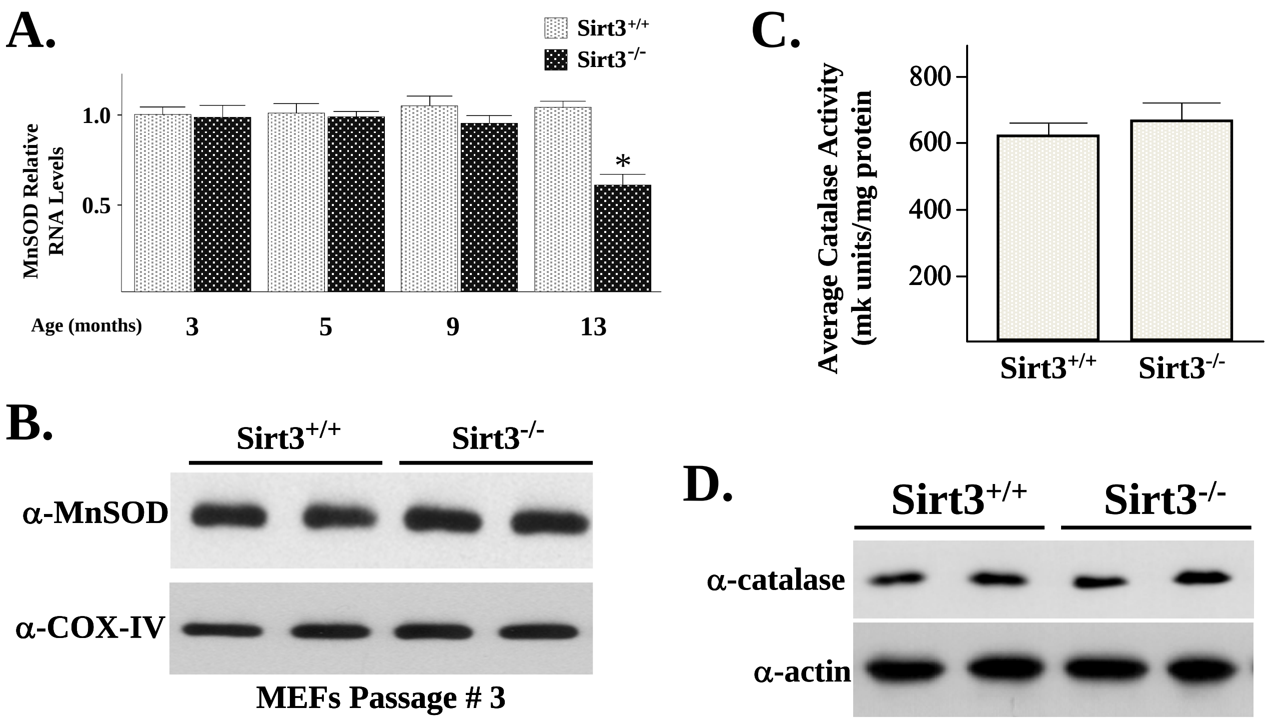


**Figure S1.** ***MnSOD*** **Levels in** ***Sirt3*** **Wild-Type and Knockout Mouse Livers at 5 and 13 Months and the Sirt3 Knockout MEFs at Passage Number Three**

(A) *MnSOD* RNA levels are decreased in the Sirt3$^{-/-}$ mice between 9 and 13 months of age. Mouse livers were harvested and RNA was prepared as previously described (Gius et al., 1990) in isogenic, age-matched wild-type and *Sirt3* knockout mouse livers extracts at 3, 5, 9, and 13 months. *MnSOD* expression was determined by qRT-PCR using *MnSOD* and *β-actin* Taqman probes (ABI) as previously described (Kim et al., 2010).

(B) MnSOD protein levels in Sirt3$^{+/+}$ and Sirt3$^{-/-}$ MEFs at early cell passage number. MEFs at passage three were isolated and whole cell extracts were harvested, separated by SDS-PAGE, transferred onto nitrocellulose, and processed for immunoblotting with an anti-MnSOD antibody (Santa Cruz Biotechnology, Inc). A representative gel is shown.

(C) Catalase activity in the wild-type and *Sirt3* knockout mice is similar. Liver extracts were isolated from Sirt3$^{+/+}$ and Sirt3$^{-/-}$ mice as previously described (Kim et al., 2010). Catalase activity was determined as previously described (Grdina et al., 2009) spectrophotometrically from aliquots of the same whole tissue homogenates (20–200 μg) used for SOD analysis by measuring the disappearance of 10 mM $H_2O_2$ at 240 ηm in 3 ml reaction volumes of potassium phosphate buffer pH 7.0 and calculated as κ units and normalized to protein content.

(D) The liver samples described in (C) were separated by SDS-PAGE and immunoblotted with either an anti-catalase (Abcam) or anti-actin (Santa Cruz Biotechnology, Inc) antibody. All the results in this figure are from at least three separate experiments. Data are presented as the average +/- SD. * indicates $P < 0.05$ by t-test. Figure S1A relates to Figure 1A. Figure S1B relates to Figure 1C. Figure S1C relates to Figure 1. Figure S1D relates to Figure 1.

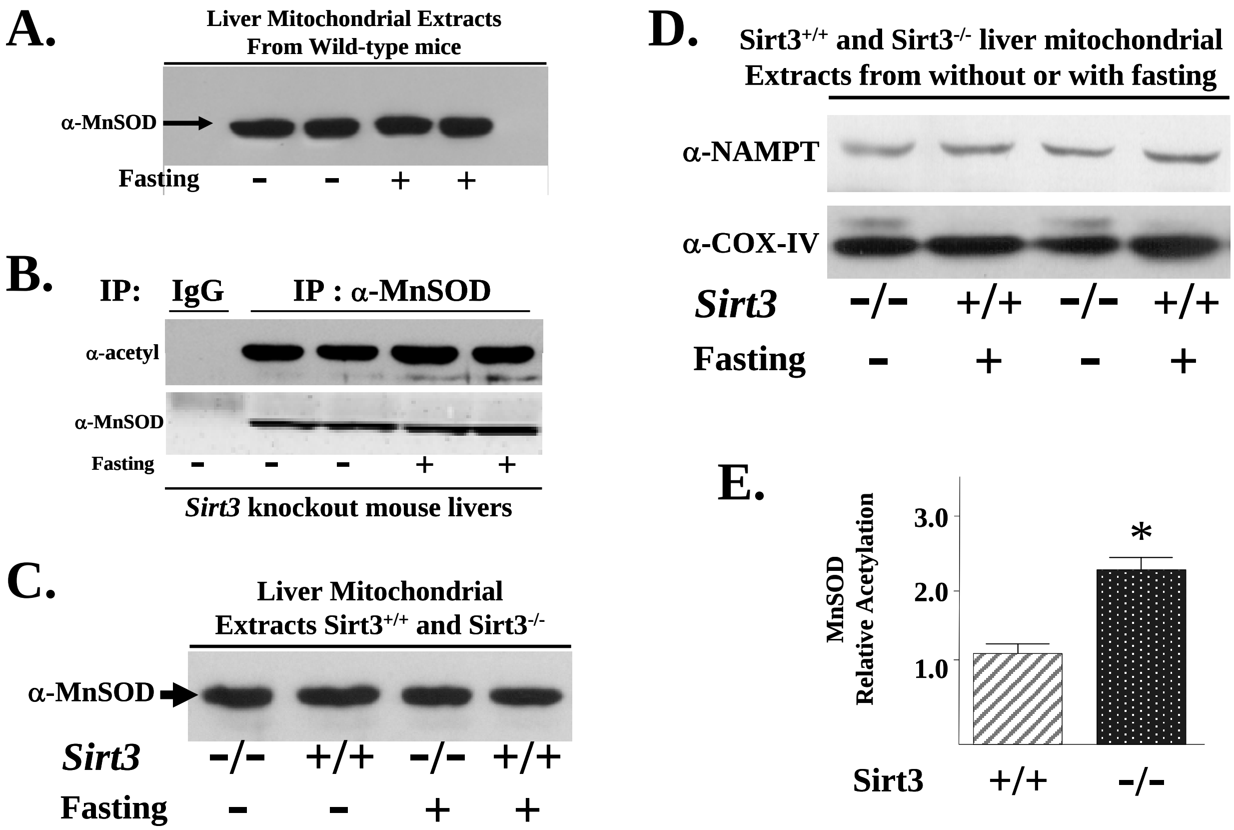


**Figure S2. MnSOD Contains a Reversibly Acetylated Lysine and Protein Deacetylation and SOD Activity Are Decreased in *Sirt3*$^{-/-}$ Cells**

(A) MnSOD levels from livers from 3-month-old age-matched Sirt3$^{+/+}$ mice are unchanged with fasting. Mitochondrial liver extracts were harvested as previously described (Kim et al., 2010) and immunoblotted with an anti-MnSOD antibody (Santa Cruz Biotechnology, Inc) to determine total mitochondrial protein levels.

(B) Fasting does not alter MnSOD acetylation in mice lacking Sirt3. Mitochondrial liver extracts were harvested as described above from Sirt3$^{-/-}$ mice, IPed with an anti-MnSOD antibody, split into two equal fractions, and immunoblotted with either an anti-acetyl (Abcam) or anti-MnSOD antibody (Santa Cruz Biotechnology, Inc).

(C) Total MnSOD mitochondrial protein is similar in the livers of *Sirt3* wild-type and knockout mice at 3 months of age with or without fasting. Mitochondrial liver extracts were harvested, separated by SDS-PAGE, transferred onto nitrocellulose, and processed for immunoblotting with an anti-MnSOD antibody.

(D) Liver extracts were isolated from Sirt3$^{-/-}$ and Sirt3$^{+/+}$ mice, as well as from mice that were fasted for 36 hr, separated, and immunoblotted with either an anti-NAMPT or anti-COX-IV antibody. Representative gels are shown.

(E) Acetylation of MnSOD lysine 122 is increased in the livers of mice lacking the *Sirt3* gene. At 3 months of age Sirt3$^{+/+}$ and Sirt3$^{-/-}$ mouse livers (6 mice in each group) were harvested, and mitochondria were isolated and analyzed for acetylation of MnSOD lysine 122 via mass spectrometry (Schwer et al., 2009). Results are presented as fold change from the untreated, wild type mouse livers. All the results in this figure are from at least three separate experiments. Representative gels are shown. Data are presented as the average +/- SD. * indicates $P < 0.05$ by t-test. Figure S2A relates to Figure 2A. Figure S2B relates to Figure 2A. Figure S2C relates to Figures 2A and 2B. Figure S2D relates to Figures 2A and 2B. Figure S2E relates to Figure 2E.

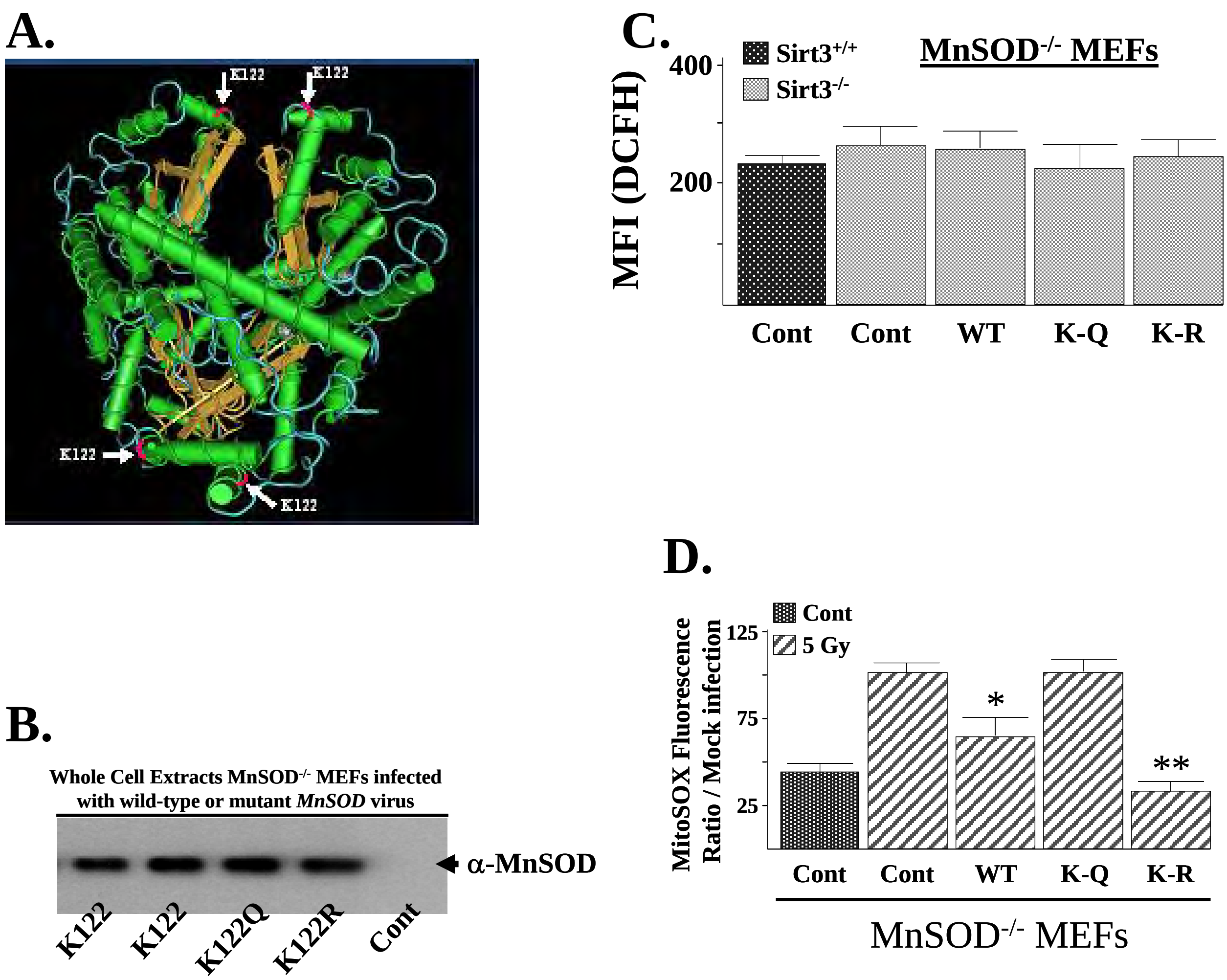


**Figure S3. MnSOD Contains an Evolutionarily Conserved Lysine Residue that Regulates SOD Activity**

(A) A representative 3D rendering of the protein structure for the MnSOD complex, which is a functional tetramer. Lysine 122 is shown in red and identified by a white arrow. As can been seen, lysine 122 is on the outside of the protein and as such, is in an ideal position to interact with other proteins such as the Sirt3 deacetylase.

(B) Infection of *MnSOD* knockout MEFs with the various *MnSOD* lentiviruses results in similar levels of expressed exogenous protein. MnSOD$^{-/-}$ MEFs were infected with a control virus (lane 5), lenti-MnSOD$^{K122}$ (lanes 1-2) or one of the lysine site-directed mutants (lenti-MnSOD$^{K122\text{-}Q}$, lane 3 or lenti-MnSOD$^{K122\text{-}R}$, lane 4). After 48 hr cells were harvested and extracts were separated by SDS-PAGE and immunoblotted with an anti-myc antibody (Santa Cruz Biotechnology, Inc.). Experiments were done in triplicate. A representative gel is shown.

(C) $H_2O_2$ levels were determined in the MnSOD$^{-/-}$ MEFs infected with the MnSOD lentiviruses. Forty hr after infection, steady-state levels of $H_2O_2$ were determined using the PEG–CAT-inhibitable signal from the oxidation-sensitive CDCFH2 probe and flow cytometry analysis (Hadzic et al., 2010). Cells were labeled with the oxidation-sensitive CDCFH2 fluorescent probe for 15 min at 37°C. PEG–CAT-inhibitable mean fluorescence intensity (MFI) was calculated by subtracting the MFI value with PEG–CAT versus the absence of PEG–CAT.

(D) Mitochondrial superoxide levels in *Sirt3* knockout MEFs exposed to IR are decreased by infection with lenti-MnSOD$^{K122\text{-}R}$. Sirt3$^{-/-}$ MEFs were exposed to 5 Gy of IR and mitochondrial

superoxide levels were determined by the addition of Mito-SOX (1 µM) as described (Kim et al., 2010). Results for all the panels in this figure are the mean of at least three separate experiments and error bars represent one standard deviation. * indicates $P < 0.05$ and ** indicates $P < 0.01$ by t-test. Figure S3A relates to Figure 5A. Figure S3B relates to Figure 5C-G. Figure S3C relates to Figure 5B-G. Figure S3D relates to Figure 5H.

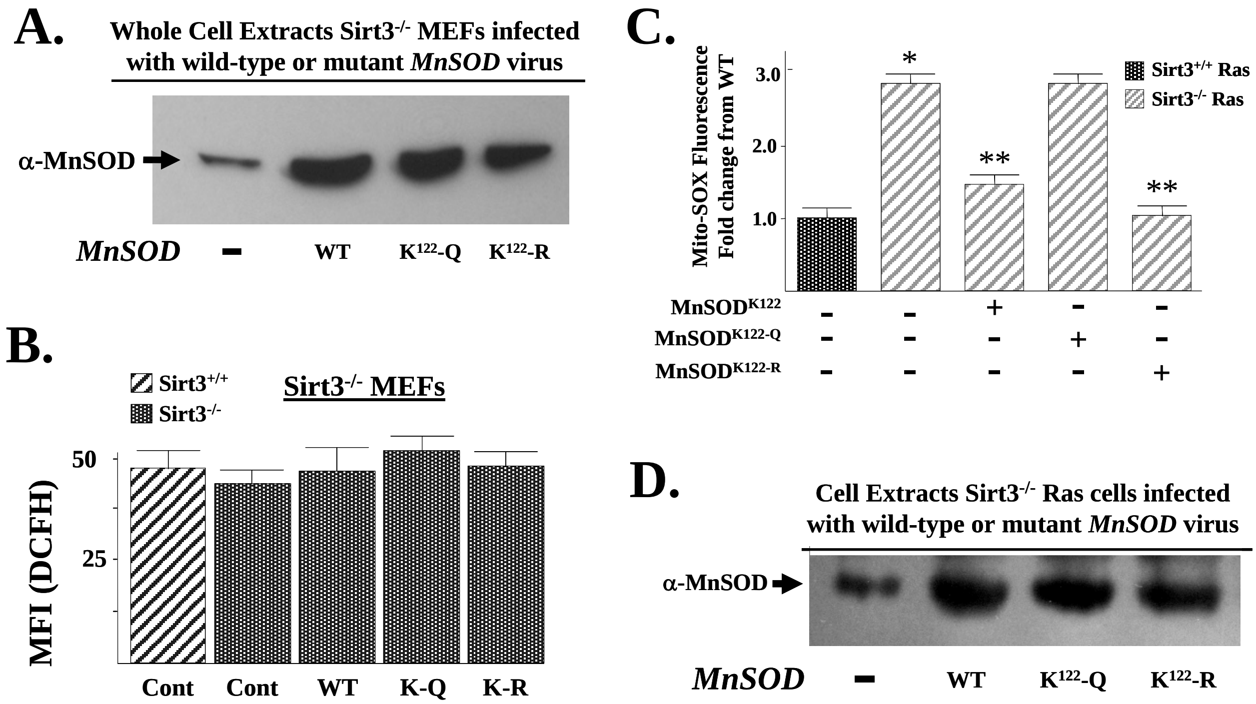


**Figure S4. Expression of the *MnSOD*$^{K122-R}$ Mutant Results in the Expression of Immunoreactive MnSOD Protein and Reverses the Increased Superoxide Levels Seen in Sirt3$^{-/-}$ Ras MEFs**

(A) Sirt3$^{-/-}$ MEFs were infected with a control virus (lane 1), a lentivirus expressing the wild-type *MnSOD* gene (lenti-MnSOD$^{K122}$, lane 2) or one of the lysine mutants that substitutes a glutamine (lenti-MnSOD$^{K122-Q}$, lane 3) or an arginine (lenti-MnSOD$^{K122-R}$, lane 4). After 48 hr cells were harvested and extracts were separated by SDS-PAGE, transferred onto nitrocellulose, and processed for immunoblotting with an anti-MnSOD antibody (Santa Cruz Biotechnology, Inc).

(B) $H_2O_2$ levels were determined in the Sirt3$^{-/-}$ MEFs infected with the MnSOD lentiviruses. Forty hr after infection, steady-state levels of $H_2O_2$ were determined as described in figure legend S3 (Hadzic et al., 2010).

(C) Infection of the transformed Sirt3$^{-/-}$ Ras cells with lenti-MnSOD$^{K122}$ and lenti-MnSOD$^{K122-R}$, but not lenti-MnSOD$^{K122-Q}$, reverses the increased mitochondrial superoxide levels in the Sirt3$^{-/-}$ Ras cells. Sirt3$^{-/-}$ Ras cells were infected with either wild-type or one of the site directed mutant *MnSOD* genes. Forty hr after infection, the cells were analyzed for mitochondrial superoxide levels as described (Kim et al., 2010).

(D) Infection of *Sirt3* knockout MEFs transformed with Ras (referred to as Sirt3$^{-/-}$ Ras cells) with the various *MnSOD* lenti-viruses results in similar levels of endogenous MnSOD immuno-reactive protein. The transformed Sirt3$^{-/-}$ Ras cells were infected with a control virus (lane 1), lenti-MnSOD$^{K122}$ (lane 2), lenti-MnSOD$^{K122-Q}$ (lane 3), or lenti-MnSOD$^{K122-R}$ (lane 4). After 48 hr cells were harvested as described above and immunoblotted with an anti-MnSOD antibody (Santa Cruz Biotechnology, Inc). The infection experiments in this figure were done in triplicate and representative gels are shown. Results are from at least three separate experiments. Data are presented as the average +/- SD. * indicates $P < 0.05$ and ** indicates $P < 0.01$ by t-test. Figure S4A relates to Figure 6a-b. Figure S4B relates to Figure 6a-b. Figure S4C relates to Figure 6c-d. Figure S4D relates to Figure 6c-d.

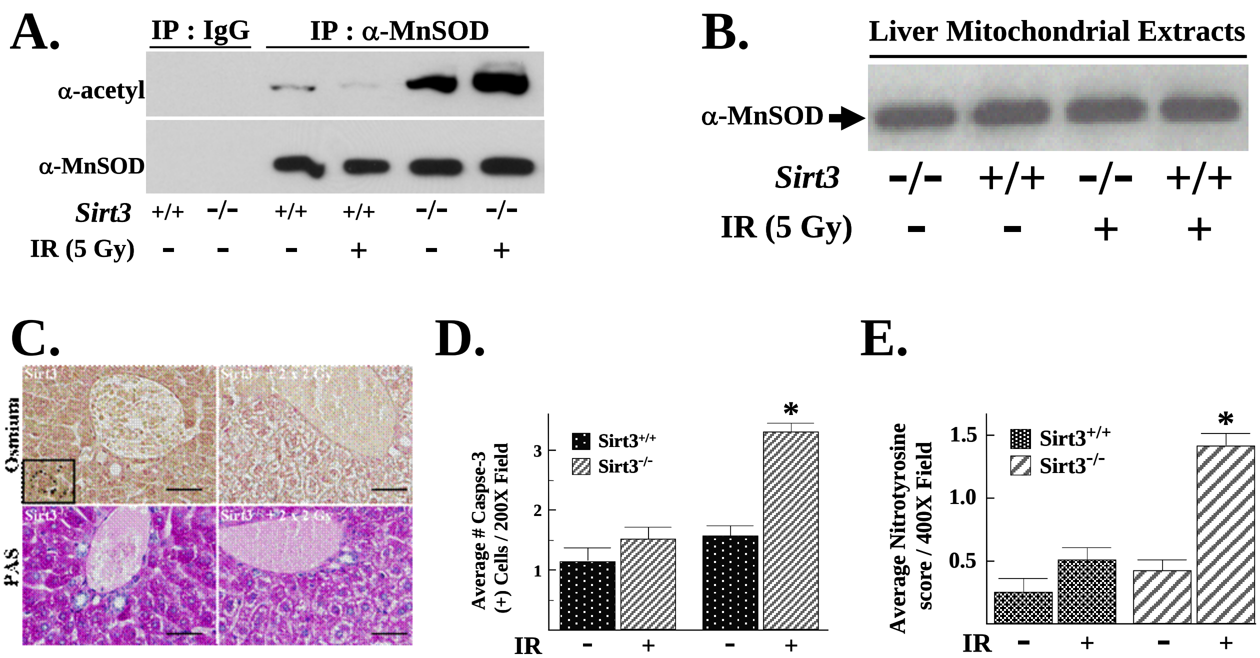


**Figure S5. MnSOD Lysine Acetylation Is Altered by IR in Livers from Irradiated Sirt3$^{+/+}$ Animals but Not Sirt3$^{-/-}$ Animals and Sirt3$^{-/-}$ Livers Showed Increased Caspase-3 Activation in Response to IR, Relative to Sirt3$^{+/+}$**

(A) Sirt3$^{+/+}$ and Sirt3$^{-/-}$ mice at 12 weeks were exposed to sham or 2 x 2 Gy Cesium 137 exposure on consecutive days and harvested after 24 hr and mitochondria were isolated. Mitochondrial liver extracts were harvested, IPed with an anti-MnSOD antibody, split into two equal fractions, separated, and immunoblotted with either an anti-K122-MnSOD antibody (Epitomics, Inc, The Rabbit Monoclonal Antibody Company, see Supplemental Information for antibody description) or anti-MnSOD antibody (Santa Cruz Biotechnology, Inc).

(B) The same samples as above were immunoblotted with an anti-MnSOD antibody. Representative gels are shown.

(C) Liver sections from Sirt3$^{-/-}$ and Sirt3$^{-/-}$ irradiated mouse livers were processed with osmium (top) to identify hepatocellular lipid or stained with periodic acid-Schiff reagent (bottom) to identify glycogen. There were minimal to no osmium positive lipid vacuoles within periportal hepatocytes from either group. There was abundant glycogen (magenta) in hepatocytes from non-irradiated Sirt3$^{-/-}$ mice. Hepatocytes from Sirt3$^{-/-}$ exposed to irradiation had moderate cytoplasmic glycogen with poorly defined cytoplasmic clear space. Bar = 25 mm.

(D) Apoptosis was determined in the Sirt3$^{+/+}$ and Sirt3$^{-/-}$ livers exposed to IR as above. Apoptotic cells were identified in liver sections by staining with an anti-activated-caspase-3 antibody. Cleaved-caspase-3 positive cells were counted in 20 randomly selected fields per liver section. Results are reported as the average number of positive cells per 200X field.

(E) Irradiated Sirt3$^{-/-}$ mouse livers exhibit increased anti-nitrotyrosine staining. Nitrotyrosine immunohistochemical staining was quantified by counting positive cells (cytoplasmic or nuclear staining) per 400X field with the following scoring system: 0 (0 positive cells), 1 (1-10 positive cells), 2 (10-20 positive cells), 3 (>20 positive cells). A total of 10, 400X fields were scored and means of these scores were calculated for further statistical analysis. Results are from at least three separate experiments. Data for S5D-E are presented as the average +/- SD. * indicates $P < 0.05$. Figure S5A relates to Figure 7b. Figure S5B relates to Figure 7b. Figure S5C relates to Figure 7b. Figure S5D relates to Figure 7e. Figure S5E relates to Figure 7f.

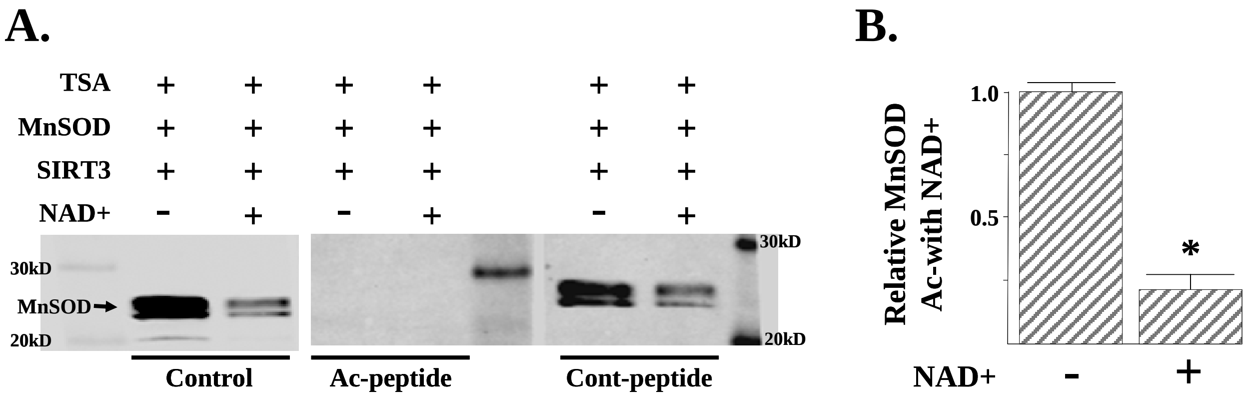


**Figure S6. SIRT3 Deacetylated MnSOD In Vitro and the Anti-MnSOD$^{Ac\text{-}K122}$ Specific Antibody Is Specific for Acetyl Lysine 122 of MnSOD**

(A) A flag-tagged MnSOD expression vector was transfected into HEK 293T cells that contained TSA (1 μM) and after 48 hr Flag-MnSOD was immunoprecipitated with an anti-Flag antibody (Sigma, Inc). The samples were subsequently washed, and incubated with purified SIRT3 protein (BioMol, Inc.) without (lane 1 or with (lane 2) NAD. After 2hr mixtures were immunoblotted with an anti-MnSOD acetyl 122 lysine antibody (Epitomics, Inc, Burlingame, CA). Identical experiments were done with the 13 amino acid lysine 122 acetylated peptide (Ac-peptide) or the control non-acetylated lysine 122 peptide (Cont-peptide).

(B) The samples from lanes 1 and 2 were also sent for mass spectrometry at the Vanderbilt Proteinomics Core to determine the difference in MnSOD 122 lysine acetylation as previously described (figure 2f). Data are presented as the average +/- SD. * indicates $P < 0.05$

**Table S1. MnSOD Prevents Immortalization of Sirt3$^{-/-}$ MEFs by a Single Oncogene**

| MEFs | Control | Myc | Ras | Myc/Ras |
|---|---|---|---|---|
| Sirt3$^{+/+}$ | None | None | None | Immort |
| Sirt3$^{-/-}$ | None | Immort | Immort | Immort |
| Sirt3$^{-/-}$ + lenti-MnSOD$^{K122\text{-}Q}$ | None | Immort | Immort | Immort |
| Sirt3$^{-/-}$ + lenti-MnSOD$^{K122\text{-}R}$ | None | None | None | Immort |

None, no MEF immortalization.
Immort, immortalization.
lenti-MnSOD 10 MOI.
Immortalization experiments were done in triplicate.

# APPENDIX B

# OSCP Contains an Evolutionarily Conserved Lysine that is Deacetylated by Sirt3 that Directs ATP Synthase Activity

J. Daniel Pennington [1,2,4], Thorkell Andresson [1,3], David Rees [2], Allen Bosely [3], Kaitlin A. Ray [4], Helen Cooper [5], Hans Spelbrink [5], Ian M. Fearnley [2], John Walker [2,6], and David Gius [4,6]

[1] The first two authors contributed equally to this manuscript.

[2] Medical Research Council Mitochondrial Biology Unit, Wellcome Trust/Medical Research Council Building, Hills Road, Cambridge CB2 0XY, United Kingdom, [3] Technologies, Advanced Technology Program, SAIC-Frederick Inc., NCI at Frederick, P.O. Box B, Frederick, MD 21702-1201, USA, [4] Department of Cancer Biology, Pediatrics, and Radiation Oncology, Vanderbilt University Medical Center, Nashville, TN 37232, USA, [5] Mitochondrial DNA Maintenance Group, Institute of Medical Technology, University of Tampere, Finland

<u>Running Title</u>: OSCP activity is directed by Sirt3 deacetylation

| | |
|---|---|
| Abstract | 150 |
| Pages | 16 |
| Characters | 31,904 |
| Figures | 4 |

<u>Keywords</u>: OSCP, *SIRT3*, Mitochondria, ATP synthase

[6] Co-corresponding authors:

David Gius, M.D., Ph.D.
Associate Professor
Department of Radiation Oncology
Department of Pediatrics
D4105 MCN
Nashville, TN 37232
David.Gius@vanderbilt.edu

John Walker, Ph.D.
Professor and Head,
Medical Research Council Mitochondrial Biology Unit
Wellcome Trust/Medical Research Council Building
Hills Road, Cambridge, UK
walker@mrc-mbu.cam.ac.uk

## ABSTRACT

Genetic deletion of mitochondrial sirtuin-3 (*Sirt3) in vitro* and *in vivo* decreases mitochondrial ATP levels suggesting a mechanistic connection to energy homeostasis. OSCP sits atop the ATP synthase ($F_1F_o$ ATPase) that uses chemiosmotic energy across the inner mitochondrial membrane to convert ADP and orthophosphate to ATP. OSCP contains a nutrient status-reversible acetyl-lysine that is evolutionarily conserved in multiple species. Mass spectrometry demonstrated that lysine 139 is hyperacetylated in *Sirt3* knockout livers. Re-introduction of wild-type, but not deacetylation null *Sirt3*, into Sirt3$^{-/-}$ MEFs deacetylated OSCP and increased mitochondrial ATP levels. IP experiments showed a physical interaction between OSCP and Sirt3. A series of *in vitro* and *in vivo* analysis demonstrated that OSCP lysine 139 is deacetylated by Sirt3. Finally, OSCP lysine 139 was mutated to arginine, mimicking deacetylation (CMV-OSCP$^{K139\text{-}R}$) and expression of CMV-OSCP$^{K139\text{-}R}$ increased mitochondrial ATP levels demonstrating that Sirt3 post-translational acetyl signaling contributes to mitochondrial energy homeostasis by deacetylating OSCP.

## INTRODUCTION

An intriguing finding from our previous work (Kim et al., 2010), and that of others (Ahn et al., 2008), demonstrated that cells lacking *Sirt3* exhibited altered mitochondrial metabolism, including a significant decrease in mitochondrial ATP levels. Mitochondria are central to aging and age-related diseases such as insulin resistance, neurodegeneration and carcinogenesis by tightly regulating the reactive oxygen species (ROS) generated as a byproduct of normal respiration activities (Singh, 2006).

Chemical reactions in a cell that are critical for the maintenance for cellular viability are thermodynamically dependent on the mitochondria to maintain a mass action ratio of ATP and ADP up to ten orders of magnitude away from equilibrium. The ATP synthase ($F_1F_o$ ATPase), an evolutionarily ancient protein complex, uses chemiosmotic energy stored in a gradient across the mitochondrial inner membrane to convert ADP and orthophosphate to ATP (Watt et al., 2010). The mammalian mitochondrial ATP synthase complex consists of 16 different subunits plus two accessory subunits (DAPIT and 6.8 kDa) peripheral to the synthesis of ATP, whose presence is dependent on the retention of phospholipids (Walker and Dickson, 2006). There is a membrane-bound portion ($F_o$) and a central stalk ($F_1$) containing a catalytic domain, held by a peripheral stalk stator that extends into the matrix.

Rotational energy is generated by protons entering the $F_o$ portion of the ATP synthase complex via a channel or channels between stationary subunit a and a rotary ring consisting of 8 c subunits (Watt et al., 2010). The rotational movement is transmitted through a central stalk consisting of subunits γ, δ, and ε. The γ subunit of this asymmetrical stalk interacts with the non-rotating catalytic subunits consisting of 3 each of alternating α and β subunits. The spinning central stalk of the ATP synthase is held in place by an external stalk consisting of subunits oligomycin sensitivity-conferring protein OSCP, β, F6, and δ; and OSCP sits on the top of the

ATP synthase complex and appears to hold the alpha and beta proteins in specific 3-dimenstional complexes (Rees et al., 2009)  This stator is flexible, a trait which may have a role in maintaining contact with the rotating portion of the $F_1$ complex during ATP synthesis as well as in regulating enzymatic function (Rees et al., 2009).

Lysine acetylation has recently emerged as an important, and perhaps the primary, post-translational modification employed to regulate mitochondrial proteins (Choudhary et al., 2009; Schwer et al., 2006).  Several proteomic surveys have identified a disproportionately high number of acetylated proteins in the mitochondria, and many appear to be associated with energy metabolism (Choudhary et al., 2009; Kim et al., 2006).  Based on these results, it seems reasonable to suggest that acetylation of mitochondrial proteins may play a role in maintaining and regulating mitochondrial metabolism and function.  Sirt3 is the primary mitochondrial deacetylase (Lombard et al., 2007), and genetic knockout of *Sirt3* results in decreased cellular ATP levels *in vitro* and *in vivo* (Ahn et al., 2008).  Thus, we believe it is a logical extension to hypothesize that Sirt3 functions as a mitochondrial regulatory protein, maintaining mitochondrial homeostasis via changes in the acetylation status of mitochondrial metabolic proteins, including perhaps those that comprise the ATP synthase complex.  This idea would mechanistically connect a metabolic sensing / signaling proteins, such as Sirt3, to the direct regulation of ATP synthase.

## RESULTS

### *Sirt3 knockout cells have increased mitochondrial acetylated protein*

Tissues from mice genetically altered to delete *Sirt3* expression were removed and mitochondria were isolated from organs pooled from several mice via homogenization and differential centrifugation. Western blotting with an antibody against Sirt3 (a kind gift from Michael Sack, NIH, Bethesda, Maryland) confirmed that the Sirt3$^{-/-}$ animals lacked Sirt3 (Fig. 1a). Global acetylation in the mitochondrial proteome was examined in the mitochondria of Sirt3$^{+/+}$ and Sirt$^{-/-}$ mice livers as well as mice fasted for 24 hours that has been shown to activate sirtuin proteins (Finkel et al., 2009). Proteins containing acetylated lysine residues were detected after resolution by 1-D SDS-PAGE and immunoblotting with an anti-acetyl lysine antibody (Cell Signaling, Inc.). Elevated levels of mitochondrial lysine acetylation were detected in the Sirt3$^{-/-}$ mice as well as mice fasting for 24 hours (Fig. 1b), and further analysis via ion-exchange chromatography clearly showed a difference in total acetylation (Supplemental Fig. S1A).

### *OSCP contains a reversible acetyl lysine that is deacetylated by Sirt3*

Evidence that OSCP contains reversibly acetylated lysine residues was obtained when wild-type mice were fasted for 36 hours and their livers were harvested and immunoprecipitated (IPed) with an anti-OSCP antibody. These samples were subsequently divided into equal fractions, resolved by SDS-PAGE, and immunoblotted with either an acetyl (Fig. 1c, upper panel) or an anti-OSCP antibody (Fig. 1c, lower panel) showing that OSCP acetylation was increased in the livers from fasting mice.

To determine if Sirt3 directly deacetylates OSCP, two lentiviruses were constructed that expressed either the wild-type (lenti-Sirt3-wt) or a deacetylation null mutant (lenti-Sirt3-dn) *Sirt3* gene (a gift from Dr. Toren Finkel, NIDDK) in which amino acid 248 was changed from a

histidine to tyrosine (Ahn et al., 2008). Sirt3$^{-/-}$ mouse embryonic fibroblasts (MEFs) were infected with these two viruses and a control lentivirus, IPed with an anti-OSCP antibody, divided into equal fractions, resolved by SDS-PAGE, and then immunoblotted with either an acetyl (Fig. 1e, upper panel) or and anti-OSCP antibody (Fig. 1e, lower panel). These experiments demonstrated that wild-type, but not deacetylation-null *Sirt3*, decreases OSCP acetylation (Fig. 1e, lane 2 versus 3) and increases mitochondrial ATP levels in a Sirt3$^{-/-}$ MEFs (Fig. 1f), though not to the levels observed in Sirt3$^{+/+}$ MEFs. Equal levels of exogenously expressed Sirt3 were confirmed by immunoblotting with an anti-Sirt3 antibody (Supplemental Fig. S1B). These results support the hypothesis that Sirt3 directly deacetylates OSCP as well as increases total mitochondrial ATP.

***OSCP physically interacts with SIRT3***

To identify substrates that interact with human SIRT3, a co-IP was done with embryonic kidney (HEK 293) cells genetically altered to express SIRT3 tagged with a FLAG epitope. The SIRT3 deacetylation null mutant was also used, as well as the other mitochondrial sirtuins, SIRT4 and SIRT5, and ACAT2, which served as a control for any non-specific mitochondrial protein binding to the FLAG epitope. Expression of flag tagged proteins was induced by tetracycline followed by FLAG-IP. These proteins were then resolved by PAGE, and stained with Coomassie (Fig. 2a), and protein bands were excised, digested with trypsin (via an in-gel digestion protocol) and identified by peptide mass fingerprinting using a MALDI-TOF-TOF mass spectrometer (Supplemental Section, Fig. S2). Two proteins, ATP synthase subunit OSCP and ATPase family AAA domain-containing protein 3A isoform 1 (ATAD3), were identified as potential SIRT3 interacting proteins that did not also bind to SIRT4, SIRT5, or ACAT2. No other subunits from the F1Fo ATP synthase were detected in this experiment or in replicate experiments.

OSCP was IPed from HCT116 cells genetically altered to overexpress either the wild-type (HCT116-wt) or deacetylation null *SIRT3* gene (HCT116-dn) as previously described (Jacobs et al., 2008). These samples were subsequently resolved by PAGE and immunoblotted with an anti-SIRT3 antibody and show an OSCP interaction with SIRT3 (Fig. 2b). A myc-IP SIRT3 immunoblot was also done as an internal control (Fig. 2b). The reverse SIRT3 IP/anti-OSCP immunoblot confirmed the interaction between these two proteins (Fig. 2c). Finally, HCT116 cells constitutively expressing wild-type *SIRT3* were stained by immunohistochemistry (IHC) with antibodies to OSCP and SIRT3 (Fig. 2d) or mitotracker and SIRT3 (Fig. 2e) and these results confirmed that OSCP and SIRT3 both localize to the mitochondria.

***SIRT3 deacetylates lysine 139 of OSCP***

To determine if SIRT3 was capable of deacetylating specific lysine residues in OSCP, an *in vitro* deacetylation assay using human recombinant SIRT3 (BioMol) and purified bovine ATP synthase was performed (Fig. 3a). Reaction products were separated by PAGE and detected with an anti-acetyl antibody showing that SIRT3 deacetylates OSCP. In addition, the decrease in lysine acetylation is inhibited with nicotinamide (lane 3), an inhibitor of sirtuin reactions, and removal of NAD+ (lane 4), suggesting that deacetylation is directly due to SIRT3.

Total mouse liver mitochondrial protein from Sirt3$^{+/+}$ and Sirt3$^{-/-}$ mice was resolved, and the part of the gel containing OSCP was digested with trypsin. The peptide mixtures were analyzed by mass spectrometry in an OrbiTrap mass spectrometer. OSCP was identified in both samples, as expected, but peptides modified by acetylation of lysine 139 were only detected in the OSCP sample from Sirt3$^{-/-}$ samples. A representation of the tandem mass spectrum demonstrating the acetylation of lysine 139 in a tryptic peptide is shown (Fig. 3b). Of the 13 most intense peaks in this tandem mass spectrum, 8 are attributable to OSCP fragments. Six peaks correspond to a

series of y+ type fragment ions defining a partial amino acid sequence of K(Ac)SFLS. One peak is a b+ type ion, b2, and an additional peak of high intensity corresponds to the 126.0913 m/z immonium ion produced by the fragmentation of peptides containing ε-acetylated lysine and is diagnostic of this modification. The lysine in the K(Ac)SFLS sequence is located at OSCP amino acid position 139.

The specificity of the lysine deacetylation was determined using recombinant human SIRT3 and a synthetic peptide (JPT Peptide Technologies, Berlin) corresponding to a 20 amino acid sequence of OSCP that contains lysine 139. This synthetic peptide (sequence EEATLSELKTVL(AcK)SFLSQGQ) was incubated with recombinant SIRT3 (BioMol) and NAD+, and the reaction was monitored by MALDI-TOF measurement of the peptide mass (Fig. 3c). Following incubation of the acetylated synthetic peptide with recombinant SIRT3, all of the peptide was reduced in mass by 42 m/z. A control reaction with nicotinamide (an inhibitor of sirtuins) caused no shift in the signal, nor did a control with NAD+ and no SIRT3 (data not shown). Similar experiments were performed for a related peptide with acetylated threonine instead of lysine (sequence EEATLSELK(AcT)VLKSFLSQGQ). No mass change was observed for the threonine acetylated peptide (Fig. 3d).

Finally, livers from Sirt3$^{+/+}$ and Sirt3$^{-/-}$ mice were harvested, and tandem mass spectrometry showed a significant increase in the acetylation of OSCP lysine 139 in the Sirt3$^{-/-}$ , as compared to the Sirt3$^{+/+}$ mice (Fig. 3e). The results of these experiments confirm that OSCP is a SIRT3 deacetylation target *in vitro* and *in vivo* and that OSCP lysine 139 is an amino acid targets.

***OSCP contains an evolutionarily conserved lysine that alters mitochondrial ATP levels***

OSCP is an old, evolutionarily conserved protein present in almost all species and as such, if a specific OSCP lysine is an acetylation target in the regulation of enzymatic activity, it seems

reasonable that this lysine would be conserved in multiple mammalian and non-mammalian species. A BLAST search demonstrated a conserved 17 amino acid motif (LSELKTVLK*SFL SQGQV) around the lysine of interest at amino acid position 139 that is present in human, murine, bovine, *C. elegans*, and yeast (Fig. 4a). Thus, it seems reasonable to propose that this conserved 17 amino acid motif, which has remained roughly intact in multiple species, may be of biological and physiological importance.

It has previously been shown that substitution of a lysine with an asparagine mimics the acetylated state, while substitution with an arginine mimics deacetylation (Li et al., 2007; Schwer et al., 2006). Thus, mutating lysine 139 to arginine would be predicted to mimic a deacetylated lysine, while substitution with an asparagine would be expected to mimic an acetylated lysine (Fig. 4b). As such, pCMV-OSCP$^{K139}$ (wild-type), pCMV-OSCP$^{K139\text{-}R}$, and pCMV-OSCP$^{K139\text{-}N}$ were used to transfect HCT116 cells to make permanent cell lines by selection with neomycin. These cells were used to determine mitochondrial ATP levels. These experiments demonstrated that the OSCP$^{K139\text{-}R}$ mutant moderately increased ATP levels, while cells expressing the OSCP$^{K139\text{-}N}$ mutant slightly decreased ATP levels (Fig. 4c). The levels of exogenously expressed OSCP in these permanent cell lines were roughly equal (Fig. 4d). These results suggest that acetylation of OSCP plays a role, but only in part, in regulating ATP synthase activity.

An examination of the published 3-dimensional structure of the ATP synthase protein complex OSCP (Rees et al., 2009) from the side (Fig. 4e, see arrow) as well as from the top (Fig. 4f) shows that lysine 139 is on the outside of the OSCP protein as well as the outer part of the ATP synthase complex. This location is an ideal position to interact with other proteins, such as Sirt3.

**DISCUSSION**

One intriguing finding from our and others previous work was that cells lacking *Sirt3* exhibited altered mitochondrial metabolism, including a significant decrease in mitochondrial ATP levels (Ahn et al., 2008; Kim et al., 2010). These results suggest a potential connection between the regulation of ATP production and SIRT3. In this regard, Sirt3 is the primary mitochondrial deacetylase (Lombard et al., 2007), and lysine acetylation has recently emerged as an important, and perhaps the primary, post-translational modification employed to regulate mitochondrial proteins (Choudhary et al., 2009; Schwer et al., 2006). In addition, large-scale mass spectrometry screening pre- and post-caloric restriction identified reversibly acetylated lysines in 72 mitochondrial proteins from a wide variety of metabolic pathways (Schwer et al., 2009). Based on these results, it seems reasonable to suggest that deacetylation of mitochondrial proteins by SIRT3 may play a role in maintaining and regulating mitochondrial metabolism and function.

A fundamental paradigm in biology is the presence of intracellular sensing proteins that recognize specific cellular conditions and initiate post-translational signaling cascades (Lombard et al., 2007), and these pathways activate the cellular machinery that maintains cellular homeostasis. The most common example of this is the cytoplasmic activation of kinases that phosphorylate a series of downstream targets in response to different environmental conditions, thereby minimizing any potentially permanent cellular detrimental effects (Kim et al., 2010). In this regard, lysine acetylation has recently emerged as an important and perhaps primary post-translational modification employed to regulate mitochondrial proteins (Choudhary et al., 2009; Lombard et al., 2007). The results presented above support this hypothesis, and together with recent findings (Kim et al., 2010), suggest that mitochondrial sirtuins, including Sirt3, may function as fidelity proteins whose loss of function may result in a damage permissive phenotype that leads to aberrant mitochondrial function.

The active site in the ATP synthase complex is formed by subunits α and β, and thus OSCP may not represent an intuitively obvious place for alteration of protein complex activity through post-translational modification. However, as OSCP is the location of contact between the peripheral stator stalk and the enzymatically active α and β subunits, it may serve to alter overall enzymatic function of the protein compels. Indeed, small alterations in or removal of OSCP can decouple the ATP synthetic activity of the complex from the protonmotive force (Rees et al., 2009). As OSCP lysine 139 is part of a beta-helix which interacts with neighboring subunit b, modification of this residue could reasonably alter activity of the ATP synthase complex.

Given that x-ray crystallography and intact mass spectrometric measurement of molecular mass of this subunit has failed to detect ε-acetylation of any lysine in OSCP, lysine 139 is either acetylated in a small portion of intact ATP synthase, or else this lysine is acetylated at times other than when this protein is assembled into fully formed and functional ATP synthase complex. For example, a modification present in only a few percent of protein complexes could be associated with a secondary function such as uncoupling from the protonmotive force, or for assembly or disassembly of the complex.

**ACKNOWLEDGMENTS**

DG is supported by 1R01CA152601-01, DOD BC093803, and SPORE P50CA98131. JDP is supported by NIA F30AG030839. We thank Mike Runswick, MBE for providing bovine heart ATP synthase. We thank Kamburapola Jayawardena and Mike Harbour for technical assistance with mass spectrometry. We thank Melissa Stauffer, PhD, of Scientific Editing Solutions, for editorial assistance.

## Materials and Methods

### *Cell lines and Purification of proteins by immunoprecipitation*

MEFs were isolated from E14.5 isogenic $Sirt3^{+/+}$ and $Sirt3^{+/+}$ mice and maintained in a 37° C incubator with 5% $CO_2$ and 6% oxygen. $Sirt3^{+/+}$ or $Sirt3^{-/-}$ MEFs (Kim et al., 2010) were infected at passage 3 with lentiviral vectors expressing either the wild-type or a deacetylation null *Sirt3* gene (Ahn et al., 2008), made by Applied Biological Materials, Inc. (Richmond, British Columbia). Levels of exogenous Sirt3 and OSCP were confirmed by western blot analysis and PCR analysis (data not shown).

Mitochondria were solubilized at with 1% w/v DDM and diluted to a protein concentration of 5.5 mg/mL. IPs was performed using either antibody already cross-linked to beads, or with free antibody. IPed samples were divided into equal samples, separated by SDS-PAGE, and immunoblotted with anti-acetyl (Cell Signaling, Inc.) and anti-OSCP antibodies.

### *Mouse tissues*

All work with mice was performed at the National Cancer Institute, National Institutes of Health, Bethesda, Maryland, USA. All protocols were approved by the National Cancer Institute's Animal Care and Use Committee as described in protocol ROB-118. Tissues were rinsed in sucrose, Tris, and EGTA (STE) buffer and immediately frozen on dry ice.

### *IP, transfections, and immunoblot analysis*

IP with anti-OSCP and anti-Sirt3 antibodies and the subsequent western analyses were done as previously described (Kim et al., 2010). The control for these IP experiments is normalized to rabbit IgG as well as immunoblotting with the control, IPed antibody. Transfections of $pCMV\text{-}OSCP^{K139}$ (wild-type), $pCMV\text{-}OSCP^{K139\text{-}R}$, or $pCMV\text{-}OSCP^{K139\text{-}Q}$ were

done as previously described (Kim et al., 2010). Blots were incubated with horseradish peroxidase-conjugated secondary antibody, analyzed using an ECL protocol (Amersham Biosciences, Piscataway, NJ), and visualized in a Fuji Las-3000 darkbox (FujiFilm Systems, Stamford, CT).

***Measurement of mitochondrial ATP levels, immunohistochemical staining and Protein identification by mass spectrometry***

ATP levels were monitored using a CellTiter-Glo Luminescent Cell Viability Assay as per the manufacturer's instructions (Promega). CellTiter-Glo was added to $10^6$ cells and placed on an orbital shaker to induce cell lysis, and samples were read on a chemiluminescence plate reader (Tecam Safire; integration time of 1 s). Data are presented as mean ± SE of luminescence readings from three separate experiments. IHC was done as previously described (Kim et al., 2010). For mass spectrometry see supplemental section, methods.

**REFERENCES:**

Ahn, B.H., Kim, H.S., Song, S., Lee, I.H., Liu, J., Vassilopoulos, A., Deng, C.X., and Finkel, T. (2008). A role for the mitochondrial deacetylase Sirt3 in regulating energy homeostasis. Proc Natl Acad Sci U S A 105, 14447-14452.

Choudhary, C., Kumar, C., Gnad, F., Nielsen, M.L., Rehman, M., Walther, T.C., Olsen, J.V., and Mann, M. (2009). Lysine acetylation targets protein complexes and co-regulates major cellular functions. Science 325, 834-840.

Finkel, T., Deng, C.X., and Mostoslavsky, R. (2009). Recent progress in the biology and physiology of sirtuins. Nature 460, 587-591.

Jacobs, K.M., Pennington, J.D., Bisht, K.S., Aykin-Burns, N., Kim, H.S., Mishra, M., Sun, L., Nguyen, P., Ahn, B.H., Leclerc, J., Deng, C.X., Spitz, D.R., and Gius, D. (2008). SIRT3 interacts with the daf-16 homolog FOXO3a in the Mitochondria, as well as increases FOXO3a Dependent Gene expression. International journal of biological sciences 4, 291-299.

Kim, H.S., Patel, K., Muldoon-Jacobs, K., Bisht, K.S., Aykin-Burns, N., Pennington, J.D., van der Meer, R., Nguyen, P., Savage, J., Owens, K.M., Vassilopoulos, A., Ozden, O., Park, S.H., Singh, K.K., Abdulkadir, S.A., Spitz, D.R., Deng, C.X., and Gius, D. (2010). SIRT3 Is a Mitochondria-Localized Tumor Suppressor Required for Maintenance of Mitochondrial Integrity and Metabolism during Stress. Cancer cell 17, 41-52.

Kim, S.C., Sprung, R., Chen, Y., Xu, Y., Ball, H., Pei, J., Cheng, T., Kho, Y., Xiao, H., Xiao, L., Grishin, N.V., White, M., Yang, X.J., and Zhao, Y. (2006). Substrate and functional diversity of lysine acetylation revealed by a proteomics survey. Molecular cell 23, 607-618.

Li, X., Zhang, S., Blander, G., Tse, J.G., Krieger, M., and Guarente, L. (2007). SIRT1 deacetylates and positively regulates the nuclear receptor LXR. Molecular cell 28, 91-106.

Lombard, D.B., Alt, F.W., Cheng, H.L., Bunkenborg, J., Streeper, R.S., Mostoslavsky, R., Kim, J., Yancopoulos, G., Valenzuela, D., Murphy, A., Yang, Y., Chen, Y., Hirschey, M.D., Bronson, R.T., Haigis, M., Guarente, L.P., Farese, R.V., Jr., Weissman, S., Verdin, E., and Schwer, B. (2007). Mammalian Sir2 homolog SIRT3 regulates global mitochondrial lysine acetylation. Mol Cell Biol 27, 8807-8814.

Rees, D.M., Leslie, A.G., and Walker, J.E. (2009). The structure of the membrane extrinsic region of bovine ATP synthase. Proc Natl Acad Sci U S A 106, 21597-21601.

Schwer, B., Bunkenborg, J., Verdin, R.O., Andersen, J.S., and Verdin, E. (2006). Reversible lysine acetylation controls the activity of the mitochondrial enzyme acetyl-CoA synthetase 2. Proc Natl Acad Sci U S A 103, 10224-10229.

Schwer, B., Eckersdorff, M., Li, Y., Silva, J.C., Fermin, D., Kurtev, M.V., Giallourakis, C., Comb, M.J., Alt, F.W., and Lombard, D.B. (2009). Calorie restriction alters mitochondrial protein acetylation. Aging Cell.

Singh, K.K. (2006). Mitochondria damage checkpoint, aging, and cancer. Ann N Y Acad Sci 1067, 182-190.

Walker, J.E., and Dickson, V.K. (2006). The peripheral stalk of the mitochondrial ATP synthase. Biochim Biophys Acta 1757, 286-296.

Watt, I.N., Montgomery, M.G., Runswick, M.J., Leslie, A.G., and Walker, J.E. (2010). Bioenergetic cost of making an adenosine triphosphate molecule in animal mitochondria. Proc Natl Acad Sci U S A.

## FIGURE LEGENDS

**Figure 1. *Sirt3* knockout cells have increased mitochondrial acetylated protein and decreased ATP levels and OSCP contains a reversible acetyl lysine. (a)** Mouse liver mitochondria were purified from $Sirt3^{+/+}$ or $Sirt3^{-/-}$ mice that were either fed (Fed) or fasted (Fasting) for 24 hours. Protein extracts were solubilized and separated via electrophoresis, transferred to a PVDF membrane, and then probed with a mouse Sirt3 antibody (A kind gift from Dr. Michael Sack, NILHK). Immunoblotting with an F1Fo ATP synthase subunit β antibody (MitoSciences, Inc.) served as a loading control. **(b)** Fasting and $Sirt3^{-/-}$ genotype increase total mitochondrial protein acetylation in mouse liver. $Sirt3^{+/+}$ (WT) and $Sirt3^{-/-}$ (KO) mouse liver mitochondria were purified as described above and immunoblotted with an anti-acetyl lysine (AcK) antibody (Cell Signaling). An antibody against ATP synthase subunit γ was used as a loading control. Coomassie staining of the PVDF membrane serves as an additional loading control (right hand panel). **(c)** OSCP contains a reversibly acetylated lysine. Livers from isogenic, three-month-old age-matched $Sirt3^{+/+}$ mice fasted for 36 hours were harvested, IPed with an anti-OSCP antibody (Santa Cruz Biotechnology, Inc.), and immunoblotted with an anti-acetyl antibody (Cell Signaling, Inc) or anti-OSCP antibody. **(d)** Mitochondrial ATP levels in *Sirt3* wild-type and knockout cells. $Sirt3^{+/+}$ and $Sirt3^{-/-}$ MEFs were lysed, and ATP levels were measured using chemiluminescence. Data are presented as arbitrary luminescence units for ATP levels as a ratio of the level in $Sirt3^{+/+}$ MEFs. Re-expression of wild-type, but not a deacetylation null mutant of *Sirt3*, **(e)** deacetylates OSCP and **(f)** restores ATP levels in $Sirt3^{-/-}$ MEFs. Fifth passage $Sirt3^{-/-}$ MEFs were transfected with a control lentivirus (Con), virus expressing a wild-type *Sirt3* (wt), or one expressing the deacetylation null gene (dn) in which amino acid 248 has been changed from a histidine to tyrosine (Ahn et al., 2008). Forty hours after infection, $Sirt3^{-/-}$ MEFs were harvested and mitochondrial extracts were IPed with an anti-OSCP antibody (Santa Cruz Biotechnology, Inc) followed by immunoblotting with an anti-acetyl or anti-OSCP antibody. These extracts were also used to measure ATP levels as described above. The results of all the experiments in this figure were obtained from at least three independent replicates. Representative gels are shown. Error bars represent one standard deviation. * indicates $P < 0.05$ by t-test.

**Figure 2. OSCP physically interacts with and co-localizes with Sirt3 in the mitochondria. (a)** Identification of proteins that co-IP with SIRT3. The pcDNA5 plasmids expressing *ACAT2*, *SIRT3*, deacetylation null mutant (*H248Y SIRT3*), *SIRT4*, or *SIRT5* with a FLAG-tag and under the control of a tetracycline-inducible promoter were transfected into HEK cells. After induction or control, cells were lysed and IP was performed using anti-FLAG antibody. Protein bands excised from the resulting Coomassie-stained polyacrylamide gel were identified by peptide mass fingerprinting using a MALDI-TOF-TOF mass spectrometer. Mitochondrial proteins ATAD3 (arrowhead) and ATP synthase subunit OSCP (arrow) are shown. **(b-c)** Sirt3 physically interacts with OSCP. HCT116 cells were constructed to constitutively express either a myc tagged wild-type (WT) or deacetylation null mutant (DN) *SIRT3*. Cell extracts from WT or DN cells were **(b)** IPed for OCSP and immunoblotted with an anti-SIRT3 antibody or **(c)** IPed for SIRT3 and immunoblotted with and anti-OSCP antibody. HCT116 cells expressing a myc tagged *SIRT3* were stained with **(d)** SIRT3 and OSCP antibodies or with **(e)** SIRT3 antibody and mitotracker and the images were merged. Representative micrographs are shown. Error bars represent one standard deviation. * indicates $P < 0.05$ by t-test.

**Figure 3. SIRT3 deacetylates lysine 139. (a)** SIRT3 directly deacetylates two subunits of ATP synthase. Fifty mg purified bovine ATP synthase were mixed without or recombinant human

SIRT3 with nicotinamide or NAD+. After one hour samples were separated by PAGE, followed by immunoblotting with an anti-acetyl antibody (Cell Signaling, Inc.). Antibody against ATP synthase subunit $\gamma$ was used as a loading control. **(b)** Tandem mass spectrum from OSCP demonstrates acetylated lysine 139 i*n vivo*. Liver mitochondria from wild-type and SIRT3$^{-/-}$ mice were resolved by SDS-PAGE followed by in-gel trypsin digestion, separation by nano-scale reverse-phase chromatography on reverse-phase columns, and analysis by OrbiTrap analyser via an electro-spray interface. The spectrum represents the fragmentation of the peptide with a mass of 1628.9501 corresponding to the sequence TVL(AcK)SFLSPNQILK. **(c)** *In vitro* deacetylation of synthetic peptides. Synthetic peptide including acetylated lysine, corresponding to the sequence of ATP synthase subunit OSCP (sequence EEATLSELKTVL(AcK)SFLSQGQ), was measured by MALDI-TOF (left). The predicted m/z for acetylated lysine 139 is 2250.57 and for deacetylated peptide is 2208.56 m/z. **(d)** Peptides deacetylated by SIRT3 *in vitro*. Peptides from the sequence of OSCP were synthesized with acetylated lysine 139, or threonine 136. A peptide derived from Acetyl CoA synthetase 2 (AceCS2) served as a positive control. **(e)** OSCP acetylation in *Sirt3* wild-type and knockout mice. Livers from Sirt3$^{+/+}$ and Sirt3$^{-/-}$ mice were used to isolate mitochondrial extracts that were used to determine the acetylation levels of OSCP amino acid 139. Error bars represent one standard deviation. * indicates $P < 0.05$ by t-test.

**Figure 4. OSCP contains an evolutionarily conserved lysine residue that regulates mitochondrial ATP levels. (a)** Multiple species contain a potential reversibly acetylated lysine amino acid. The OSCP protein sequence from multiple species was BLASTed based on the reversibly acetylated lysine located at amino acid 139 in humans and mice. A 17 amino acid motif (LSELKTVLK*SFLSQGQV) was identified and this motif is present in multiple species. **(b)** Schematic for the substitution of a lysine with asparagine (N) to mimic an acetylated amino acid state, and with arginine (R) to mimic a deacetylated amino acid state (Li et al., 2007; Schwer et al., 2006). **(c)** OSCP lysine acetylation status directs mitochondrial ATP levels. HCT116 cells were transfected with OSCP wild-type and mutant expression vectors (pCMV-OSCP$^{K139}$, pCMV-OSCP$^{K139\text{-}N}$, pCMV-OSCP$^{K139\text{-}R}$) and analyzed for mitochondrial ATP levels as described in the legend to Fig. 1. **(d)** Expression of exogenous OSCP in the HCT116 permanent cell lines is similar. The HCT116 cells expressing pCMV-OSCP$^{K139}$, pCMV-OSCP$^{K139\text{-}N}$, pCMV-OSCP$^{K139\text{-}R}$ were harvested and extracts were separated by SDS-PAGE, followed by immunoblotting with an anti-OSCP antibody (Santa Cruz Biotechnology, Inc). Experiments were done in triplicate. A representative gel is shown. **(e-f)** A representative side view **(e)** or co-axial view **(f)** 3-dimensional rendering of the protein structure for OSCP as part of the complete ATP synthase (Rees et al., 2009). Lysine amino acid 139 is identified by a white arrow. As can been seen, lysine 139 is on the outside of the protein and as such, is in an ideal position to interact with other proteins such as the Sirt3 deacetylase. Error bars represent one standard. * indicates $P < 0.05$ and ** $P< 0.01$ by t-test.

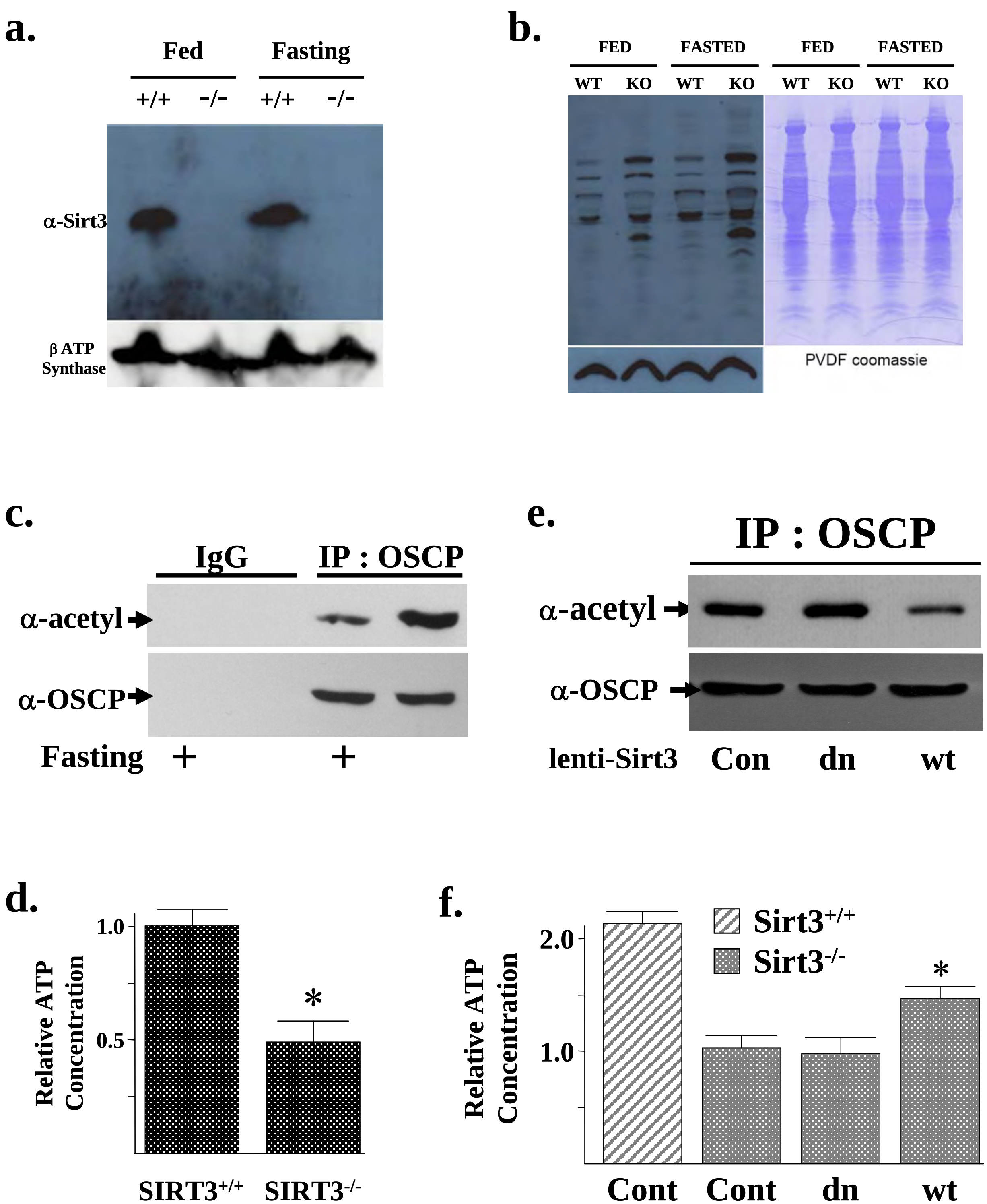
a.
Fed
Fasting
+/+
-/-
+/+
-/-
α-Sirt3
β ATP Synthase
b.
FED
FASTED
FED
FASTED
WT
KO
WT
KO
WT
KO
WT
KO
PVDF coomassie
c.
IgG
IP : OSCP
α-acetyl
α-OSCP
Fasting
+
+
e.
IP : OSCP
α-acetyl
α-OSCP
lenti-Sirt3
Con
dn
wt
d.
Relative ATP Concentration
1.0
0.5
*
SIRT3+/+
SIRT3-/-
f.
Relative ATP Concentration
2.0
1.0
Sirt3+/+
Sirt3-/-
*
Cont
Cont
dn
wt

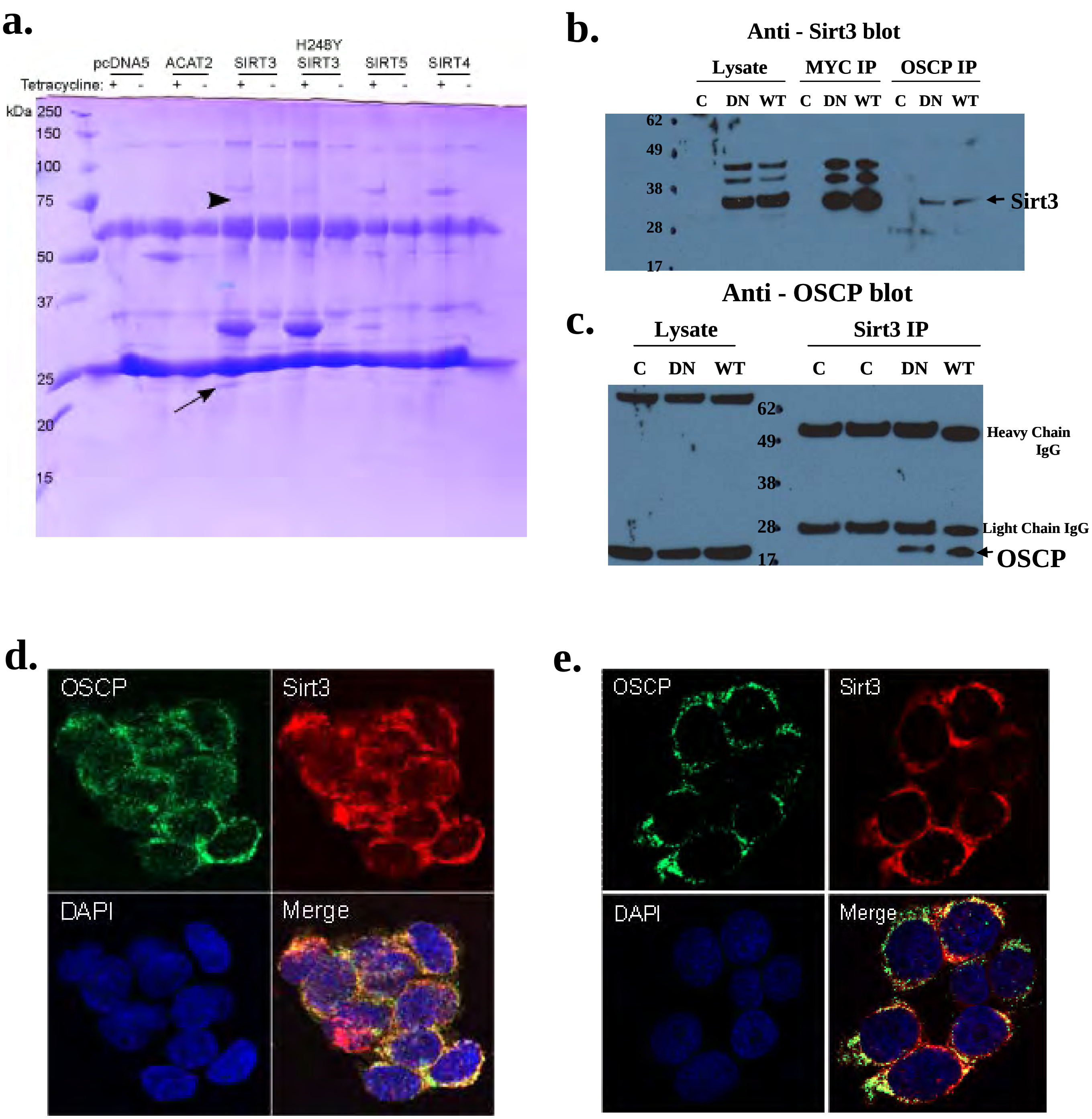
a.
pcDNA5
ACAT2
SIRT3
H248Y SIRT3
SIRT5
SIRT4
Tetracycline: + - + - + - + - + - + -
kDa 250
150
100
75
50
37
25
20
15
b.
Anti - Sirt3 blot
Lysate
MYC IP
OSCP IP
C DN WT C DN WT C DN WT
62
49
38
28
17
Sirt3
Anti - OSCP blot
c.
Lysate
Sirt3 IP
C DN WT C C DN WT
62
49
38
28
17
Heavy Chain IgG
Light Chain IgG
OSCP
d.
OSCP
Sirt3
DAPI
Merge
e.
OSCP
Sirt3
DAPI
Merge

Pennington et al.
Figure 3

**a.**

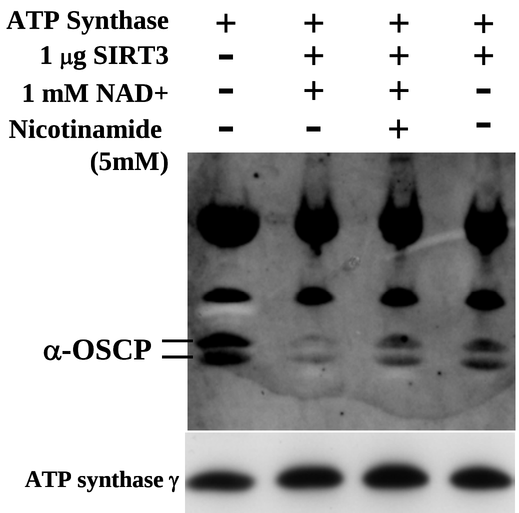


**b.**

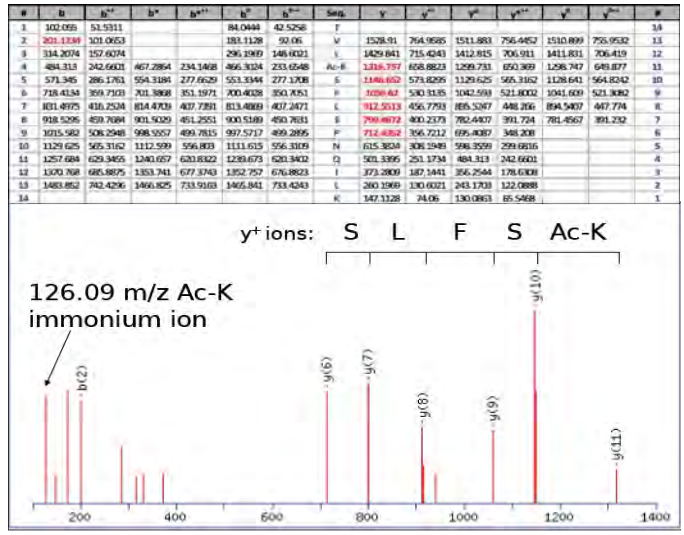


**c.**

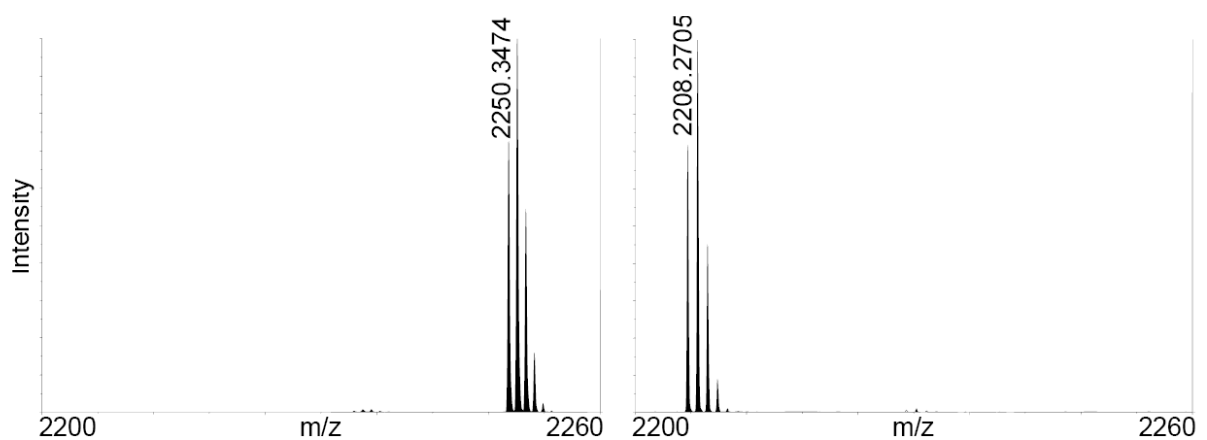


EEATLSELKTVL(Ac-K)SFLSQGQ + NAD+ $\xrightarrow{\text{SIRT3}}$ EEATLSELKTVL(Ac-K)SFLSQGQ + Nicotinamide + 2’-O-acetyl-ADPR

**d.**

| Description | Sequence | 42 kDa mass loss |
|---|---|---|
| AcK162 | EEATLSELKTVL(AcK)SFLSQGE | + |
| AcT159 | EEATLSELK(AcK)TVLKSFLSQGQ | No loss |
| AceCS2 | TRSG(AcK)VMRRLLR | + |

**e.**

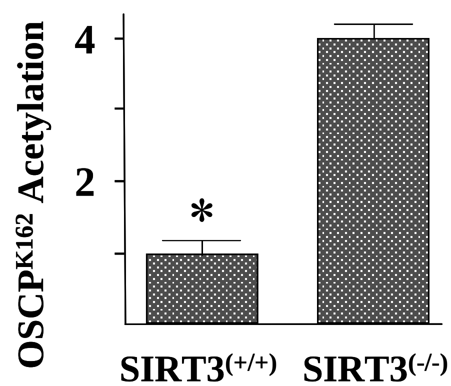

Pennington et al.
Figure 4

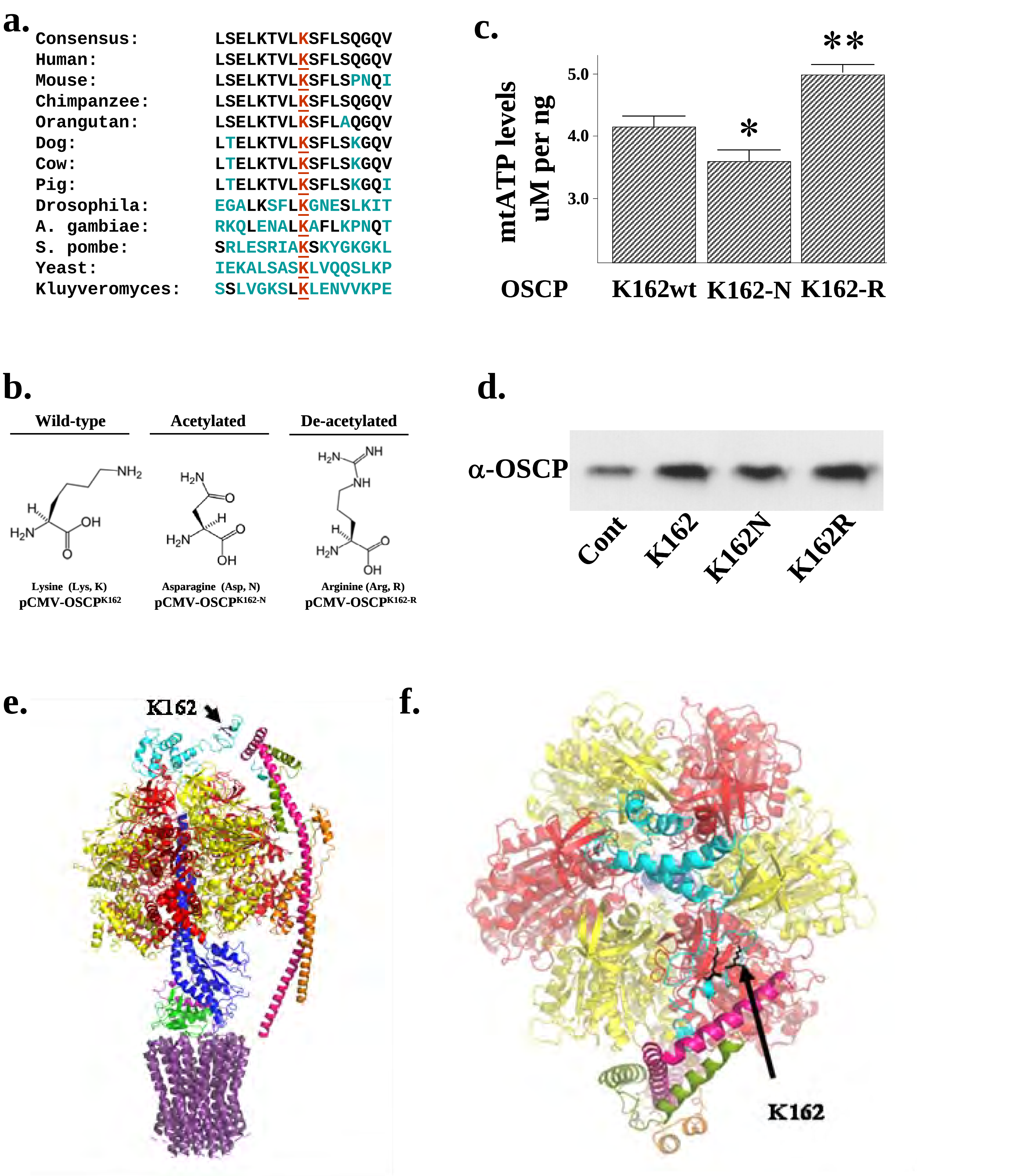

Pennington et al.
Figure 5

a.

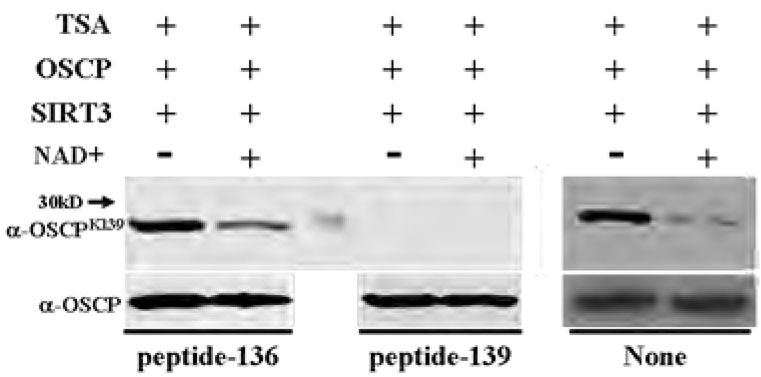


b.

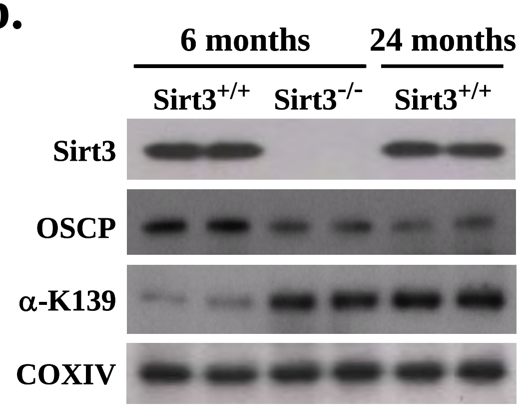


c.

d.